Evaluating the genotypic and phenotypic stability of CRISPRi essential gene mutants in *Burkholderia cenocepacia* K56-2

by

Zayra Yael Batun Hernandez

A Thesis submitted to the Faculty of Graduate Studies of The University of Manitoba in partial fulfilment of the requirements of the degree of

MASTER OF SCIENCE

Department of Microbiology

University of Manitoba

Winnipeg, Manitoba, Canada

ABSTRACT

Essential genes encode the processes required for cell growth and survival within specific environments. Understanding the products of essential genes is important for antibiotic discovery, as many essential genes encode the targets of antibiotics. Also, controlling the products of essential genes is a potential approach to reversibly inhibit growth while exploiting beneficial traits. A genetic tool to investigate essential gene function by controlling gene expression is CRISPR interference (CRISPRi). This tool comprises a nuclease-inactive Cas9 (dCas9) and a synthetic guide RNA (sgRNA), forming a ribonucleoprotein complex that binds to the target gene and sterically blocks transcription. Previously, we constructed a CRISPRi system in strains of the *Burkholderia cepacia* complex, opportunistic bacterial pathogens with biotechnological potential. Our CRISPRi system uses a chromosomally encoded, rhamnose-inducible dCas9 and a sgRNA constitutively expressed from a plasmid. We and others have observed that CRISPRi mutants spontaneously lose their conditional growth phenotype (CGP), hampering their potential use in controlling bacterial growth. To understand this phenotypic reversion, we performed experimental evolution experiments in selected 15 CRISPRi mutants under dCas9-inducing and non-inducing conditions. At time points, we performed targeted gene repression by RT-qPCR and whole genome sequencing (WGS) in parental and evolved mutants. While analysis across generations revealed diverse CGPs, all mutants reverted to wild-type growth phenotypes. K-medoids clustering identified 3 clusters with different relationships between essential gene functions and the CGP. Under consistent inducing conditions, Cluster 1 exhibited severe gene repression of 78-fold, dropping to 3-fold. Cluster 2 decreased from 46-fold to 0.5-fold, whereas Cluster 3 demonstrated wide diversity in gene repression. There was no evidence of single nucleotide polymorphisms (SNPs) in the dCas9, rhamnose system regions, or the encoded sgRNAs maintained on a plasmid. However, WGS identified SNPs in a porin and a LysR-type global regulator. Immunoblot analysis confirmed the absence of dCas9, indicating a lack of expression possibly due to porin malfunction affecting rhamnose uptake or protein degradation caused by unregulated proteases. Together, while the CRISPRi machinery is genetically stable, compensatory mutations compromised its function at longer times. Our work highlights the strengths and limitations of CRISPRi for extended control of bacterial growth.

Keywords: Essential genes, CRISPR interference (CRISPRi), conditional growth phenotype (CGP), gene repression, *Burkholderia*

ACKNOWLEDGEMENTS

As I look back three years ago and reflect on the moments that led to the completion of this thesis, I would like to thank primarily my supervisor, Dr. Silvia Cardona. Her mentorship and guidance allowed me to become the person I am today and pushed me to pursue a better version of myself, both scientifically and personally. Her knowledge, expertise, guidance, and motivation directed me during this journey, and I am deeply thankful for that.

I would like to express my deepest appreciation to my committee members, Dr. Aleeza Gerstein and Dr. Nediljko Budisa. Your support, encouragement, and kindness motivated me in every way. Thank you for guiding me, listening to me, and helping me find beauty in the chaos. I wouldn't have completed this without both of you. A big thank you to Dr. Marike Palmer for believing in me and helping me through the final stretch of my degree. I would also like to thank Dr. Chris Rathgeber for believing in me and for all his advice and empathy. I want to thank the funding agencies that have made this work possible over the years: Mitacs Inc., Research Manitoba, NSERC, and the Faculty of Graduate Studies.

To the members of the Cardona lab, both past and present. You made the stressful days less heavy and cheered me when life was complicated. Thank you for all the moments we've shared. I want to thank Dr. Andrew Hogan for being more than just a mentor; you have been a friend and helped me when I felt like drowning. Thank you for inspiring me to become a better scientist and helping me in so many ways. I want to thank all my friends in Mexico and Canada, inside and outside the Department of Microbiology. To my amazing family, who believes in me more than I believe in myself, I wouldn't be here without you. To my extraordinary mother, for always bringing me down to earth and reminding me of the purpose I came for, her love that kept me going and every phone call that made me feel I was never alone.

Finally, I am incredibly grateful to my partner and best friend, Marko Gajic, for his understanding during these years, his support during tough times, and his patience. He always motivates and reminds me that I am strong, but I must admit that I am stronger when I am with him. Thank you for being my rock, boosting my spirits, always looking out for me and warming my heart in every possible way.

DEDICATION

I dedicate this work to my mom. The person who has always believed in me through the best and the worst times. The one that gives me strength in every situation. The one that pushes me to believe in myself. My source of inspiration and my lucky charm.

I also want to dedicate this work to my God because when I think I can't do this anymore, somehow, I get through it. When I tried to give up, there was a glimpse of light. Through every rough experience, I was reminded of how blessed I am.

TABLE OF CONTENTS

LIST OF TABLES

List of Supplementary Tables

LIST OF FIGURES

List of Supplementary Figures

LIST OF ABBREVIATIONS

ANOVA	Analysis of variance
Bcc	*Burkholderia cepacia* complex
BCIP	5-bromo-4-chloro-3-indoyl phosphate
cDNA	Complementary DNA
CDS	Coding Sequence
CF	Cystic Fibrosis
CGD	Chronic Granulomatous Disease
CGP	Conditional growth phenotype
COG	Cluster of Orthologous Genes
CRISPRi	Clustered regularly interspaced short palindromic repeats interference
C_T	Threshold cycle
dCas9	Deactivated (dead) Cas9
ddNTP	Dideoxynucleotides
DMSO	Dimethyl sulfoxide
DNA	Deoxyribonucleic acid
EG	Essential gene
GMO	Genetically Modified Organism
HSD	Honestly Significant Difference
IPTG	Isopropyl ß-D-1-thiogalactopyranoside
LB	Lysogeny broth
LTTR	LysR-type transcriptional regulators
MA	Mutation accumulation
Mb	Megabases
n0	Initial population size
NGS	Next Generation Sequencing
NTC	Non-targeting Control
OD	Optical density
OD_{600nm}	Optical density measured at 600nm
ONT	Oxford Nanopore Technology
PAM	Partitioning Around Medoids

PAM	Protospacer Adjacent Motif
PCR	Polymerase Chain Reaction
PHA	Polyhydroxyalkanoates
PVDF	Polyvinylidene fluoride
Rha	L-rhamnose
RNA	Ribonucleic acid
RNP	Ribonucleoprotein
RT-qPCR	Reverse-transcription quantitative polymerase chain reaction
SBS	Sequencing by Synthesis
sgRNA	Synthetic guide RNA
SNP	Single Nucleotide Polymorphism
SyRI	Synteny and Arrangement Identifier
Tp	Trimethoprim
Tp^R	Trimethoprim resistant
WGS	Whole Genome Sequencing
WT	Wild-type

CHAPTER 1: LITERATURE REVIEW

1.1 Insights into the Genus *Burkholderia*

1.1.1 History and Properties

The genus *Burkholderia* was characterized and separated from the genus *Pseudomonas* in 1992, based on biochemical and nucleic acid differences such as their abilities to metabolize specific compounds, lipid composition, G+C content, and ribosomal RNA (Yabuuchi *et al.,* 1992). Over time, this genus has been classified within the Burkholderiaceae family, the Burkholderiales order, and the Betaproteobacteria class. *Burkholderia* are Gram-negative, motile, flagellated, rod-shaped bacteria (**Figure 1**) with over 60 characterized species. They are typically urease, catalase, and oxidase positive and thrive in aerobic conditions (Coenye, 2014; Elshafie & Camele, 2021). These characteristics allow them to inhabit a wide range of environments, including water, soil, and plants, where they can form symbiotic relationships that promote growth or act as biocontrol agents (Eberl, 2006; Eberl & Vandamme, 2016). Such properties have led to a positive association of some *Burkholderia* species with agricultural applications and environmental interactions.

From a phylogenetic perspective, the analysis of 16S rRNA sequences has revealed distinct lineages within the genus. While these species have been classified into different lineages, assigning a specific lineage to species with varying traits remains a challenge (Eberl & Vandamme, 2016; Depoorter *et al.,* 2016). This versatility is likely due to their large genomes, which consist of two to four chromosomes or large plasmids (megaplasmids), ranging up to 9 million base pairs. These large genomes contribute to their genomic plasticity, encoding a broad array of metabolic functions (Holden *et al.,* 2004; Vial *et al.,* 2007; Holden *et al.,* 2009).

1.1.2 Beneficial Traits versus Pathogenicity

The genus *Burkholderia* can be divided into two major lineages: one containing species with pathogenic properties and another with environmentally beneficial traits (Eberl & Vandamme, 2016). This division was originally based on the 16S ribosomal RNA sequences of

55 *Burkholderia* species. However, Depoorter *et al*. (2016) proposed additional lineages based on further analysis of these sequences, including species that have been recovered from contaminated sources and possessed the ability to degrade various compounds. The adaptability of *Burkholderia* allows it to thrive in acidic soils, contaminated water, plants, and clinical environments, making it an opportunistic pathogen that poses a risk to human health, particularly in individuals with compromised immune systems, such as those with cystic fibrosis (CF) (Glowicz *et al*., 2018).

Infection typically occurs through direct exposure, but individuals with weakened immune systems, especially CF patients, are more susceptible. Some *Burkholderia* species, including *B. multivorans*, *B. cenocepacia*, and *B. gladioli*, have been identified in clinical settings, while others have been found in pharmaceutical solutions and water supplies (Coenye & Vandamme, 2003). Over time, *Burkholderia* species have developed resistance to a wide range of antibiotics, making treatment more complicated and raising significant health concerns (Rhodes & Shweizer, 2016). Despite the pathogenic potential of some *Burkholderia* species, many also exhibit beneficial environmental traits. For example, *B. cepacia* has been identified in crops and water, where it acts as a biocontrol agent, producing antimicrobials to combat fungal pathogens. Similarly, *B. contaminans* (strain MS14) synthesizes occidiofungin, an antifungal compound that inhibits cell wall formation (Govan *et al*., 1996; Deng *et al*., 2016). Furthermore, *B. vietnamiensis* serves as a biofertilizer for rice plants, enhancing growth by fixing nitrogen in the soil (Compant *et al*., 2008). Many *Burkholderia* species also produce secondary metabolites, which are not required for growth but are produced in response to stress, competition for nutrients, or environmental factors. For instance, *B. cepacia* produces pyrrolnitrin, which inhibits the growth of various fungi and some Gram-positive bacteria, while *B. glumae* produces toxoflavin, a yellow-colored toxic compound harmful to plants, fungi, and other microorganisms (Depoorter *et al*., 2016; Elshafie & Camele, 2021).

In addition, some *Burkholderia* species can degrade and synthesize biopolymers like polyhydroxyalkanoates (PHA). For example, *B. cepacia* (strain JC-1) can produce PHA from various carbon sources, including simple carbohydrates and animal fat, while *B. cepacia* (strain DP1) can degrade PHA in optimal conditions, increasing depolymerase enzyme activity up to nine

times (Chin *et al*., 2022; Azami *et al*., 2017). *B. glumae* (strain MA13) has also been shown to produce PHA using glycerol as a carbon source, presenting an ecological alternative for plastic synthesis (De Paula *et al*., 2021).

1.1.3 Burkholderia cepacia Complex (Bcc)

The *Burkholderia cepacia* complex (Bcc) is a closely related group of bacteria within the genus *Burkholderia*. This complex consists of at least 20 species, which can be found in both natural and human environments. The genetic plasticity of these species allows them to proliferate in diverse ecosystems and contribute to their rapid mutation and adaptation (Tavares *et al*., 2020). Bcc species are particularly concerning as they can cause infections in humans, especially those with compromised immune systems, the elderly, and individuals with respiratory diseases such as CF or chronic granulomatous disease (CGD), leading to a decline in lung function and increased mortality (Courtney *et al*., 2004; Tavares *et al*., 2020). Treating these infections has been challenging due to the intrinsic resistance of *Burkholderia* species to various antibiotics, including carboxypenicillins, first- and second-generation cephalosporins, aminoglycosides, polymyxins, and most β-lactam antibiotics (Drevinek & Mahenthiralingam, 2010; Sfeir, 2018; Ragupathi & Veeraraghavan, 2019).

The primary species within the Bcc complex include *B. cepacia*, *B. vietnamiensis*, *B. ambifaria*, and *B. cenocepacia* (Courtney *et al*., 2004; Sfeir, 2018; Ragupathi & Veeraraghavan, 2019; Tavares *et al*., 2020; Gutiérrez-Santana & Coria-Jiménez, 2024). Among these, *B. cenocepacia* and *B. multivorans* are the most problematic species in CF patients, with an infection prevalence exceeding 80% (Drevinek & Mahenthiralingam, 2010). Interestingly, some strains of *B. cenocepacia* have demonstrated antimicrobial and antifungal properties. For instance, one strain has been shown to reduce fungal growth (Ho *et al*., 2015), while another produces an oxidizing compound that exhibits antimicrobial activity against *Enterobacter soli*, inhibiting its growth (Hunter & Manter, 2014). These examples underscore the dual nature of certain *Burkholderia* species, which can simultaneously pose risks to human health while offering potential for biotechnology and agricultural applications. The versatility of *Burkholderia* species highlights their potential in biotechnology; however, their pathogenic properties pose a risk to

human health if not properly contained (**Figure 2**). Therefore, it is important to explore targeted alternatives that enhance their beneficial traits while mitigating their pathogenic properties.

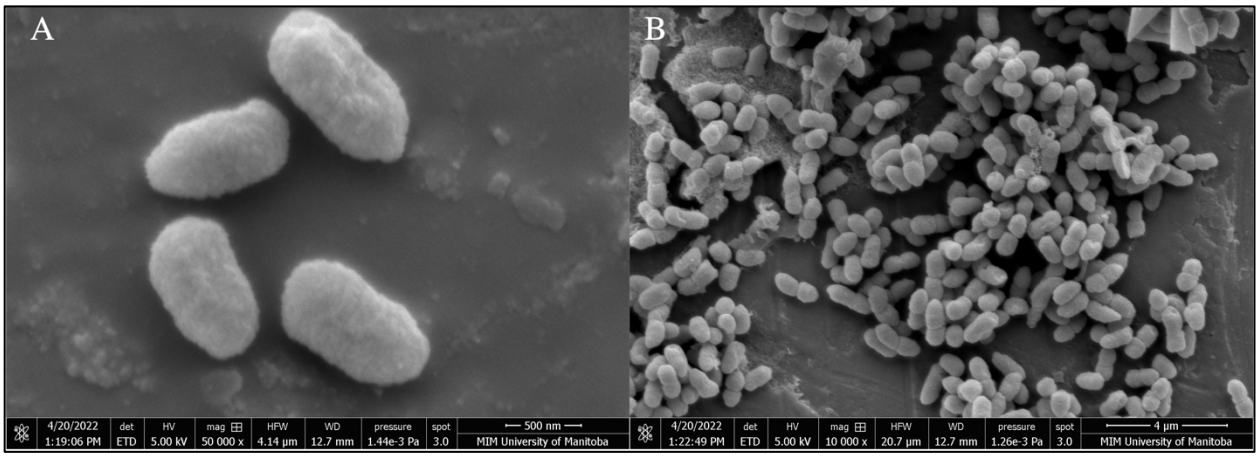

Figure 1. *Burkholderia cenocepacia* K56-2 morphology under Scanning Electron Microscopy.

(A) High-magnification view with a scale bar of 500 nm at 50,000x, showing four bacterial cells with characteristic rod-shaped morphology. (B) Lower magnification view with a scale bar of 4 µm at 10,000x, showing a cluster of cells, with the rod shape and cellular arrangement distinctly visible.

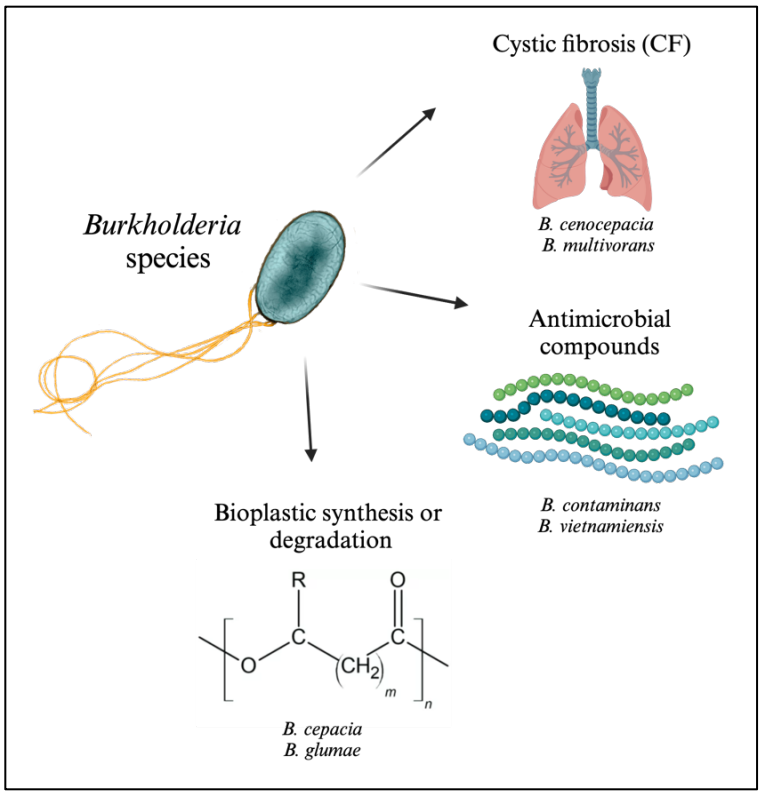

Figure 2. Versatility in the genome of *Burkholderia*.

Visual representation of the genome plasticity in *Burkholderia*'s different species, as an opportunistic pathogen in people with cystic fibrosis (*B. cenocepacia* and *B. multivorans*), biocontrol agent due to its capacity as a producer of antimicrobial compounds (*B. contaminans* and *B. vietnamiensis*), and as a biotechnology promise for its traits in the bioplastic industry (*B. cepacia* and *B. glumae*).

1.2 Gene essentiality and essential genomes

1.2.1. Definition of essential genes

Essential genes encode the products or processes indispensable for cellular proliferation and survival in a specific environment (Rancati *et al*., 2018; Dilucca *et al*., 2018; Luo *et al*., 2020). Identifying the essential genes for bacterial survival poses a challenge across different fields of study. The focus may vary depending on whether the goal is to investigate pathogenicity, antimicrobial resistance, or growth and secondary metabolite production processes. Nonetheless, studying essential genes is necessary to obtain information related to evolution and cell

functionality (Rocha & Danchin, 2003). These essential genes allow bacteria to adapt to diverse environments, and they can vary among species (Bloodworth *et al*., 2013; Luo *et al*., 2015; Gislason *et al*., 2017; Hogan & Cardona, 2022). Some examples of genes considered essential across the board are those involved in DNA replication, membrane biogenesis, transcription and translation (Juhas *et al*., 2012; Acevedo-Rocha *et al*., 2013).

1.2.2 Conserved essential genes in Burkholderia

Building on this general understanding of essential genes, research into *Burkholderia* species has provided insight into the conservation and variability of essential genomes. Ussery *et al*. (2009) analyzed 56 genomic sequences of diverse *Burkholderia* species and strains, including a comparative analysis in *B. cenocepacia* strains; by comparing the genome of four strains, it was found that out of the three chromosomes in *B. cenocepacia* (García-Romero & Valvano, 2020), chromosome 1 is the most conserved, whereas the plasmid is the least conserved. Furthermore, multiple studies have shown that the majority of genes encoding processes required for survival are contained in chromosome 1 in different strains of *Burkholderia cenocepacia* (Juhas *et al*., 2012; Wong *et al*., 2016; Higgins *et al*., 2017; Cardona *et al*., 2006), suggesting that this chromosome harbours the most conserved genes among species.

To address the variability in gene essentiality across different bacterial species, transposon mutagenesis followed by next generation sequencing (NGS) can be used to identify essential genetic elements across genomes. For instance, Gislason *et al*. (2017) employed transposon mutagenesis combined with Illumina sequencing in *B. cenocepacia* K56-2, revealing an essential gene set of 508 genes under a rich medium. Moreover, when comparing these results against *B. thailandensis, B. pseudomallei* and *B. cenocepacia* strain J2315, they identified 158 essential genes conserved across all three species, strongly suggesting that these are essential across different *Burkholderia* species.

1.2.3 Identification of essential genes in Burkholderia cenocepacia K56-2

Expanding on this genomic work, researchers have developed innovative systems to explore gene essentiality. In 2006, Cardona *et al*. developed a system utilizing a rhamnose-inducible promoter combined with transposon mutagenesis to identify essential genes and operons in *B. cenocepacia* K56-2. This approach addressed the potential misidentification of essential genes within operons, where one gene may regulate the expression of others, leading to incorrect conclusions about which genes are truly essential. In such cases, an entire gene cluster may be required for cell survival. The study used a rhamnose-inducible system to identify essential genes in *B. cenocepacia* K56-2 by controlling gene expression in the presence of rhamnose. They engineered the genome to introduce transposon insertions and paired these with a rhamnose-inducible promoter. This setup allowed them to regulate gene expression and determine which genes are essential based on whether bacteria could grow in a rhamnose-supplemented medium, conferring a conditional growth phenotype (CGP). They defined an essential gene cluster as a group of genes with a minimum distance of 150 base pairs between them.

Subsequent studies were built on this research to determine the essential genome of *B. cenocepacia* K56-2. As mentioned previously, work by Gislason *et al*. (2017) identified an essential gene set containing 508 genes by performing transposon mutagenesis and determining genes essential as those not interrupted by a transposon insertion. Moreover, when comparing this gene set by homology against *Burkholderia cenocepacia* strain J2315, they found 175 unique essential genes for K56-2, enriched in categories such as cell wall biogenesis, translation, replication and metabolism according to the cluster of orthologous genes (COG). These findings underscore the importance of genome analysis in uncovering essential processes. Moreover, understanding essential genes offers insights into the critical processes required for bacterial survival.

1.3 Next-generation sequencing (NGS) and whole genome sequencing (WGS) for bacterial genomes

Sequencing millions of DNA base pairs simultaneously using a specific platform that detects molecules individually is known as next-generation sequencing (NGS). Based on the structure of the molecules, different signals are generated at once, producing thousands of reads, which are then translated into a DNA sequence (Mitchell & Simner, 2019). This tool is versatile, as it can help understand genetic diseases, crucial mutations across species for adaptation, population analysis, or even infectious diseases (Satam *et al.,* 2023). This technology has advanced over the years, being classified from first-generation to third-generation or next-generation sequencing since the 1970s. One example of the first generation is Sanger sequencing, which consists of fluorescently or radioactively labelled dideoxynucleotides (ddNTPs) that terminate the chain elongation of DNA; then, this fluorescence is used for further sequencing by fragments (Sanger *et al.,* 1977; Slatko *et al.,* 2018; Satam *et al.,* 2023). Next-generation sequencing is characterized by its ability to sequence in parallel, meaning that it reads multiple fragments at once; for example, Illumina sequencing uses a process called sequencing-by-synthesis (SBS), which enables the simultaneous reading of multiple short DNA fragments added to a flow cell. Specific adapters and primers bind to the sequences, and a DNA polymerase generates many copies of the original sequence (Mardis, 2008). During each cycle, four different nucleotides with a unique fluorescent label are added to the flow cell, acting as reaction terminators and the signal emitted by the fluorescence is detected; this process is repeated for more than 300 cycles (Slatko *et al.,* 2018). This technology has enabled many developments for targeted approaches and whole-genome sequencing (WGS) across species. However, it has limitations, such as DNA polymerase accuracy, the amount of DNA template added or the number of cycles needed (Slatko *et al.,* 2018; Satam *et al.*, 2023).

An approach to sequence long DNA fragments is Oxford Nanopore Technology (ONT), which involves passing single-stranded DNA through a membrane embedded with nanopores. Each nucleotide passing through these nanopores will generate a specific electrical signal that is measured and then translated to create a sequence (Wick *et al.,* 2019). ONT platforms can sequence between 10,000 and 30,000 base pairs on average; however, it has a higher error rate, between 5-

15% (Wick *et al*., 2017; Satam *et al*., 2023). Nonetheless, this technology has been employed for bacterial genome assemblies or to identify bacterial strains based on its ability to detect base modifications (Wick *et al*., 2017; Slatko *et al*., 2018). ONT has been improved over the last few years by increasing read length up to 2.273 megabases (Mb) or by coupling with Illumina sequencing to reduce error rates (Wang *et al*., 2021), resulting in hybrid sequencing. This alternative combines short and long reads since the first one can quantify abundance, whereas the second one is used to assess for higher coverage (Wick *et al*., 2017; Satam *et al*., 2023). Overall, ONT has diverse applications, such as the generation of de novo genome assemblies, characterization of genomic rearrangements and identification of bacterial species (Wang *et al*., 2021).

1.3.1 Whole-genome sequencing (WGS) and spontaneous mutations

The first time WGS of a bacterium was performed, happened in 1995 using Sanger sequencing (Fleischmann *et al*., 1995). Since it has revolutionized the way strains are identified, typically, the generated sequences from WGS are assembled into larger contigs, which are then used to reconstruct the complete genome. WGS has opened the opportunity to compare the genomes of pathogenic and non-pathogenic strains plus it has posed as the first tool to analyze single nucleotide polymorphisms (SNPs) and antimicrobial resistance genes (Mustafa, 2024). Some studies have demonstrated a phenotype-genotype correlation higher than 95% (Mitchell & Simner, 2019), confirming that a phenotype can be inferred using WGS, granting the potential to understand pathogen evolution related to virulence (Mustafa, 2024).

Another approach of WGS is its potential to study mutations potentially causing diverse phenotypes across lineages. However, mutation rate can vary between species, especially in those with high G+C content and multiple chromosomes, such as *Burkholderia* (Dillon *et al*., 2015). Therefore, WGS could allow to understand mutation effects since its sensitivity allows us to analyze SNPs such as insertion-deletions (indels) and base-substitutional changes (Dillon & Copper, 2016). Depending on different factors, such as natural selection, acquired mutations from evolved lineages adapting to the environment are still under study. In previous years, exploring microbial evolution was limited to characterization at a phenotype level (Brockhurst *et al*., 2011);

however, with NGS and WGS technologies, experimental evolution can be enhanced to study phenotypic-genotypic relationships and those spontaneous mutations that have conferred variation among lineages and further adaptation (Hassan *et al.,* 2020). NGS is advancing incredibly, allowing more specific approaches like phenotypic-genotypic relationships in pathogens to move forward.

1.3.2 Burkholderia cenocepacia K56-2 genome

The genome of *Burkholderia cenocepacia* K56-2 was previously sequenced in our lab (Bloodworth *et al.,* 2015, GenBank accession LAUA00000000*)*. The sequencing data was assorted into 17 contigs and further assembled into three chromosomes and one megaplasmid. However, improvement in NGS technologies led García-Romero and Valvano, in 2020, to sequence the genome of *Burkholderia cenocepacia* K56-2 using a hybrid approach: Oxford Nanopore and Illumina sequencing. Similarly, four replicons were obtained and assembled with a coverage of 107.62x, meaning that each nucleotide of the genome was approximately sequenced 107 times for each strain. The characteristics of these four replicons are as follows: 3 circular chromosomes of 3,673,077 bp (chromosome 1: 66.89% GC content), 3,211,025 bp (chromosome 2: 67.29% GC content), and 765,157 bp (chromosome 3: 66.92% GC content) plus a megaplasmid of 92,661 bp (62.76% GC content). These replicons contained 3453, 2902, 660 and 106 genes, respectively. As we move forward, newer technologies such as next-generation sequencing (NGS) have revolutionized bacterial genomics, enabling deeper insights into genetic variation and bacterial evolution.

1.4 Experimental evolution and spontaneous mutations

1.4.1 Experimental evolution in bacteria

Understanding the processes of natural selection can be achieved through experimental evolution, which investigates those changes in a population by manipulating the environmental conditions in a laboratory setting (Elena & Lenski, 2003; Kawecki *et al.,* 2012; Van den Bergh *et*

al., 2018). For many years, scientists have been studying natural selection to underlie the mechanisms of adaptation in the environment. In bacteria, short-term evolution experiments study diversification in early generations to gain insights into population dynamics, where less than 150 generations are usually studied (Rozen & Lenski, 2000; McElroy *et al*., 2014). In contrast, long-term evolution experiments (LTEE) have been assessed to measure bacterial fitness under different conditions. These experiments allow to track ancestral populations propagated down to many generations, even up to 60,000 (Crozat *et al*., 2004; Tenaillon *et al*., 2016; Lenski, 2017; Good *et al*., 2017) and enable the study of evolved strains from a common ancestor and compare their fitness, in other words, their capacity of adaptation in a specific environment over time. This bacterial fitness can be analyzed under diverse environments, for example, increasing or decreasing salt and sugar concentrations or shifting environments from rich to minimal media (McDonald, 2019). In contrast, other more complex evolution experiments study the competition between two bacterial species populations under a specific environment and their interaction (Elena & Lenski, 2003). Throughout the adaptation process, mutations frequently arise to confer the adapted phenotype to this new environment; these mutations are typically known as beneficial (Lenski, 2017; McDonald, 2019).

1.4.2 Beneficial mutations

Mutations can be considered the origin of variation that has led to species diversification (Rana *et al*., 2021). However, they can also confer beneficial properties that allow an organism to evolve. In bacteria, these mutations can determine the adaptation of species to diverse environments, potentially conferring pathogenicity or improving fitness, an organism's ability to thrive in a given environment. These changes can be measured in conventional practice by counting colonies from a plate to address phenotypic and morphology changes, such as colony size, elevation and color. The occurrence of beneficial mutations depends on many factors, such as competing for environmental resources, for example, an available carbon source (Lenski, 2017). On top of that, these beneficial mutations might trigger the development of more SNPs, such as insertions, deletions, or base-substitutional changes, resulting in hypermutability strains that grow at a faster rate (Lenski, 2017; McDonald, 2019).

In the laboratory, evolution experiments allow the study of beneficial mutations and their role in adaptation processes (Crozat *et al*., 2004). These assays can reveal the dynamic of beneficial versus neutral mutations related to the improvement of fitness over time (Tenaillon *et al*., 2016) in diverse microorganism populations. According to Brockhurst *et al*. (2011), there could be three potential possibilities: a) beneficial mutations decrease when the progeny becomes more adapted to the environment; b) if the mutation is now constant across lineages, its effects are not visible at a phenotypic level, slowing the mutation rate, or c) there is a competition between beneficial mutations in a population where only the most beneficial prevails.

1.4.3 Spontaneous mutations in Burkholderia cenocepacia

Research in *Burkholderia cenocepacia* HI2424 performing studies for over 5000 generations in rich and minimal media applying a mutation accumulation approach found changes in bacterial growth. Dillon & Cooper (2016) performed WGS of 43 lineages and found that those with reduced fitness presented a higher number of SNPs in coding regions, where a decrease in bacterial growth rate reduced fitness in all environments tested. Using these 43 lineages, Rana *et al*., 2021, performed a mutation accumulation experiment and identified that in 27 lineages, the mutations were either beneficial or deleterious. These lineages had significant changes in fitness when compared to the ancestral strain and the mutations were primarily in a transcriptional regulator and a DNA repair enzyme. These studies illustrate the importance of spontaneous mutations in bacterial fitness. However, further research is needed to better understand genotype-phenotype relationships in *Burkholderia cenocepacia*, particularly under stronger selective pressures. Given the importance of spontaneous mutations in shaping bacterial fitness, experimental evolution assays are key to understanding how these mutations confer adaptative advantages.

While understanding essential genes offers insights into the processes required for bacterial survival and creates a baseline for exploring how bacteria adapt under selective pressures, experimental evolution builds on this knowledge by observing how bacterial populations acquire beneficial mutations and adapt to various environmental conditions.

1.5 Synthetic biology as a biocontainment strategy

1.5.1 Biocontainment

Biocontainment or safeguard mechanisms refer to methodologies that aim to control the growth of genetically modified organisms (GMOs) and prevent their release into the environment (Mandell *et al.,* 2015). These strategies employ genetic engineering to condition microorganisms to a defined environment, decreasing escape frequency (Gallagher *et al.,* 2015). An example of these genetic modifications to control growth is auxotrophy, a condition where a microorganism is genetically engineered not to produce an essential metabolite (such as an amino acid); therefore, it must be provided externally (Arnolds *et al.,* 2021). On the other hand, toxin expression, an approach that involves introducing a gene encoding a lethal protein into a microorganism's DNA, can cause cell death when expressed under controlled conditions or in response to environmental factors. This approach ensures that cells only survive in laboratory conditions, while cells that escape these conditions are killed (Molin *et al.,* 1987; Mandell *et al.,* 2015; Arnolds *et al.*, 2021).

Another safeguard mechanism is regulating one or more essential genes by using inducible promoters that control gene expression; it is argued that this has fewer negative effects on cell growth than toxins, which are more likely to disrupt cellular systems (Cai *et al.,* 2015; Gallagher *et al.,* 2015). These different approaches target diverse cellular mechanisms, but they all have the same purpose: to contain GMOs in a confined environment. Simultaneously, these techniques can be employed for biotechnology purposes (Cai *et al.*, 2015), combining the possibility of scaling up metabolite production while maintaining microorganisms within controlled conditions.

1.5.2 Synthetic biology

Synthetic biology, an approach based on DNA manipulation to engineer organisms for a specific task (Stano, 2010; Fan *et al.,* 2020), has developed novel editing tools to apply them in diverse biotechnology fields, from research to environmental and medical purposes (Lee *et al.*, 2018). Some of these tools involve diverse mechanisms to introduce genetic changes into a microorganism's DNA or uncover those genes required for survival to build what is known as a

minimal genome, to further create a cell that is viable with only those sets of essential functions (Acevedo-Rocha *et al*., 2013). The efforts to build a minimal genome have focused on essential genes. However, conserved essential genes narrow down as more species are compared (Acevedo-Rocha *et al*., 2013; Juhas *et al*., 2012; Forster & Church, 2006). Nevertheless, synthetic biology tools that aim to create minimal genomes enable the identification of essential genes across species. These tools will help uncover the core genes necessary for survival and facilitate their use in controlling growth for targeted applications.

1.5.2.1 CRISPR interference (CRISPRi)

One of the tools synthetic biology has developed in recent years to study essential genes is the application of clustered regularly interspaced short palindromic repeats interference or CRISPRi. This system consists of 3 main components: first, a critical protospacer-adjacent motif (PAM), a sequence from 2-6 base pairs (bp) unique to the target region that confers specificity (Qi *et al*., 2013); second, a synthetic guide RNA (sgRNA) located downstream of the PAM, complementary to any strand of the target DNA (Hogan & Cardona, 2022); and third; a CRISPR-associated nuclease protein from *Streptococcus pyogenes*, without endonuclease activity due to mutations in two catalytic domains (RuvC and HNH), resulting in a "dead" or deactivated Cas9 (dCas9) unable to cleave DNA but with the ability to bind to the target region (Wu *et al*., 2014; Depardieu & Bikard, 2020; Cai *et al*., 2023). These components form a ribonucleoprotein (RNP) complex, where the sgRNA directs the dCas9 to the DNA target region, and the PAM confers binding specificity. Once dCas9 is placed on the target, two events can occur: 1) interference with transcription initiation by sterically blocking transcription factors or the RNA polymerase complex, and 2) interference with elongation by sterically blocking RNA polymerase. Both events depend on whether the targeted site is the promoter or downstream of the promoter region (gene body) (Wu *et al*., 2014; Hogan & Cardona, 2022; Byun *et al*., 2023).

Studies in bacterial cells, have shown the potential of CRISPRi, due to its high specificity which allows to identify and study essential genes, understand gene function, and bacterial fitness (Rousset *et al*., 2018; Liu *et al*., 2017; Zhao *et al*., 2016). Moreover, CRISPRi has been demonstrated to knock down genes and enabled the study of a tunable system when the dCas9 is

under an inducible promoter, allowing tight gene regulation and displaying up to 1000-fold gene repression (Qi *et al*., 2013; Cai *et al*., 2023).

1.5.2.2 CRISPRi toolkit in Burkholderia

Previously, the Cardona group developed a CRISPRi toolkit for various *Burkholderia* species, including *B. cenocepacia* K56-2, *B. multivorans* ATCC17616, and *B. thailandensis* E264 (Hogan *et al*., 2019) (**Figure 3**). This toolkit consists of a chromosomally integrated codon-optimized dCas9 under the control of a rhamnose-inducible promoter (P_{rhaB}) and sgRNAs constitutively expressed from a plasmid with an antibiotic selection cassette (pSCB2-sgRNA). Upon induction, they observed a 25-fold- to 30-fold growth inhibition across all species with 0.2% rhamnose. The sgRNAs were designed to target promoter regions (including transcription start sites and near start codons) on both template and non-template strands of genes involved in the phenylacetic acid degradation pathway. However, growth inhibition occurred regardless of the targeted sgRNA template.

To confirm phenotypic assays, they performed RT-qPCR in *B. cenocepacia* K56-2. They found that gene repression was most effective (~114-fold) when the sgRNA targeted near the start codon of the non-template strand. These experiments were performed under non-inducing and dCas9-inducing conditions (-/+ rhamnose), with no apparent growth inhibition or gene repression under non-inducing conditions, allowing regular gene expression (**Figure 4**). To assess the modularity of the CRISPRi toolkit, a mutant with a non-targeting sgRNA was created as a control (NTC). This mutant contains all CRISPRi genetic elements, but the sgRNA does not target any gene in the genome. The NTC control showed no growth defects in either non-inducing or dCas9-inducing conditions (-/+ rhamnose). However, induction with rhamnose concentrations above 0.5% was shown to cause general growth inhibition, possibly causing toxicity due to high levels of dCas9 expression.

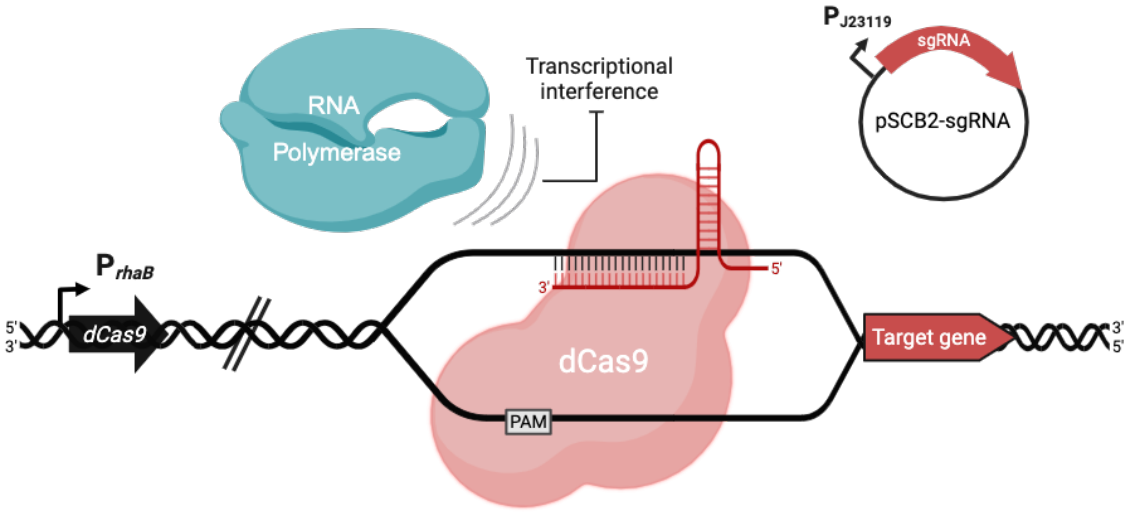

Figure 3. CRISPRi toolkit in *Burkholderia*.

Representation of the genetic elements introduced into *Burkholderia* species to express a dCas9 chromosomally inserted into the genome, causing inhibition of transcription by blocking an RNA polymerase. The vector containing a sgRNA is constitutively expressed from a plasmid, which guides the dCas9 to the target gene and a PAM conferring binding specificity. Modified from Hogan *et al*., 2019, *ACS Synthetic Biology*, **8**(10): 2372-2384.

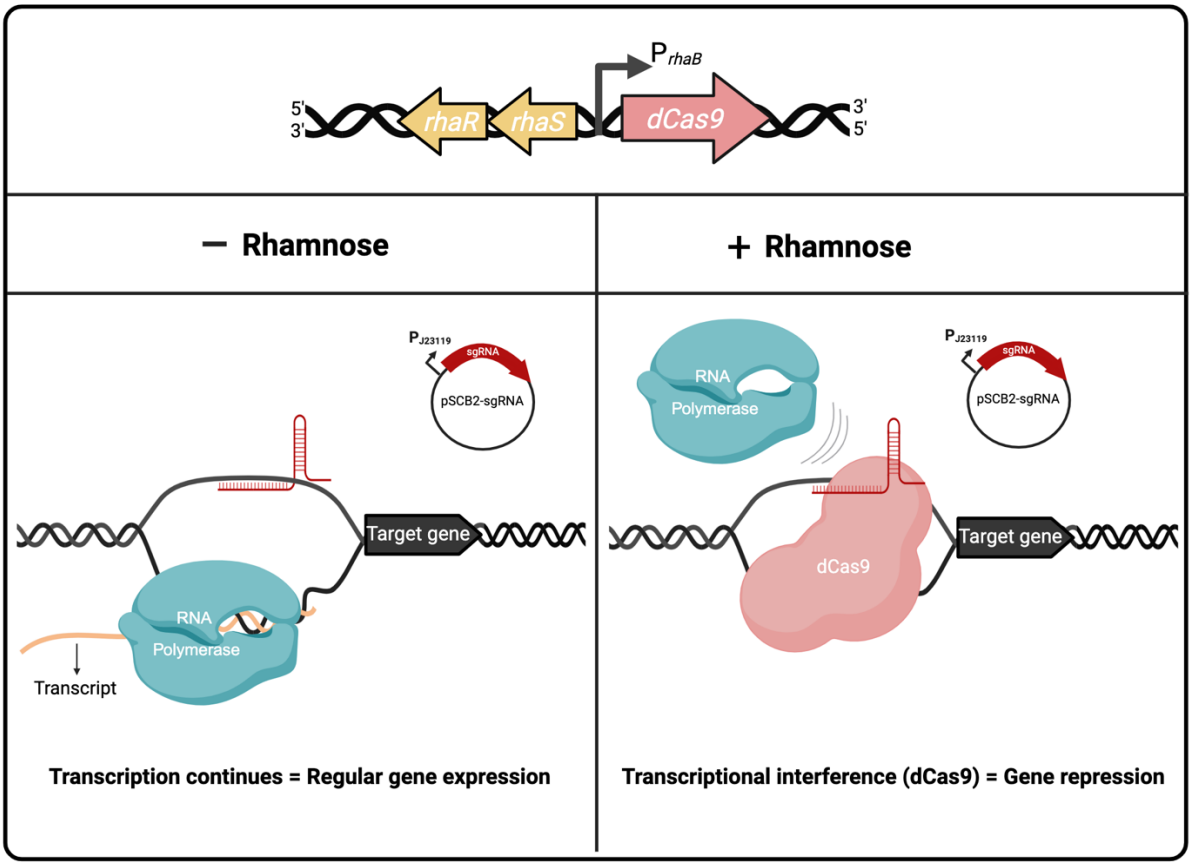

Figure 4. Rhamnose-inducible CRISPRi machinery in *B. cenocepacia* K56-2.

Graphic representation of the CRISPRi inducible system with a dCas9 regulated by a rhamnose-inducible promoter. The promoter is inactive under non-inducing conditions (– rhamnose); therefore, dCas9 is not expressed, allowing regular gene expression. Under dCas9-inducing conditions (+ rhamnose), rhamnose activates the promoter, leading to dCas9 expression, which then blocks transcription by sterically blocking an RNA polymerase, causing gene repression.

1.5.2.3 CRISPRi library in Burkholderia cenocepacia K56-2

Using the CRISPRi toolkit from Hogan *et al*. (2019), Rahman *et al*. (2024) developed a comprehensive CRISPRi-based essential gene mutant library for *B. cenocepacia* K56-2, targeting over 400 essential genes. This library was constructed based on predicted operons in the closely related *B. cenocepacia* J2315. Multiple sgRNAs were designed for each gene to target promoter regions and translation start sites. Upon induction of dCas9 with 1% rhamnose, growth inhibition was observed in 92% of the mutants compared to the nontarget sgRNA control, confirming

effective gene knockdown. The development of CRISPRi-based genomic libraries provides an effective high-throughput screening approach to study essential genes for different purposes, such as antimicrobial discovery, elucidating metabolic pathways, or identifying gene networks (Peters *et al*., 2016; Beuter *et al*., 2018).

1.5.2.4 CRISPRi loss of function related to spontaneous mutations

Knocking down essential genes using CRISPRi offers several advantages, but its long-term limitations remain unexplored. Liu *et al*. (2017) investigated CRISPRi mutants in *Streptococcus pneumoniae*. They observed that some mutants restored wild-type growth after reculturing under dCas9-inducing conditions despite the expected growth inhibition due to targeting essential genes. After sequencing these strains, they detected spontaneous mutations in the dCas9 coding sequence (CDS), causing frameshifts and changes in amino acid sequences that were translated to stop codons, likely causing loss of function. Similarly, Zhao *et al*. (2016) studied CRISPRi mutants in *Bacillus subtilis* targeting essential functions and identified deletion mutations in the dCas9 gene that caused frameshifts in the coding sequence (CDS), affecting dCas9 function. Both studies employed inducible promoters for controlling dCas9 expression, IPTG and xylose, respectively. Using inducible promoters in CRISPRi systems provides modularity, offering an "on-off" switch for dCas9 expression. This allows tunable gene regulation to analyze conditional phenotypes (Zhao *et al*., 2016; Zocca *et al*., 2021). However, the impact of consecutive selective pressure from inducers on CRISPRi mutants and how this contributes to the loss of desired conditional phenotypes remains poorly understood.

The development of these CRISPRi tools for *Burkholderia* demonstrates their utility in studying and knocking down essential genes. This approach underlies the biotechnology's potential for controlling bacterial growth and discovering new antibiotics. Nevertheless, further clonal assays are needed to fully understand essential genes and optimize CRISPRi applications in bacterial research. Moreover, spontaneous mutations in the CRISPRi machinery have been found to compromise its function when targeting essential genes. Therefore, its genetic stability needs to be investigated prior to downstream applications.

1.6 Rationale and Hypothesis

Bacterial essential genes have been demonstrated to be evolutionary conserved across species, as these encode the processes necessary for cell survival and adaptation in different environments (Rancati *et al*., 2018). Thus, these have been studied to inhibit and control bacterial growth for diverse applications, such as antibiotic discovery. CRISPRi interference (CRISPRi) is a synthetic biology tool that inhibits transcription and allows gene repression. Targeting essential genes using CRISPRi is a promising combination to control growth in a specific environment for future downstream applications.

Two studies in other bacterial species applying CRISPRi to repress essential genes have identified spontaneous mutations affecting the dCas9 and sgRNAs sequences (Zhao *et al*., 2016; Liu *et al*., 2017). These mutations resulted in CRISPRi loss of function and restored wild-type phenotypes. While CRISPRi is a genetic tool that effectively inhibits gene expression, further studies are required to elucidate the mechanisms that alleviate conditional growth phenotypes, particularly those involving spontaneous mutations. *Burkholderia cenocepacia* serves as a model organism due to its versatile genome. Our long-term goal is to control *Burkholderia'*s growth for future industrial applications by partially inhibiting essential gene expression with CRISPRi. For this thesis, our goal was to investigate the compensatory effects of spontaneous mutations on CRISPRi-mediated essential gene repression. and evaluate their implications for improving this genetic tool.

I hypothesized that exploring CRISPRi genetic stability in *B. cenocepacia* K56-2 through consistent gene repression will reveal spontaneous mutations that arise as a compensatory response. This can provide a deeper understanding of genetic tools to control bacterial growth and can help us design an improved CRISPRi system toward biotechnological applications.

1.7 Research Objectives

The objectives of this research were as follows:

1. Select CRISPRi mutants by COG categories and characterize their conditional growth phenotype (CGP).
2. Quantify gene expression under non-inducing and dCas9-inducing conditions of CRISPRi mutants.
3. Identify potential spontaneous mutations in the genome of *Burkholderia cenocepacia* K56-2 and the CRISPRi toolkit.

CHAPTER 2: MATERIAL AND METHODS

2.0 Media preparation and growth conditions

Bacterial strains listed in **Table 1** were grown at 37°C in lysogeny broth (LB)-Lennox medium (Difco) with trimethoprim at a concentration of 100 µg/mL (Sigma-Aldrich) with continuous shaking at 230 rpm unless noted otherwise. Trimethoprim was used to maintain the plasmid containing an antibiotic resistance cassette. A stock solution of 20% L-rhamnose (Sigma-Aldrich) was prepared in filter-sterilized, deionized water and stored at room temperature. The sgRNA sequences and their target genes (locus tags) listed in **Table 2** were obtained from Rahman *et al*. (2024). The starting inoculum for all assays was estimated at $2.6x10^6$ cells based on a standard curve CFU/mL vs optical density at 600nm (OD_{600nm}). This estimation resulted in a starting culture with an OD_{600nm} of 0.005.

Table 1. Bacterial strains used in this study.

Strain	Plasmid	Description*	Source
Burkholderia cenocepacia K56-2::dCas9	pSCB2-sgRNAv2-*atpB*	Expressing sgRNA targeting *atpB* (K562_RS00155), clean dCas9 insertion, Tp^R	(Rahman *et al*., 2024)
Burkholderia cenocepacia K56-2::dCas9	pSCB2-sgRNAv2-*dnaN*	Expressing sgRNA targeting *dnaN* (K562_RS02185), clean dCas9 insertion, Tp^R	(Rahman *et al*., 2024)
Burkholderia cenocepacia K56-2::dCas9	pSCB2-sgRNAv2-*gyrB*	Expressing sgRNA targeting *gyrB* (K562_RS02180), clean dCas9 insertion, Tp^R	(Rahman *et al*., 2024)
Burkholderia cenocepacia K56-2::dCas9	pSCB2-sgRNAv2-*parC*	Expressing sgRNA targeting *parC* (K562_RS06290), clean dCas9 insertion, Tp^R	(Rahman *et al*., 2024)
Burkholderia cenocepacia K56-2::dCas9	pSCB2-sgRNAv2-*metG*	Expressing sgRNA targeting *metG* (K562_RS05945), clean dCas9 insertion, Tp^R	(Rahman *et al*., 2024)
Burkholderia cenocepacia K56-2::dCas9	pSCB2-sgRNAv2-*murC*	Expressing sgRNA targeting *murC* (K562_RS16815), first gene in the division and cell wall operon, clean dCas9 insertion, Tp^R	(Rahman *et al*., 2024)

Burkholderia cenocepacia K56-2::dCas9	pSCB2-sgRNAv2-*mrdAB*	Expressing sgRNA targeting *mrdAB* (K562_RS02475), clean dCas9 insertion, Tp^R	(Rahman *et al*., 2024)
Burkholderia cenocepacia K56-2::dCas9	pSCB2-sgRNAv2-*obgE*	Expressing sgRNA targeting *obgE* (K562_RS16670), clean dCas9 insertion, Tp^R	(Rahman *et al*., 2024)
Burkholderia cenocepacia K56-2::dCas9	pSCB2-sgRNAv2-*trxB*	Expressing sgRNA targeting *trxB* (K562_RS14600), clean dCas9 insertion, Tp^R	(Rahman *et al*., 2024)
Burkholderia cenocepacia K56-2::dCas9	pSCB2-sgRNAv2-*gatB*	Expressing sgRNA targeting *gatB* operon(K62_RS02505), clean dCas9 insertion, Tp^R	(Rahman *et al*., 2024)
Burkholderia cenocepacia K56-2::dCas9	pSCB2-sgRNAv2-*parAB*	Expressing sgRNA targeting *parAB* operon (K62_RS17180), clean dCas9 insertion, Tp^R	(Rahman *et al*., 2024)
Burkholderia cenocepacia K56-2::dCas9	pSCB2-sgRNAv2-*gmk*	Expressing sgRNA targeting *gmk* (K562_RS14475), clean dCas9 insertion, Tp^R	(Rahman *et al*., 2024)
Burkholderia cenocepacia K56-2::dCas9	pSCB2-sgRNAv2-*ligA*	Expressing sgRNA targeting *ligA* (K562_RS08175), clean dCas9 insertion, Tp^R	(Rahman *et al*., 2024)
Burkholderia cenocepacia K56-2::dCas9	pSCB2-sgRNAv2-*engA*	Expressing sgRNA targeting *engA* (K562_RS09275), clean dCas9 insertion, Tp^R	(Rahman *et al*., 2024)
Burkholderia cenocepacia K56-2::dCas9	pSCB2-sgRNAv2-*sodB*	Expressing sgRNA targeting *sodB* (K562_RS05385), clean dCas9 insertion, Tp^R	(Rahman *et al*., 2024)
Burkholderia cenocepacia K56-2::dCas9	pSCB2-sgRNAv2-non target	Expressing pSCB2-sgRNAv2, Clean dCas9 insertion, Tp^R	(Rahman *et al*., 2024)

* Tp^R = trimethoprim resistance

Table 2. List of sgRNAs, locus tags and protein IDs used for essential-gene knockdown in *Burkholderia cenocepacia* K56-2.

Gene (product name)	sgRNA	sgRNA GC% content	PAM	Locus tag(s)	Protein ID(s)
dcw cluster	ACTTTCCGCTCTCCCGTTCA	55	GGG	K562_RS16815	WP_006487098.1
				K562_RS16810	WP_006487084.1
				K562_RS16805	WP_006477019.1
				K562_RS16800	WP_006487155.1
				K562_RS16790	WP_006487111.1
				K562_RS16785	WP_006487095.1
				K562_RS16780	WP_006487105.1
				K562_RS16775	WP_006477014.1
				K562_RS16770	WP_006487138.1
				K562_RS16765	WP_006487140.1
engA	GGTTTCATCTGTGTTTTCTA	35	GCC	K562_RS09275	WP_006493685.1
dnaN	GGCTCTTGGCCCGCCACCAC	75	GCC	K562_RS02185	WP_006493926.1
parC	GCTGAATTTCGTCATTCATC	40	CCC	K562_RS06290	WP_006487625.1
gyrB	GCCCGCCCCAAGTGCCGAAA	70	GGA	K562_RS02180	WP_006490993.1
ligA	TTGGGTTCGGGCCATGCTGG	65	GCC	K562_RS08175	WP_006484653.1
parAB	GGTTTATGCGCATAAACGAG	45	GCC	K562_RS17180	WP_006485146.1
atpB	CGATAGTTGCAAGTGATTCA	40	TCC	K562_RS00155	WP_012492242.1
trxB	GACATGTGCGAATCCGTAAA	45	TCC	K562_RS14600	WP_006491171.1
sodB	CGGCGGGAGCGTATGAGCCA	70	GGT	K562_RS05385	WP_006489396.1
gatB	GGTCAGGGCCATGCGATCAC	65	GCC	K562_RS02505	WP_006494379.1
metG	TCGGATGCGGACATAGGGTC	60	GGT	K562_RS05945	WP_006493649.1
obgE	TCCGCTATTGTGCCGCGCGC	70	GGC	K562_RS16670	WP_006489254.1
gmk	TCATGGTTCGTCTCGCCGTC	60	GGT	K562_RS14475	WP_006486663.1
mrdAB	CGTTGAATTCGGTCATTTAA	35	GGG	K562_RS02475	WP_006482564.1
NTC*	CGCCGTGCACTCGCGCCGCC	85	NA	NA	NA

*NTC = Non-Targeting Control, NA = Not Applicable

2.1 CRISPRi conditional growth phenotype (CGP) assessment

Essential functions targeted in *Burkholderia cenocepacia* K56-2::dCas9 are listed in **Table 3**, describing the Cluster of Orthologous Genes (COG) category, pathway and function. Conditional growth phenotypes (CPG) were assessed by inducing dCas9 expression with 0.5% rhamnose (dCas9-inducing conditions). Overnight cultures were started from glycerol stocks and were grown in 5 mL LB with trimethoprim (100 μg/mL) at 37°C and shaking at 230 rpm. 96-well plate containing LB with trimethoprim (100 μg/mL) and with/without 0.5% rhamnose were inoculated with overnight culture and diluted to an OD_{600nm} 0.005 (~$2.6x10^6$ cells). Cell density (OD_{600nm}) readings were taken at 1-hour intervals for 22 hours using a BioTek Synergy 2 microplate reader and processed in R (version 4.3.2) to generate growth curves representing the average from three biological replicates.

Table 3. Essential genes in *Burkholderia cenocepacia* K56-2 selected for this study, COG category, pathway and function description.

COG category	Gene (product name)	Pathway	Function
Cycle Control, Cell Division, Chromosome Partitioning (D)	*dcw cluster*	Peptidoglycan biosynthesis	Division and cell wall cluster (*dcw*), of 15 genes responsible for peptidoglycan synthesis and cell division.
	engA	Ribosome associated	Necessary for normal cell division and for the maintenance of normal septation.
DNA Replication, Recombination and Repair (L)	*dnaN*	DNA Replication	DNA polymerase III subunit beta, confers DNA tethering and processivity to DNA polymerases and other proteins. Acts as a clamp, forming a ring around DNA which diffuses in an ATP-independent manner freely and bidirectionally along dsDNA.
	parC	DNA Replication	DNA topoisomerase IV, essential for chromosome segregation. It relaxes supercoiled DNA. Performs the decatenation events required during the replication of a circular DNA molecule.
	gyrB	DNA Replication	Type II topoisomerase (DNA gyrase) that negatively supercoils closed circular double-stranded (ds) DNA to modulate DNA topology and maintain chromosomes in an underwound state.

	ligA	Base excision repair	DNA ligase that catalyzes the formation of phosphodiester linkages between 5'-phosphoryl and 3'-hydroxyl groups in double-stranded DNA.
	parAB	Chromosome and associated proteins	parA parB operon, chromosome partitioning protein systems that ensure active segregation of plasmid copies prior to cell division.
Energy Production and Conversion (C)	*atpB*	Metabolic pathways	ATP synthase subunit A, key component of the proton channel; plays a direct role in the translocation of protons across the membrane
	trxB	Pyrimidine metabolism	Thioredoxin reductase, belongs to the class-II pyridine nucleotide-disulfide oxidoreductase family.
	sodB	Ethylene biosynthesis	Superoxide dismutase, destroys radicals which are normally produced within the cells and which are toxic to biological systems.
Translation (J)	*gatB*	Aminoacyl-tRNA biosynthesis	Amidotransferase subunit B, allows the formation of correctly charged Asn-tRNA(Asn) or Gln-tRNA(Gln).
	metG	Aminoacyl-tRNA biosynthesis	Methionine tRNA ligase, required not only for elongation of protein synthesis but also for the initiation of all mRNA translation through initiator tRNA(fMet) aminoacylation.
	obgE	Ribosome biogenesis biogenesis	GTPase, which plays a role in control of the cell cycle, stress response and ribosome biogenesis.
Nucleotide transport and metabolism (F)	*gmk*	Purine metabolism	Guanylate kinase, essential for recycling GMP and indirectly, cGMP.
Cell Wall, Membrane, Envelope Biogenesis (M)	*mrdAB*	Peptidoglycan biosynthesis	Cell wall shape-determining proteinC, catalyzes cross-linking of the peptidoglycan cell wall.

2.2 Short-term experimental evolution assay

A short-term experimental evolution assay was designed to achieve prolonged growth inhibition during dCas9-inducing (0.5% rhamnose) and non-inducing conditions (0% rhamnose), performing three consecutive passages. Bacterial cultures of *Burkholderia cenocepacia* K56-2::dCas9 strains were grown overnight in 5 mL of LB (trimethoprim 100 μg/mL) at 37°C with shaking at 230 rpm. Overnight cultures were diluted to an OD_{600nm} 0.005 (~$2.6x10^6$ cells) and inoculated in a 96-well plate containing LB (trimethoprim 100 μg/mL) with and without 0.5% rhamnose. OD_{600nm} readings were taken at 1-hour intervals for 22 hours using a BioTek Synergy 2 microplate reader. Cell aliquots were collected as glycerol stocks (20% glycerol) at the end of each subculture (16 hours) and immediately stored at -80°C. Next, overnight cultures from these stocks (5 μL) were inoculated in 5 mL of LB (trimethoprim 100μg/mL) with and without 0.5% rhamnose to perform growth curves after the overnight period. This process was repeated over three passages (~72 generations). The data from the microplate reader was processed in R (version 4.3.2) to generate growth curves representing the average from three biological replicates.

2.3 Measurement of growth parameters

Growth data from the short-term evolution assay was processed in R (version 4.3.2). using the "*growthcurver*" of the R package (Sprouffske & Wagner, 2016). The following parameters were obtained using the function 'SummarizeGrowthByPlate': growth rate, generation time, carrying capacity, maximum OD, deceleration phase and initial population size. Apparent lag phase time was calculated separately, as this function is not provided by the package. The description of each parameter is listed in **Table 4.** The data was fitted to a standard logistic growth equation to generate the parameters.

Table 4. Selected growth parameters obtained with R package "*growthcurver*" to characterize the conditional growth phenotypes (CGPs) and cluster CRISPRi essential gene mutants.

Argument/Parameter	Description
Initial population size (n0)	Initial population size at the beginning of the growth curve.
Growth rate (r/μ)	Increase of cells proportional to the number of bacteria present at that time. The constant of proportionality, μ, is an index of the growth rate and is called the growth rate constant.
Deceleration phase (t_mid)	The time at the inflection point of the logistic curve (end of logarithmic phase), also known as deceleration or stationary phase.
Generation time (t_gen)	Defined by the time (or predictable time) needed under optimal conditions, for a population of cells (bacteria) to double in number.
Apparent lag time (lag)	Starting point of the S-curve, cells are adapting. Although cells are active, they do not start dividing during the lag phase. The length of the lag phase will also depend on the age and general viability of the cells in the inoculum.
Maximum OD (Max OD)	Maximum optical density (OD) at the end of the curve.

2.4 Partitioning Around Medoids (PAM) Method or K-medoids Clustering

To perform dimensionality reduction with the growth parameters obtained in Section 2.3 the following R (version 4.3.2) packages were used: Kassambara (2020) ("*factoextra*") and Maechler *et al.,* 2024 ("*cluster*"). First, the data was scaled using the function 'scale' for standardization. Then, the values were reorganized into a table format, with growth parameters, biological replicates and genes assigned as columns. Distances between these values were calculated using the function 'dist' for further clustering. The optimal number of clusters was determined by the within sum of squares (WSS) and Silhouette methods using the function 'fviz_nbclust' (methods "wss" and "silhouette"). The PAM or K-medoids algorithm was applied under the function 'pam', specifying the number of clusters. The function 'fviz_cluster' was used to visualize the results from the clustering.

2.5 Reverse transcription quantitative PCR (RT-qPCR) for parental and evolved strains

To quantify relative gene expression across bacterial passages, stocks generated in Section 2.2 were grown with or without 0.5% rhamnose as necessary. Cells from glycerol stocks (5 µL) were grown overnight in 5 mL of LB (trimethoprim 100 µg/mL) with or without 0.5% rhamnose at 37°C with shaking at 230 rpm. Specifically, parental strains were incubated without rhamnose, whereas evolved strains were incubated with rhamnose. Overnight cultures were diluted at an OD_{600nm}) of 0.01 and subcultured into fresh LB medium with trimethoprim (100 µg/mL), both in the presence of 0.5% rhamnose and in the absence of rhamnose. The absence of rhamnose served as non-inducing conditions for the comparative method (C_T). The subcultures were incubated until an OD_{600nm} of 0.7 was reached. Cells were pelleted by centrifugation (5 min at 4000g) and immediately used or stored at −80 °C until RNA extraction.

2.5.1 RNA extraction, purification and cDNA synthesis

RNA was extracted using the PureLink™ RNA Mini Kit (Invitrogen) with some modifications. Bacterial pellets were lysed in 100 µL of lysozyme (100 mg/mL in 10 mM Tris, 0.1

mM EDTA, pH 8.0). After adding 600 µL of lysis buffer with 1% β-mercaptoethanol, samples were mixed with an equal volume of 70% ethanol and vortexed. A 700 µL aliquot was loaded onto a spin column, centrifuged at 12,000 g for 15 seconds at room temperature, and the filtrate was discarded. This process was repeated twice. Subsequent washes with 700 µL Wash Buffer 1 and 500 µL Wash Buffer 2 were performed under the same centrifugation conditions. Finally, the RNA bound to the membrane was eluted in 30 µL RNase-free water, followed by incubation for 2 minutes. RNA purity (A260/280 ~2.0) was assessed by NanoDrop, and concentrations ≥150 ng/µL were used for cDNA synthesis. Samples were stored at −80°C or processed immediately for DNase treatment. To remove genomic contamination, treatment with DNase (ezDNAse™, Invitrogen) was performed at 37°C for 60 minutes. RNA integrity post-treatment was assessed by agarose gel electrophoresis (2% agarose) to confirm the absence of genomic DNA. Next, cDNA synthesis was performed using the SuperScript™ IV One-Step RT-PCR System (Invitrogen) with reaction volumes adjusted for 1600 ng of RNA in a 15 µL reaction.

2.5.2 Primer design and efficiency

Primers targeting the mid-region of coding sequences were designed with the following parameters: Tm between 58–62°C, GC content of 35–65%, and product sizes of 75–150 bp. Sequences of forward and reversed primers are listed in **Table 5.** Primer efficiencies (90–110%) were evaluated using standard curves, as recommended by Rocha *et al.,* 2020. Data was analyzed using the comparative C_T method. Genes were normalized to a reference or "housekeeping" gene, the RNA polymerase sigma factor *sigE* (K562_RS21810).

Table 5. List of designed and validated primers for RT-qPCR targeting essential genes in *Burkholderia cenocepacia* K56-2, linear regression analysis was performed to obtain primer efficiency and R^2.

Target Gene	Primer sequences (5'- 3')	Locus Tag	Efficiency (%)	R^2
atpB	Forward: CATGTGGAGCTTCGGTGG	K562_RS00155	94.90	0.997
	Reverse: CCGAGATACACCAGCGTCAG			

dnaN	Forward: CGTGACGTTGAAGCCGATG Reverse: GATCAGGAAGAGGCGCAGG	K562_RS02185	93.69	0.985
dcw cluster	Forward: GATCAGGAAGAGGCGCAGG Reverse: CGAGATGGACAAGTGCTTCCAG	K562_RS16765	97.03	0.996
gatB	Forward: GTCGGCCAGGAGAAGTTCG Reverse: CTTCGTAATTGATCGCTTCCTCG	K562_RS02510	100.34	0.995
gyrB	Forward: GAAGATGAACGACAAGCACG Reverse: CCTTGTAGCTGTTCTGGTCG	K562_RS02180	94.19	0.991
engA	Forward: GGAAACCTACAAGCGCTACC Reverse: CGGAACTCTATGCGCAATGG	K562_RS09275	96.52	0.989
ligA	Forward: GCTCGACTTCTTCCGCAAG Reverse: GTTGACCTTGTAGACGACGC	K562_RS08175	90.64	0.887
metG	Forward: GAAGGATCGGACAAGCTGC Reverse: GAAGGATCGGACAAGCTGC	K562_RS05945	108.43	0.943
parAB	Forward: CGCCTGCTCCGGAATTCAC Reverse: GATTCTCGAGACGCCACGC	K562_RS17180	90.07	0.982
parC	Forward: GCAGGCCGAGGACATTC Reverse: GAGTTCCTTCTCGATCTTGATC	K562_RS06290	100.90	0.972
trxB	Forward: CACATCCACACCGCGAAAC Reverse: CGAATCGCACGTGTACTCG	K562_RS14600	97.45	0.987

2.5.3 Statistical analysis

Statistical analysis of qPCR data was performed in R (version 4.3.2). To assess statistical differences in CT values between parental and evolved strains under dCas9-inducing conditions, Welch's t-tests and one-way analysis of variance (ANOVA) were conducted, followed by Tukey's Honestly Significant Difference (HSD) test on the significant results from the ANOVA tests to identify pairwise differences.

2.6 Illumina sequencing for encoded sgRNAs

The sgRNAs were sequenced using Illumina technology across all passages in both dCas9-inducing and non-inducing conditions. Glycerol stock samples (8 µL) from Section 2.2 were briefly thawed, and 2 µL of DMSO were added. Then, samples were treated at 95°C for 5 minutes in a thermocycler, followed by centrifugation for 4 minutes at 12,000g. From the mixture, a 2 µL sample was used for PCR amplification with different i5 and i7 primer combinations (sequences were obtained from Rahman *et al*., 2024). PCR amplification was confirmed by running a 2.5% agarose gel, resulting in a 201 bp product size. Samples with a positive amplification were pooled, and a PCR cleanup was performed using SeraMag beads (Cytiva) to remove unwanted DNA fragments. The final concentration of the pooled sample was adjusted to 20 ng/µL and sent for amplicon sequencing on a MiSeq v2 Nano platform (2x250 pair-end, output 1M clusters) at the Donnelly Centre, Toronto, Canada. Sequencing results in fastq.gz format were analyzed by pairwise comparison against the original sgRNA sequences using *Geneious* Software (Geneious Prime, version 8.1.9) (https://www.geneious.com).

2.7 Whole genome sequencing (WGS)

To identify genomic differences in CRISPRi mutants from Cluster 1, genomic DNA from selected strains was extracted using the PureLink™ Microbiome DNA Purification Kit (Invitrogen). Overnight cultures from glycerol stocks performed in Section 2.2 were briefly thawed, and a volume of 5 µL was inoculated in 5 mL of LB (trimethoprim 100 µg/mL) with and without 0.5% rhamnose for evolved and parental strains, respectively, at 37°C with shaking at 230

rpm. After incubation, cells were pelleted by centrifugation at 14,000g for 10 minutes, and the supernatant was discarded. The resulting pellet was resuspended in 800 µL of Lysis Buffer 1 and transferred to a bead tube, followed by adding 100 µL of Lysis Enhancer. Then, samples were incubated at 65°C for 10 minutes. Bead tubes were homogenized in a Bead Mill 24 Homogenizer (Fisherbrand™) at maximum speed for 10 minutes, followed by centrifugation at 14,000g for 2 minutes. A 500 µL from the supernatant was transferred to a clean tube, and 900 µL of binding buffer was added. Next, 700 µL were transferred to a spin column, and the sample was centrifuged at 14,000g for 1 minute. 500 µL of Wash Buffer was added and centrifuged for 1 minute at 14,000 g, followed by an additional 30-second centrifugation to dry the spin column containing ethanol. Subsequenctly, a 30 µL of elution buffer was added, followed by a 1-2 minute incubation at room temperature and centrifuged for 1 minute at 14,000 g to elute DNA. The concentrations were measured in a Qubit 2.0 Fluorometer. Finally, as requested by the sequencing company (Plasmidsaurus Inc., Louisville, Kentucky, United States), samples with a final concentration of 50 ng/µL in a 20 µL volume were performed and sent for Oxford Nanopore Sequencing (ONT). The raw data was received in fasta.gz format and used for further analysis.

2.7.1 Genome assembly and contig arrangement

De novo genome assembly from ONT raw sequencing data was performed using Flye 2.9.4 (Kolmogorov *et al*., 2019). The assembly process was configured with a minimum overlap of 1000 bp, utilizing 12 computational threads and performing up to 10 iterative rounds to refine the assembly. The resulting assembly consisted of 5 contigs with a minimum coverage of 150x. The fasta output file containing contigs was reordered manually in *Geneious* Software to ensure the same starting positions for both parental and evolved strains before pairwise comparison.

2.7.2 Synteny and Arragement Identifier (SyRI)

Pairwise genome comparisons were conducted using SyRI (Goel *et al*., 2019) to identify genomic differences, primarily single nucleotide polymorphisms (SNPs). Whole-genome alignments were performed using minimap2 and a minimum overlap of 1000 bp to ensure high-confidence alignments. The alignment output, in SAM format, was analyzed through SyRI and

produced several output files, including structural variants (sv.txt), syntenic regions (synout.txt), and SNPs (snps.txt).

2.7.3 Genome annotation using Prokka in Galaxy

To identify those genes affected by the mutations found using SyRI, annotation of assembled genomes was performed using Prokka (Seemann *et al.,* 2014). The analysis was conducted through the European Galaxy web server, which offers a user-friendly interface for running Prokka. Input genomes, whose contigs were arranged at the same starting positions in Section 2.7.1, were uploaded to Galaxy, where default Prokka parameters were used to predict coding sequences (CDS). The resulting annotations were saved in a GenBank file format and imported into *Geneious* software, where single SNPs between the parental and evolved strains were analyzed. Selected CDS were used as queries in BLASTn searches against the previously annotated wild-type genome from our laboratory (Bloodworth *et al.,* 2015, GenBank accession LAUA00000000), serving as a reference.

2.8 SDS-PAGE and Immunoblot to detect dCas9

Immunoblot assays were performed to observe changes in dCas9 protein abundance. A sample (5 μL) from glycerol stocks of corresponding strains was thawed and grown in 5 mL of LB (trimethoprim 100 μg/mL) at 37°C with shaking at 230 rpm. Purified dCas9, parental *gyrB* and evolved NTC mutants, were included as control. The cultures were diluted into 2 mL of fresh LB to an OD_{600nm} of 0.02 and grown until an OD_{600nm} of 0.7 was reached. Induction of dCas9 was performed by directly adding 0.5% rhamnose (50 μL from a 20% rhamnose stock) for 4 hours. The resulting cultures were centrifuged, and cell pellets were resuspended in TNG buffer (100 mM Tris-HCl, 150 mM NaCl, 10% glycerol, pH 7.4). Cell lysis was performed using sonication with three cycles of 5 seconds, resting in ice between cycles. Total proteins were separated by 8% SDS-PAGE in duplicate. One SDS-PAGE gel was transferred to a polyvinylidene fluoride (PVDF) membrane using the iBlot system and blocked in 5% skim milk-TBST. Then, dCas9 was detected using a primary mouse monoclonal antibody (ThermoFisher 10C11A12) at room temperature for one hour, followed by three washes in TBST buffer (150 mM NaCl, 10 mM Tris-HCl, 0.5% Tween

20, pH 7.5). Then, a secondary goat anti-mouse antibody (ThermoFisher G-21060), linked to alkaline phosphatase, was added at a 1:20,000 dilution for 1 hour, followed by three washes in TBST buffer. Protein detection was done by chemiluminescence using a detection solution (5-bromo-4-chloro-3-indoyl phosphate [BCIP] in 1M Tris-HCl pH 9.5, 1M $MgCl_2$, 2.5M NaCl). Results were visualized after 30 minutes.

CHAPTER 3: RESULTS

The goal of this work was to characterize growth inhibition phenotypes during repression of essential functions with CRISPRi. To that end, we decided to characterize CRISPRi essential gene mutants targeting different functions from the Cluster of Orthologous Genes (COG) categories. Subsequently, by performing a short-term experimental evolution assay, we aimed to elucidate the stability of CRISPRi in knocking down essential genes across three bacterial passages under dCas9-inducing conditions. Then, we aimed to identify trends in conditional growth phenotypes (CGP) and their relationship to gene expression through RT-qPCR. Lastly, to analyze phenotypic variations, we employed whole genome sequencing (WGS), intending to uncover genomic differences and examine the mechanisms conferring changes in CGPs.

3.1 Conditional growth phenotypes (CGPs) are diverse across CRISPRi essential gene mutants and are COG-independent

Our first objective was to repress essential genes using a rhamnose-inducible CRISPRi system (Hogan *et al.,* 2019) from a CRISPRi essential gene mutant library in *Burkholderia cenocepacia* K56-2 (Rahman *et al*., 2024). We selected fifteen CRISPRi mutants, targeting essential genes across different COG categories, such as those involved in cell division (COG D), cell envelope biogenesis (COG M), DNA replication and repair (COG L), energy production (COG C), translation (COG J) and nucleotide conversion and metabolism (COG F) (See **Table 3**). These genes were defined as essential in *Burkholderia cenocepacia* K56-2 (Gislason *et al*., 2017), as they were found to encode essential products required for survival.

To characterize the CGP of CRISPRi mutants, a catalytically inactive or "dead" Cas9 can be expressed in a rhamnose-dependent manner. It is placed under a rhamnose-inducible promoter, allowing tunable expression. A concentration of 0.5% rhamnose was selected to induce dCas9 expression since it was demonstrated to be the maximum tolerated by CRISPRi mutants; higher concentrations were shown to be lethal (Hogan *et al.,* 2019). Without rhamnose, there is no dCas9 expression, allowing regular gene expression; however, a synthetic guide RNA (sgRNA) is always constitutively expressed from a plasmid containing a trimethoprim resistance cassette for selection.

Growth curves were performed for 24 hours under dCas9-inducing (0.5% rhamnose) and non-inducing (0% rhamnose) conditions to assess the CGP. In parallel with the 15 CRISPRi mutants and their respective non-inducing controls, a CRISPRi non-targeting control (NTC) mutant was included. This mutant consists of a sgRNA that does not target any gene in the genome. Therefore, its phenotype exhibits similar wild-type (WT) growth levels.

CRISPRi mutants targeting genes from the same COG category differ in their CGP, suggesting that despite encoding essential products within the same category, their CGP is considerably diverse (**Figure 5)**. Therefore, the CGPs were independent from their COG category. We observed a spectrum of growth defects among mutants, ranging from severe, medium and mild, based on their extended lag time compared to non-inducing controls. These results demonstrated that knocking down essential genes related to the same functional category exhibit CGPs according to specific functions, degrees of essentiality or strength of gene silencing (Dilucca *et al*., 2018; Hogan & Cardona, 2022). Growth in all mutants tended to reach WT levels after 20 hours under dCas9-inducing conditions, suggesting that the CGP could be alleviated.

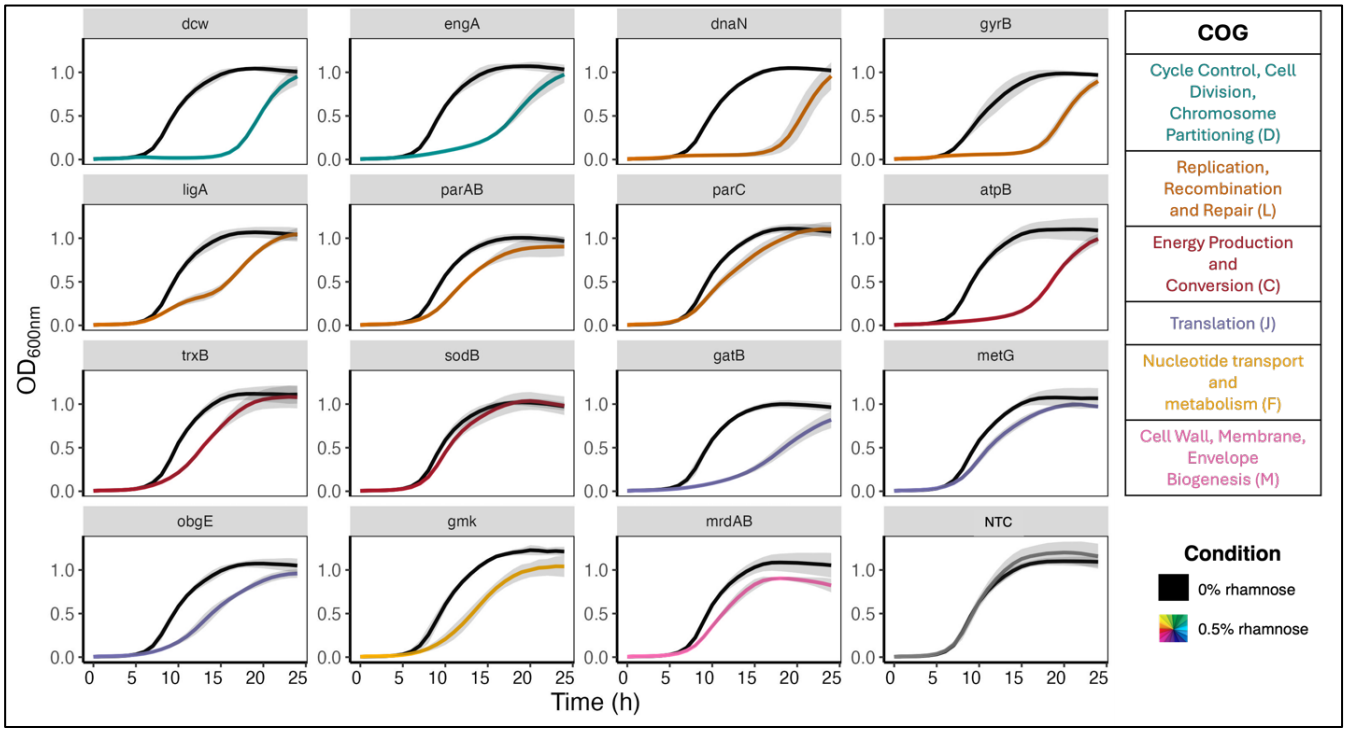

Figure 5. Conditional growth phenotype assessment of CRISPRi essential gene mutants.

Growth curves of CRISPRi mutants under dCas9-inducing conditions (0.5% rhamnose) and non-inducing conditions (0% rhamnose) are shown in different colours or in black. Each colour represents a different COG. CRISPRi mutants were grown overnight and back diluted to an OD_{600nm} 0.005 as a starting inoculum. Growth curves were performed in LB (trimethoprim 100 µg/mL) with and without rhamnose for 24 hours. Shaded areas indicate the standard deviation (arithmetic mean ± SD) from three independent biological replicates. NTC stands for "non-targeting control" mutant, serving as the negative control for this assay.

3.2 Short-term evolution experiment reveals CGP loss at different bacterial passages

To further explore the loss of the CGP in the CRISPRi mutants, We next characterized their growth phenotypes over time under consecutive dCas9-inducing and non-inducing conditions. An outline of the short-term evolution experiment is shown in **Figure 6**. The procedure consisted of three bacterial passages that originated from a common ancestor or parental strain grown without rhamnose and later exposed to dCas9-inducing (0.5% rhamnose) and non-inducing conditions during microbial growth curves reflecting their initial CGP, as characterized previously. The parental strains were further subcultured under dCas9-inducing and non-inducing conditions overnight. Consequently, after the overnight period (~16 hours), cultures from each passage were frozen at -80°C to preserve their genetic material for further analysis, and microbial growth curves were performed again to assess for the CGP after consistent selective pressure. A starting inoculum of OD_{600nm} 0.005 was selected for all microbial growth curves, with readings taken in 1-hour intervals. It was expected to observe changes in the CGP from those bacterial cultures from consistent dCas9-inducing conditions overnight (0.5% rhamnose). The experiment was conducted in three independent evolution replicates for each CRISPRi mutant, with two technical replicates throughout all bacterial passages.

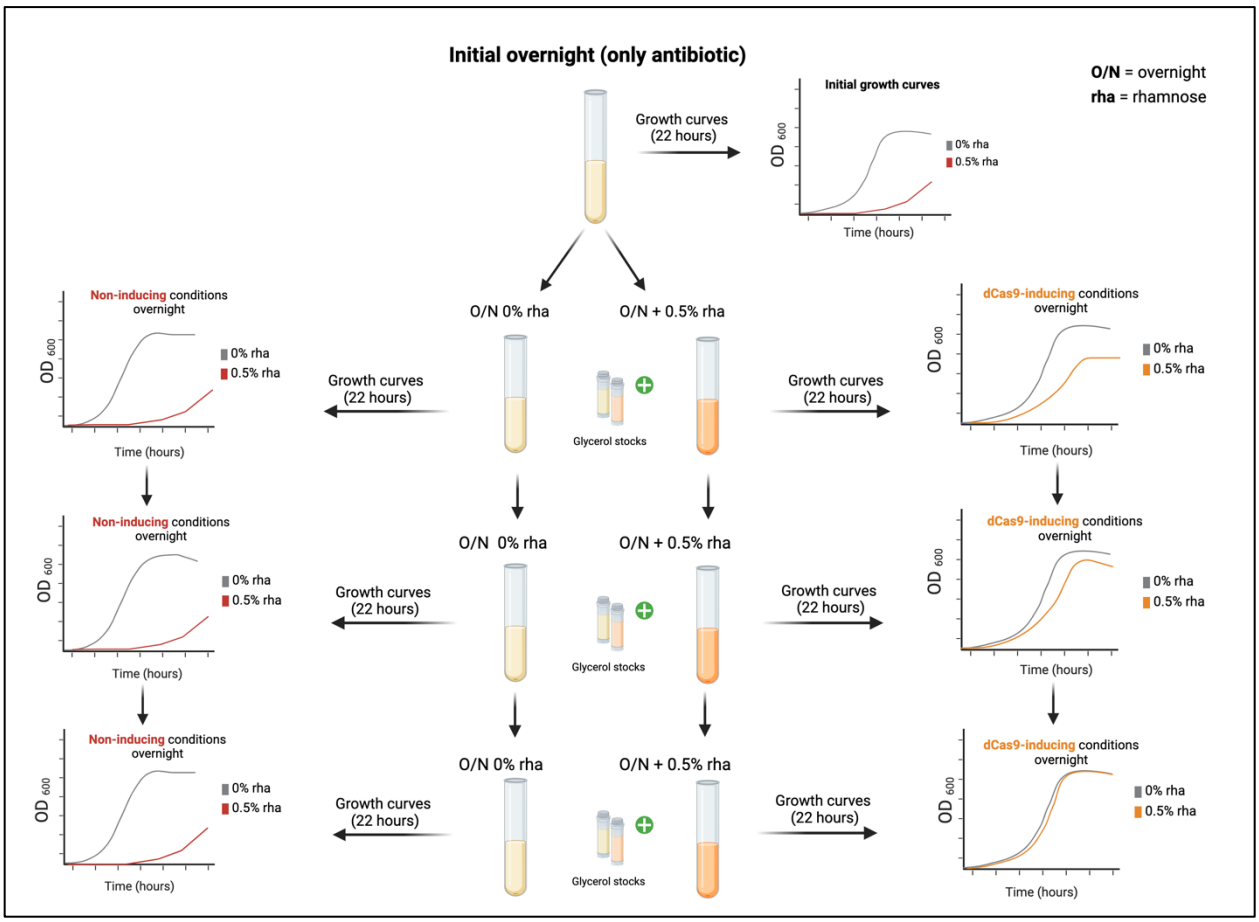

Figure 6. Short-term experimental evolution assay in CRISPRi essential gene mutants.

Workflow illustrating the steps to categorize the conditional growth phenotype (CGP) after three bacterial passages. The design consisted of a parental strain under non-inducing conditions followed by microbial growth curves under dCas9-inducing and non-inducing conditions. Next, a subculture under dCas9-inducing and non-inducing conditions was performed. After the overnight period (~16 hours), a sample of the subculture was immediately stored at -80°C as glycerol stocks. Then, these were thawed and used as inocula for the subsequent passages. This process was repeated over three passages. On the right, the final outcome is depicted: in the first column, growth curves show a maintained CGP under dCas9-inducing conditions due to non-exposure to rhamnose overnight, whereas, in the second column, growth curves illustrate a gradual CGP loss due to consistent dCas9-inducing conditions across bacterial passages. For consistency, an initial inoculum of OD_{600nm} 0.005 was used for all growth curves in the assay with three independent evolution replicates for each CRISPRi mutant.

A gradual loss of CGPs has been observed under intense selective pressure, such as antibiotic exposure or environmental stress (Zorraquino *et al*., 2016; Crow *et al*., preprint). However, the loss of CGP was not gradual in all the CRISPRi mutants (**Figure 7),** as six mutants completely lost the CGP after one passage **(Figures 7A, S2, S3, S4, S5 and S9)**. From the mutants that lost the CGP gradually, six mutants reverted to WT growth after two passages (**Figure 7B, S6, S7, S8, S10 and S11**), and three mutants after three passages (**Figure 7C, S12 and S13**). These events occurred across the three independent biological replicates. Furthermore, we observed the loss of the CGP across the three independently evolved replicates. Additionally, all CRISPRi mutants grown overnight under non-inducing conditions and later exposed to rhamnose to induce dCas9 expression showed a CGP across all passages (**Figures 8 and S2-S13**).

The NTC mutant (negative control) preserved its phenotype throughout all passages (**Figure 9**). As stated before, we found the CGP to be COG-independent, and similarly, in this assay, there was no correlation between the timing of CGP loss and the COG category. Interestingly, we observed a link between growth defects and CGP loss; thus, mutants exhibiting a severe growth defect or extended lag phase compared to the control lost the CGP and restored WT growth levels after one passage under dCas9-inducing conditions. In contrast, those with medium and mild growth defects lost the CGP after two and three passages, respectively. The media conditions and supplements, including the rhamnose stock, were identical for all experiments and passages. Therefore, variability in CGP loss cannot be attributed to media composition or preparation. Together, the different degrees of essential gene dispensability and essential protein function may create different selective pressures (Lluch-Senar *et al*., 2015; Fuentes *et al*., 2021) that contribute to differences in the timing at which the CGP is lost. Moreover, the specific placement of the dCas9 on the target region interferes with transcription initiation or elongation, leading to different levels of gene repression and, thereby, resulting in a diversity of growth defects. Thus, the sgRNA target region and the PAM are crucial elements that influence these events.

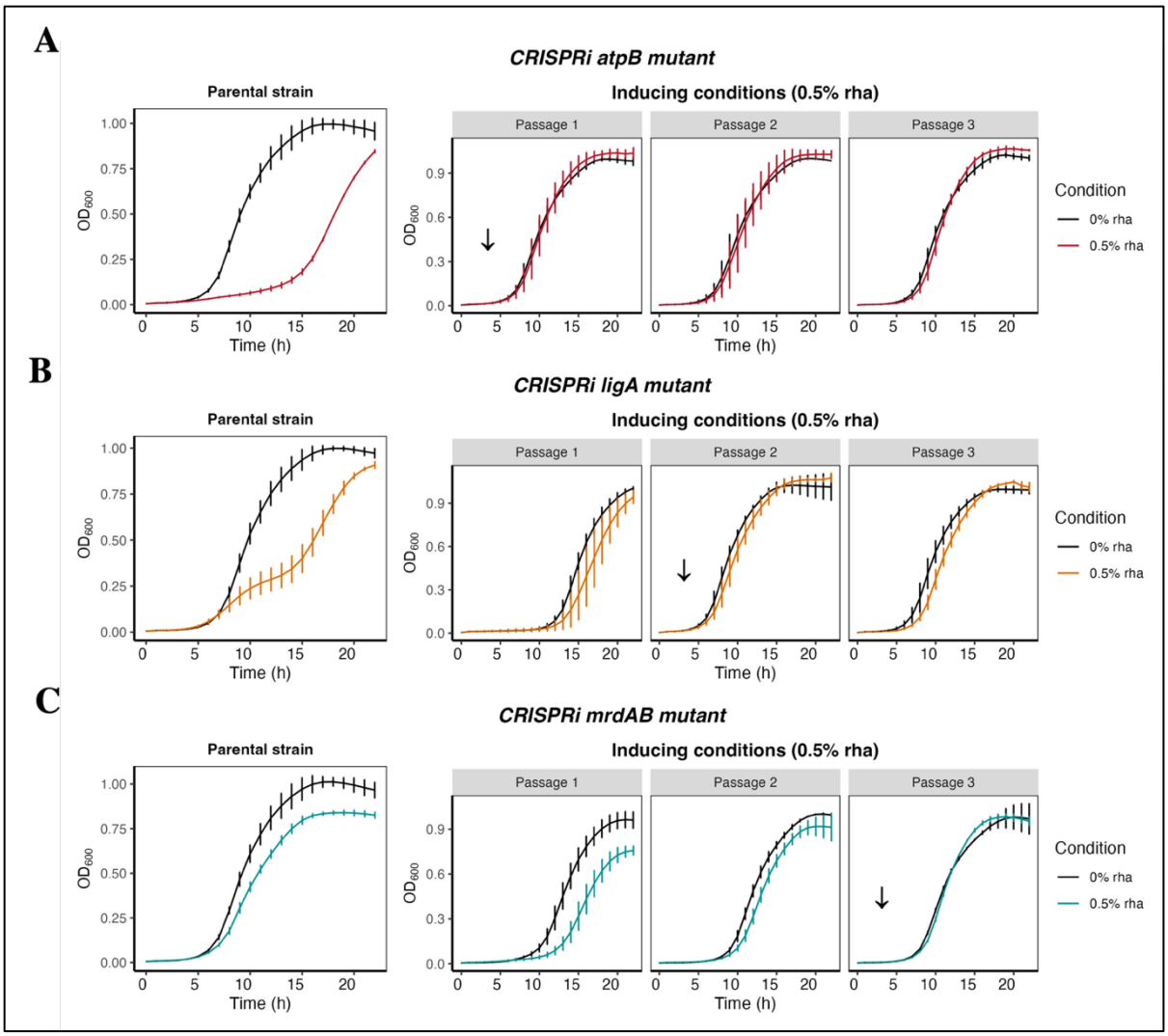

Figure 7. CGP loss after one, two, and three bacterial passages in CRISPRi mutants.

(A) Growth curves of a CRISPRi *atpB* mutant under dCas9-inducing conditions overnight show the loss of the CGP after one bacterial passage; the parental strain shows a severe CGP based on the apparent lag time. (B) Growth curves of a CRISPRi *ligA* mutant under dCas9-inducing conditions overnight indicate the loss of the CGP after two bacterial passages; the parental strain shows a medium CGP based on the apparent lag time. (C) Growth curves of a CRISPRi *mrdAB* mutant under dCas9-inducing conditions overnight demonstrate the loss of the CGP after three bacterial passages; the parental strain shows a mild CGP based on the apparent lag time. A black arrow above each panel indicates the bacterial passage at which the CGP is lost. The values represent the mean of three biological replicates; error bars indicate the standard deviation (± SD). An initial inoculum of OD_{600nm} 0.005 was used for all microbial growth curves in this assay.

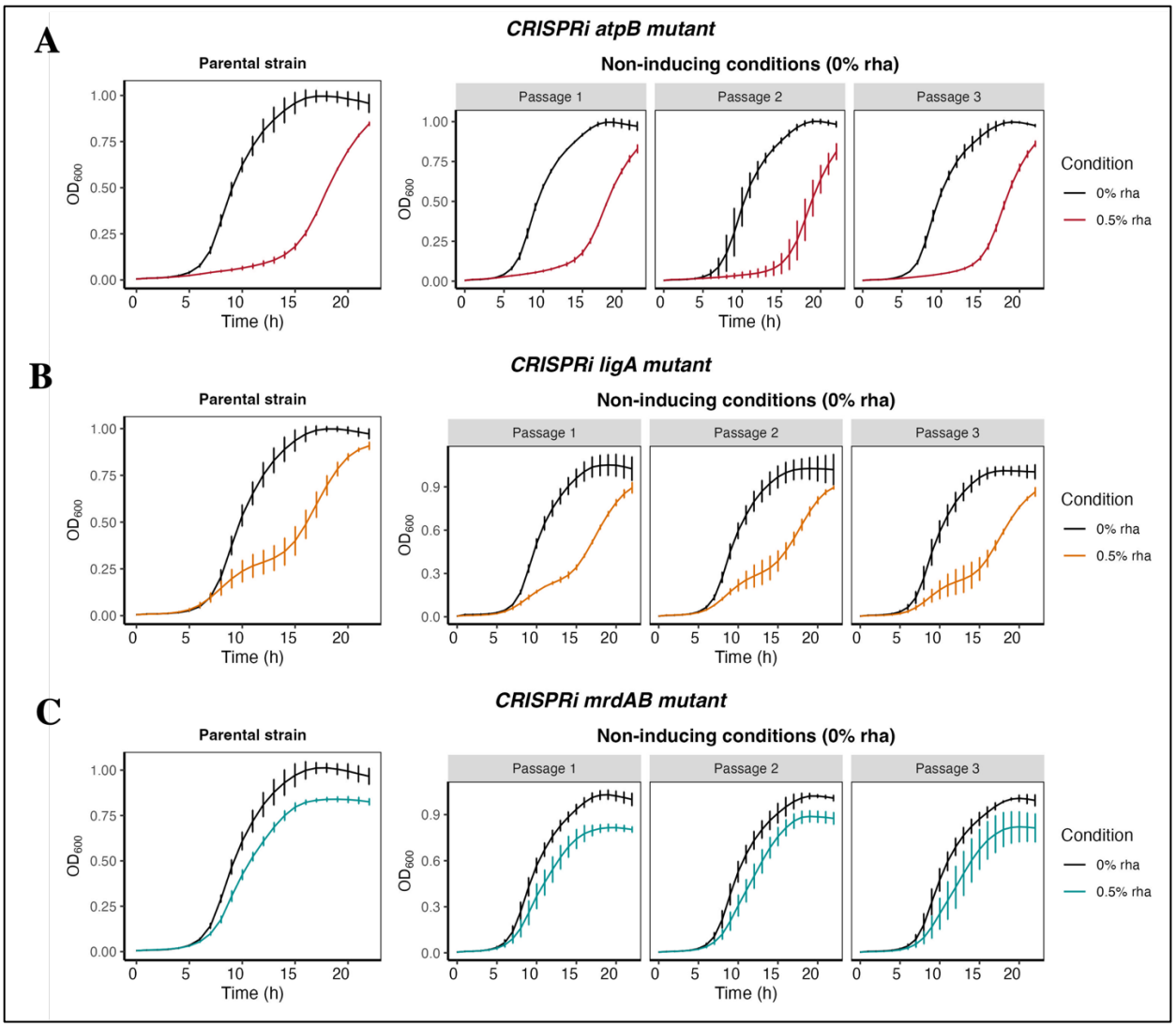

Figure 8. Maintenance of CGP across bacterial passages in CRISPRi mutants under non-inducing conditions.

(A–C) Growth curves of CRISPRi *atpB*, *ligA*, and *mrdAB* mutants show a consistent CGP across all bacterial passages when subcultured under non-inducing conditions and later exposure to rhamnose during microbial growth curves. No CGP loss is detected at any passage. The values represent the mean of three biological replicates; error bars indicate the standard deviation (± SD). An initial inoculum of OD_{600nm} 0.005 was used for all microbial growth curves in the assay.

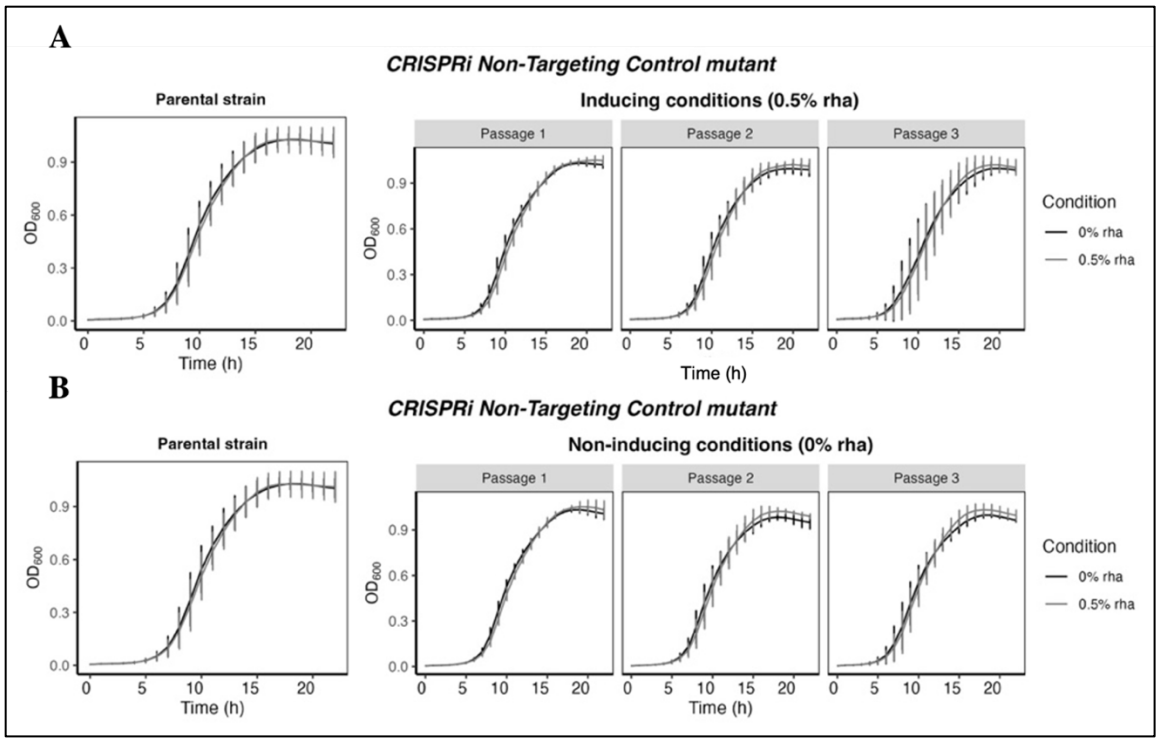

Figure 9. CRISPRi Non-Targeting Control (NTC) mutant preserves a wild-type phenotype throughout dCas9-inducing and non-inducing conditions.

(A) Growth curves under dCas9-inducing and (B) non-inducing conditions overnight; no growth defect was observed across all bacterial passages. The values represent the mean of three biological replicates, and error bars indicate the standard deviation (± SD). An initial inoculum of OD_{600nm} 0.005 was used for all microbial growth curves in the assay.

3.3 K-medoids (PAM algorithm) reveals distinct clusters based on growth curve parameters

To quantify the observed differences in the CRISPRi mutant growth curves, we calculated growth parameters using the R package "*growthcurver*" (Sprouffske & Wagner, 2016), which transforms raw optical density measurements into a logarithmic scale and fits these values into an exponential growth model. Different growth parameters were calculated (**Table 4**) from the transformed data applying the logistic equation used in experimental evolution studies (Novak *et al*., 2009; Leiby & Marx, 2014; Fuentes *et al*., 2021):

$$N_t = \frac{K}{1 + \left(\frac{K - N_0}{N_0}\right) e^{-rt}}$$

N*t* = Number of cells at time *t*

N_0 = Population size at the beginning of the growth curve

K = Carrying capacity or population size in a certain environment

r = Population growth rate

t = Time

These growth parameters were further used to cluster the CRISPRi mutant CGPs. For this analysis, a nonparametric clustering algorithm was chosen. Specifically, K-medoids or Partitioning Around Medoids (PAM) algorithm. This algorithm selects specific points from the dataset, called medoids, as reference points and assigns each data point to the nearest medoid, grouping the data based on similarity (Kaufman & Rousseeuw, 2009; Gu *et al*., 2022). The optimal number of clusters was found by applying two methods: the Within Sum of Squares (WSS) or Elbow Method and the Silhouette Method.

The WSS or Elbow method, calculates how closely data points fit around each medoid by measuring the squared distance between each point and its medoid. As the number of clusters increases, WSS generally decreases, showing a better fit (Handl *et al*., 2005). The value where a

sudden drop in WSS is observed, forming an "elbow" in the graph, is considered the optimal number of clusters. In contrast, the Silhouette method evaluates the cohesion and separation of the clusters to their medoid, specifically, how well-separated the clusters are from each other, by calculating how close points are within their own cluster versus how far they are from points in other clusters (Modak *et al*., 2020). The average silhouette score across all points indicates the best cluster number, with higher values showing better-defined clusters (Lengyel & Botta-Dukát, 2019). By applying both methods, using the R package "*factoextra*", we found that the optimal number of clusters for our dataset was three (**Figure 10**).

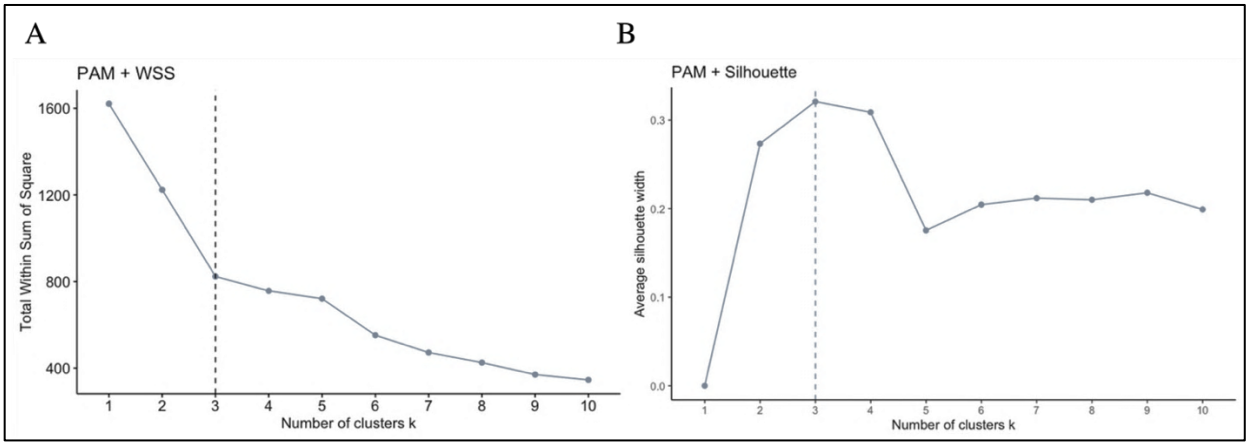

Figure 10. Determination of the optimal number of clusters using WSS (Elbow) and Silhouette methods.

(A) The Within Sum of Squares (WSS) plot, shows the "elbow" point suggesting three as the optimal number of clusters, indicated by the sharp decrease in WSS. (B) The Silhouette method displays the average silhouette width for different numbers of clusters, with the highest score observed at three clusters. Both methods identify three clusters as the best fit for the data.

Once the number of clusters was obtained, we scaled the data to obtain an equal distribution of values. Then, the data was clustered using the PAM algorithm previously described using the R package "*cluster*" under the function *pam*. We obtained three clusters with the following distribution:

- Cluster 1: Five CRISPRi mutants (*atpB, dnaN, gatB, gyrB* and *dcw)*
- Cluster 2: Two CRISPRi mutants (*ligA* and *engA*)
- Cluster 3: Eight CRISPRi mutants (*parAB, parC, metG, obgE, trxB, gmk, sodB* and *mrdAB)* plus the NTC mutant.

The resulting clusters were then visualized in two dimensions, Dim1 (Dimension 1) and Dim2 (Dimension 2), which represent the reduced projection of the data on the x-axis and y-axis, respectively. These dimensions capture the overall structure of the data, with each axis representing a combination of the growth parameters that most effectively separate the clusters. In the plot, the sum of Dim1 and Dim2 explains the combined variance, with 50.9% of the total variance captured by the growth parameters as variables. Each mutant is presented with three data points, illustrating the three biological replicates from the short-term experimental evolution assays. Each point reflects a unique interaction for each mutant, derived from the combined growth parameters measured and scaled across passages. Thus, the data points enable a thorough comparison across replicates (**Figure 11**).

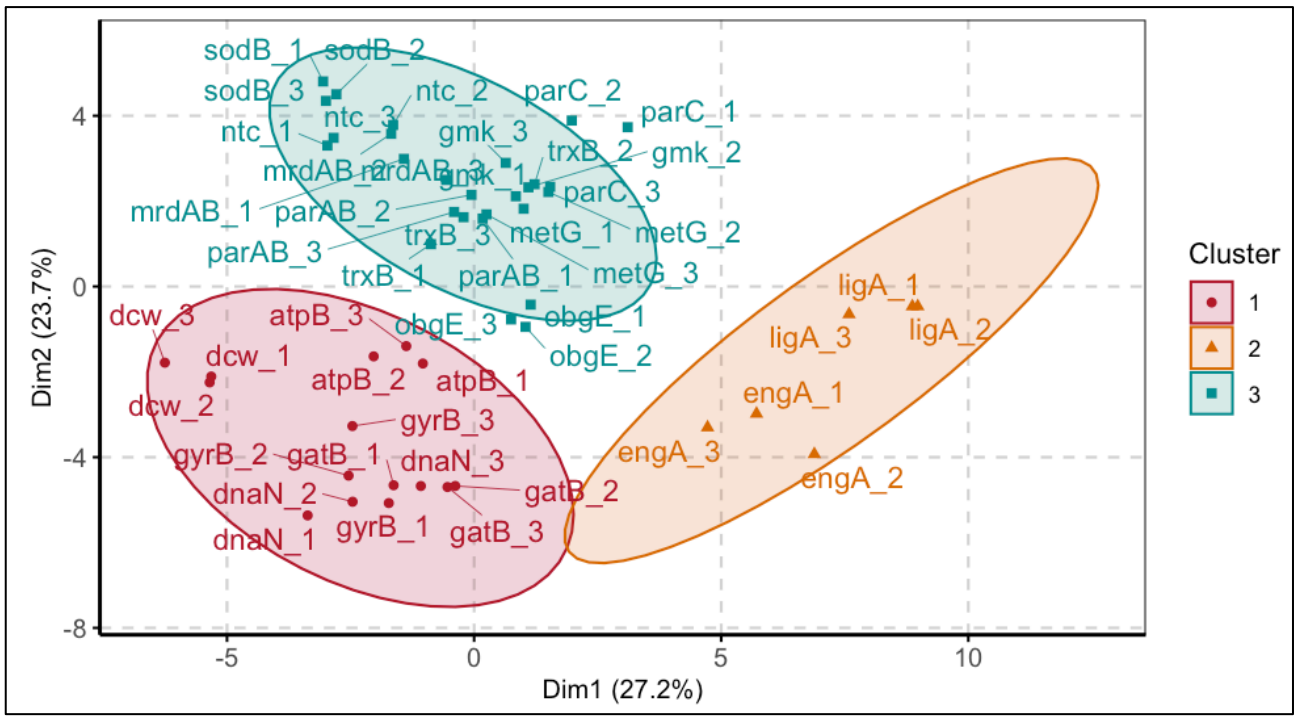

Figure 11. K-medoids (PAM) clustering of CRISPRi mutants reveals three clusters.

Cluster 1 (red dots) contains five CRISPRi mutants (*atpB, dnaN, gatB, gyrB, and dcw*), Cluster 2 (orange triangles) contains two CRISPRi mutants (*ligA* and *engA*), and Cluster 3 (cyan squares) contains eight CRISPRi mutants (*parAB, parC, metG, obgE, trxB, gmk, sodB,* and *mrdAB*) plus the NTC mutant. Dimension 1 on the x-axis captures 27.2% of the overall variance, while Dimension 2 on the y-axis captures 23.7%, explaining 50.9% of the total variance in the dataset. Each mutant is represented by three data points, reflecting values from three independent biological replicates obtained from the short-term experimental evolution assay. Each point reflects a unique interaction for each mutant, derived from the combined growth parameters as variables and scaled across bacterial passages. Each independent evolution replicate is represented as _1, _2 and _3.

To visualize the CGPs and observe trends in growth and essential gene knockdown across bacterial passages, growth curves from dCas9-inducing and non-inducing conditions were analyzed by cluster. The clustering revealed three main trends: Cluster 1 mutants exhibited a prolonged apparent lag time, lower optical density (OD) values at the end of the growth curves and CGP loss after one passage under consistent dCas9-inducing conditions. Cluster 2 mutants displayed a prolonged apparent lag time after one passage under consistent dCas9-inducing conditions and CGP loss after two passages. In contrast, Cluster 3 mutants showed milder CGPs and different CGP loss timing under consistent dCas9-inducing conditions. Under consistent non-inducing conditions, all mutants exhibited similar wild-type growth levels, as represented by the NTC mutant (**Figure 12**).

Overall, the clustering trends partially coincided with the phenotypic data from the short-term evolution experiment, with Cluster 1 showing the strongest correlation between CGP loss timing and growth defects. In contrast, Clusters 2 and 3 displayed less consistent patterns with the phenotypic data, suggesting additional variability within these groups. These results provided evidence of CGP loss under consecutive selective pressure.

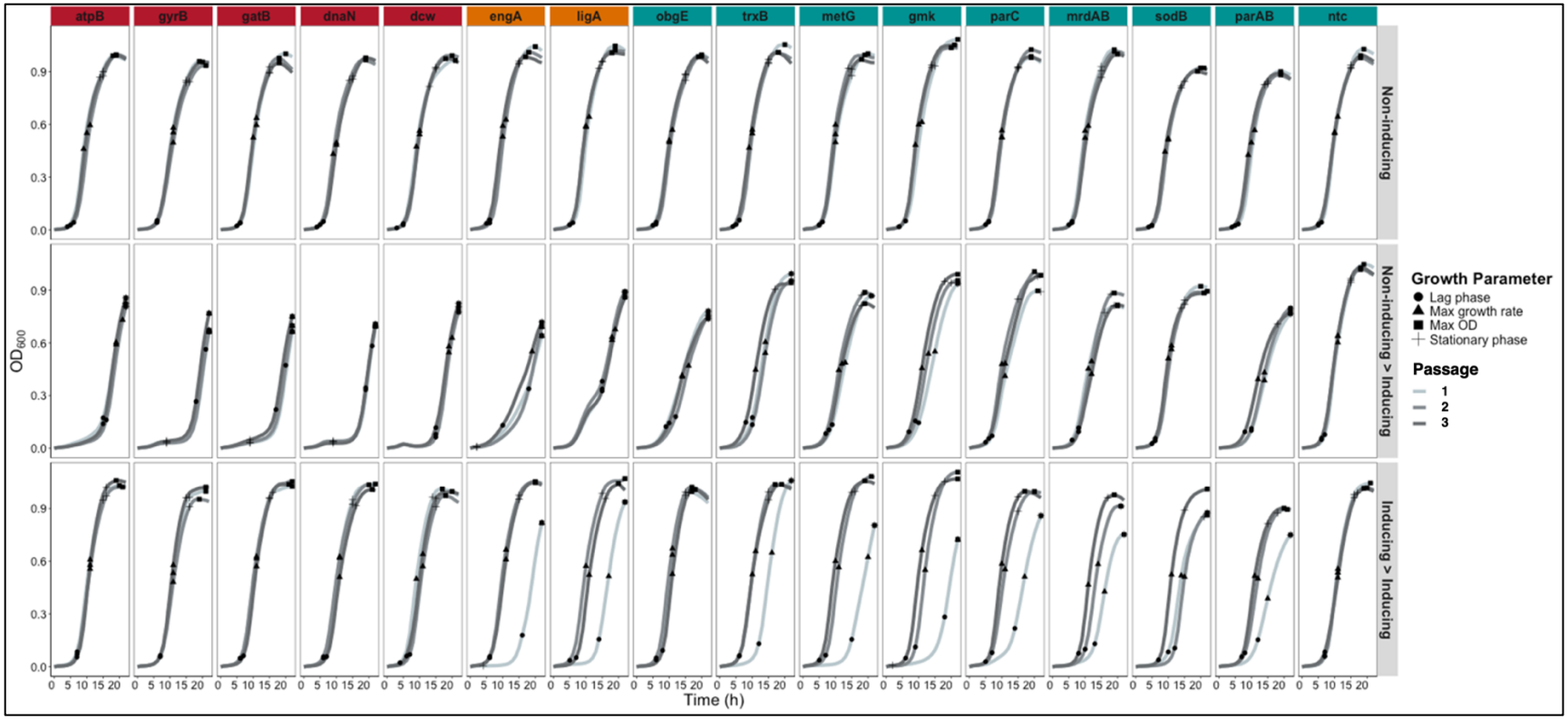

Figure 12. CRISPRi mutants distributed by cluster across bacterial passages under dCas9-inducing and non-inducing conditions.

From left to right, the CRISPRi mutants are presented by the representative cluster color. The passages are represented on a grey scale (lighter to darker) from passages one to three. The first row exhibits consistent non-inducing conditions overnight and during microbial growth curves (Non-inducing) without growth defects detected across bacterial passages. The second row exhibits consistent non-inducing conditions overnight followed by the addition of rhamnose during microbial growth curves (Non-inducing > Inducing); growth defect characteristics for each cluster are observed, ranging from severe (Cluster 1), to medium (Cluster 2), and mild (Cluster 3). The third row exhibits consistent dCas9-inducing conditions overnight and during microbial growth curves (Inducing > Inducing); CGP loss is observed after one, two or three bacterial passages for each cluster. Different symbols represent a growth parameter indicated in each growth curve across passages and conditions.

3.4 RT-qPCR reveals loss of CRISPRi-mediated repression of target genes across bacterial passages

Based on previous evidence of mutations in the sgRNA and dCas9 sequences (Zhao *et al*., 2016; Liu *et al*., 2017), we investigated whether the loss of the CGP was due to alleviation of the CRISPRi-based essential gene silencing. We quantified essential gene expression in knockdown mutants using reverse-transcription quantitative polymerase chain reaction (RT-qPCR under both dCas9-inducing and non-inducing conditions to assess changes in gene expression across bacterial passages. Given its sensitivity and accuracy, RT-qPCR has become the gold standard for quantifying and analyzing the amount of messenger RNA (mRNA) actively expressed in bacterial cells (Bengtsson *et al*., 2008; Rocha *et al*., 2020). The results from this assay can be relative or absolute, where the first uses a reference target to determine the relative quantification when normalized to a reference gene, whereas the second one uses a standard curve to compare the performance (Svec *et al*., 2015).

First, RNA was extracted from a bacterial subculture when an OD_{600nm} 0.7 was reached and converted to complementary DNA (cDNA) by reverse transcription for further quantification, as the cDNA formed serves as the template to be quantified by PCR. This reaction consists of cDNA with specific primers to be amplified and a fluorescent dye that binds to new double-stranded DNA formed (when cDNA is amplified). Finally, the fluorescence emitted is proportional to the amount of DNA present (Kubista *et al*., 2006; Gao *et al*., 2011). This happens exponentially, doubling with each amplification cycle. Finally, this logarithmic value is converted to a linear scale to calculate the relative expression against an internal control (Derveaux *et al*., 2010).

Relative quantification, or comparative C_T, was employed based on previous studies measuring gene expression in *Burkholderia cenocepacia* (Hogan *et al*., 2019). "C_T" stands for cycle threshold and is determined when the fluorescent signal from the PCR cycle crosses a certain threshold (Schmittgen & Livak, 2008). This comparative method, or $2^{-\Delta\Delta Ct}$, uses an internal control gene often known as "housekeeping", and the targets are normalized against it. Therefore, the analysis results are relative to the control, and the data can be reported in gene expression "fold-

change" (Schmittgen & Livak, 2008). The equation for generating this relative output is as follows: (Equation modified from Schmittgen & Livak, 2008)

$$2^{-\Delta\Delta Ct}(Fold\ change) = [(Ct\ target\ gene - Ct\ internal\ control)\ Sample\ A - (Ct\ target\ gene - Ct\ internal\ control)\ \text{Sample B}]$$

Sample A: dCas9-inducing conditions
Sample B: Non-inducing conditions

We included the sigma factor (σ) as an internal control (K562_RS21810) from previous research (Hogan *et al.,* 2019). This factor is conserved among bacteria, and its function is to recognize promoter regions in association with an RNA polymerase, resulting in effective transcription (Bervoets & Charlier, 2019).

Validation of RT-qPCR primers was performed to achieve an efficiency higher than 90% (See **Table 5**). This efficiency refers to the performance of the primers to amplify the target with high specificity. It is usually determined by a standard curve, performing serial dilutions of cDNA followed by a dispersion plot and linear regression analysis, where values between 0.85-1.1 (90-110%) are considered optimal efficiency (González-Bermúdez *et al*., 2019; Rocha *et al*., 2020).

We performed RT-qPCR for 11 CRISPRi mutants, all from Clusters 1 and 2, and four representative mutants from Cluster 3. We measured relative expression throughout the passages when CGP loss was observed. Specifically, for Cluster 1 mutants, we compared gene expression between the parental strain and passage one, as these mutants lost the CGP after one passage. For Cluster 2, we performed RT-qPCR on the parental strain, passage one, and passage two to track changes in gene expression as CGP loss occurred between passages one and two. For Cluster 3, we compared gene expression from the parental strain to passages one, two, and three to correlate CGP loss with gene expression changes over multiple passages. This aimed to observe a correlation between CGP loss and the restoration of gene expression levels.

3.4.1 CRISPRi mutants from Cluster 1 show restoration of gene expression after one passage under dCas9-inducing conditions

We analyzed changes in target gene expression in parental and evolved CRISPRi mutants. Four parental mutant strains from Cluster 1 exhibited between 41-fold and 78-fold reduction in target gene repression in dCas9-inducing conditions, compared to non-inducing conditions. However, the parental CRISPRi mutant *dcw* observed only 4.4-fold reduction in target gene repression. The CRISPRi *dcw* cluster mutant, which stands for "*division and cell wall*", contains 15 genes responsible for peptidoglycan synthesis and cell division. Here, we quantified the expression of *ftsZ*, the last gene in this operon. The product encoded by this gene is involved in cell division and is the primary protein responsible for locating the center of the cell, where it interacts with other proteins to form a molecular scaffold, facilitating cell septation (Mingorance *et al*., 2004; Trespidi *et al*., 2020). Gene silencing with CRISPRi has a polar effect in that it reduces the expression of all essential genes in an operon when targeting the promoter region (Peters *et al*., 2015, 2016). We quantified *ftsZ* expression, the last gene of the *dcw* operon in *B. cenocepacia* K56-2 and observed mild gene repression. Nonetheless, this mutant exhibited a severe CGP, suggesting that cumulative repression of the 15 genes in this operon contributes to the observed growth defect.

Evolved CRISPRi mutants from Cluster 1 revealed increased target gene expression after one passage under dCas9-inducing conditions, compared to non-inducing conditions. Specifically, gene expression of the CRISPRi *dnaN* mutant changed from 78-fold repression to 3-fold repression (**Figure 13A**); gene expression of the CRISPRi *gyrB* mutant went from 67-fold to 1-fold (**Figure 13B**); gene expression in the CRISPRi *atpB* mutant changed from 55-fold to 9-fold (**Figure 13C**); gene expression in the CRISPRi *gatB* mutant went from 41-fold to 0.9-fold (**Figure 13D**), and gene expression in the CRISPRi *dcw* cluster mutant changed from 4.4-fold to 1-fold (**Figure 13E**). We performed a Welch's t-test to compare parental strains against passage one under dCas9-inducing conditions, assuming unequal variances. The analysis revealed all mutants exhibited statistically significant differences in gene expression levels when compared to the parental strain (*atpB*, $p < 0.05$; *dnaN*, $p < 0.01$; *dcw*, $p < 0.01$; *gatB*, $p < 0.01$; *gyrB*, $p < 0.001$) (**Table 6).** These results indicated a correlation between CGP loss and decreased target gene expression in CRISPRi

mutants from cluster 1, suggesting that growth may be restored due to decreased CRISPRi-mediated target gene repression.

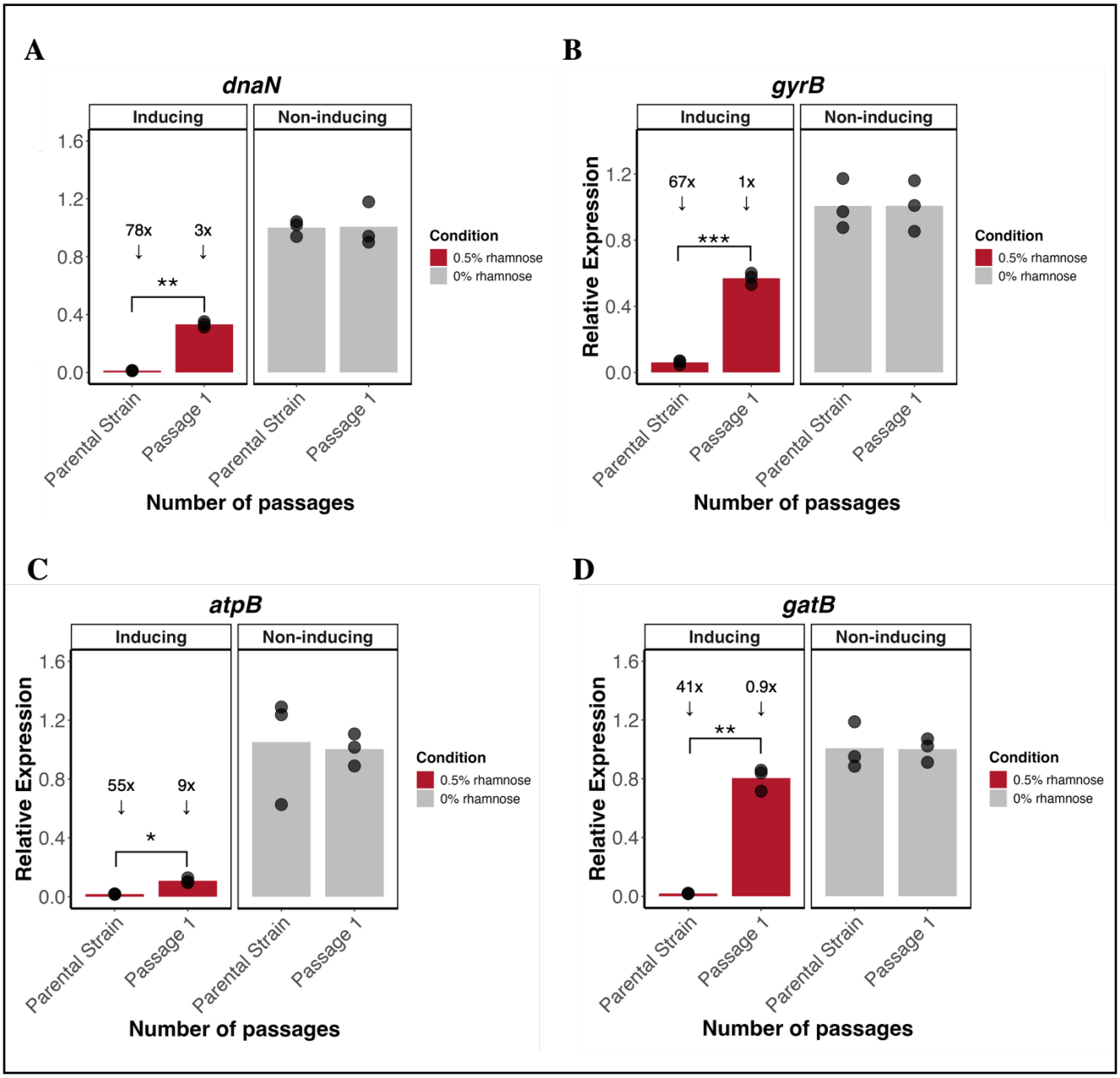

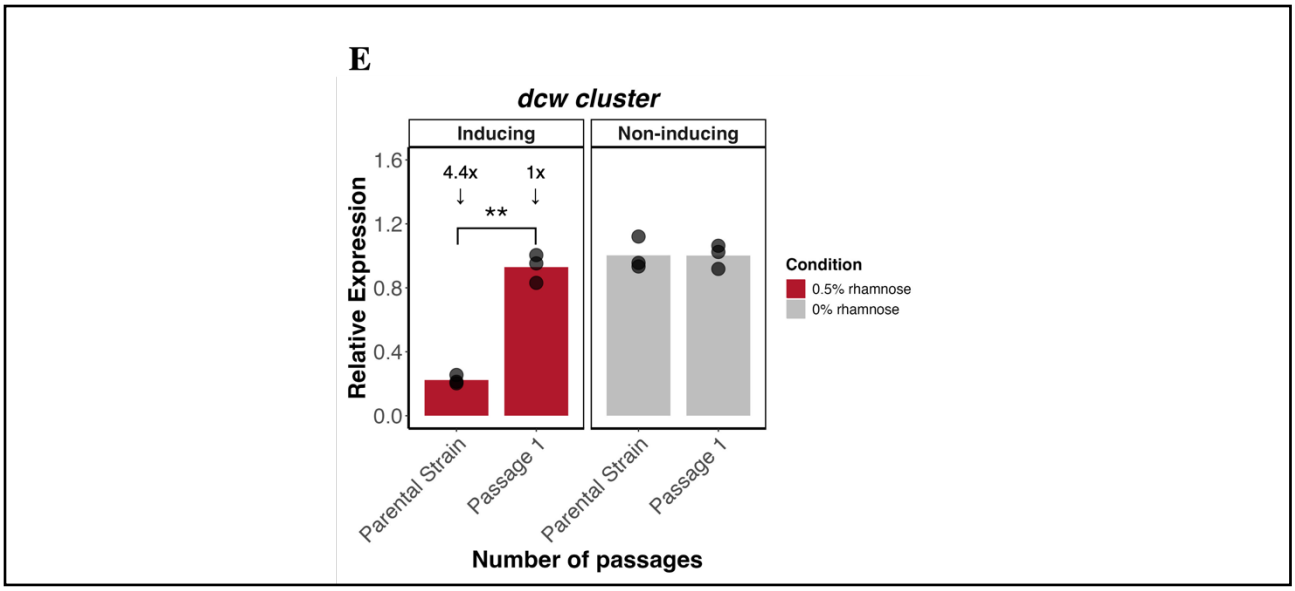

Figure 13. Relative gene expression levels in CRISPRi mutants from Cluster 1.

(A) Gene expression in the CRISPRi *dnaN* mutant exhibits a 78-fold in gene repression, dropping to 3-fold after one bacterial passage under dCas9-inducing conditions. (B) The CRISPRi *gyrB* mutant reveals gene repression of 67-fold, dropping to 1-fold after one passage under dCas9-inducing conditions. (C) The CRISPRi *atpB* mutant exhibits gene repression of 55-fold, dropping to 9-fold after one passage under dCas9-inducing conditions. (D) The CRISPRi *gatB* mutant exhibits gene repression of 41-fold in the parental strain, dropping to 0.9-fold after one passage under dCas9-inducing conditions. (E) The CRISPRi *dcw* mutant reveals gene repression of only 4.4-fold in the parental strain, dropping to 1-fold after one bacterial passage under dCas9-inducing conditions. Welch's t-tests were conducted to assess for significance between the parental strain and passage one for all mutants (***, $p < 0.001$; **, $p < 0.01$; *, $p < 0.05$). Black dots represent values from three independent biological replicates. The C_T values, quantification of relative gene expression and fold-changes for all CRISPRi mutants tested are available in the Supplementary Material: Tables S1, S2, and S3.

Table 6. Welch's t-test to analyze relative gene expression differences between parental strain and passage one, under consistent dCas9-inducing conditions of CRISPRi essential gene mutants in Cluster 1.

CRISPRi mutant	*T* statistic[a]	*diff*[b]	*df*[c]	*p. value*
atpB	-9.004	0.090	2.02	$p = 0.011$
dnaN	-28.939	0.319	2.02	$p = 0.001$
dcw cluster	-13.087	0.706	2.38	$p = 0.002$
gatB	-17.520	0.785	2.00	$p = 0.003$
gyrB	-23.573	0.508	2.53	$p = 0.0004$

[a]*T* statistic = *t* value from Welch's t-test, [b]*diff* = mean difference between passages, [c]*df* = degrees of freedom.

3.4.2 CRISPRi mutants from Cluster 2 exhibit differences in gene repression under dCas9-inducing conditions

CRISPRi mutants from Cluster 2 exhibited different gene repression levels. The CRISPRi *ligA* mutant exhibited 46-fold target gene repression in the parental strain, whereas the CRISPRi *engA* mutant showed 7.4-fold (**Figure 14**). However, both mutants increased target gene expression levels after one and two passages, surpassing non-inducing controls. A one-way ANOVA comparing gene expression across passages under dCas9-inducing conditions revealed significant differences for the CRISPRi *ligA* mutant after a Tukey HSD posthoc analysis (ANOVA, $F = 385.2$, $p = 4.62e\text{-}07$) showing significant differences between all groups. However, the CRISPRi *engA* mutant showed significant differences between the parental strain and bacterial passages but not between the evolved strains (ANOVA, $F = 60.57$, Tukey HSD, $diff_{2\text{-}1} = -0.321$, $p.adj = 0.181$) (**Table 7**).

These results partially correlate with the phenotypic data from the short-term evolution assay. Target gene repression was observed in the parental strain, which correlates with phenotypic data; however, target gene expression increased significantly after passages one and two, but mutants displayed the loss of the CGP until passage two.

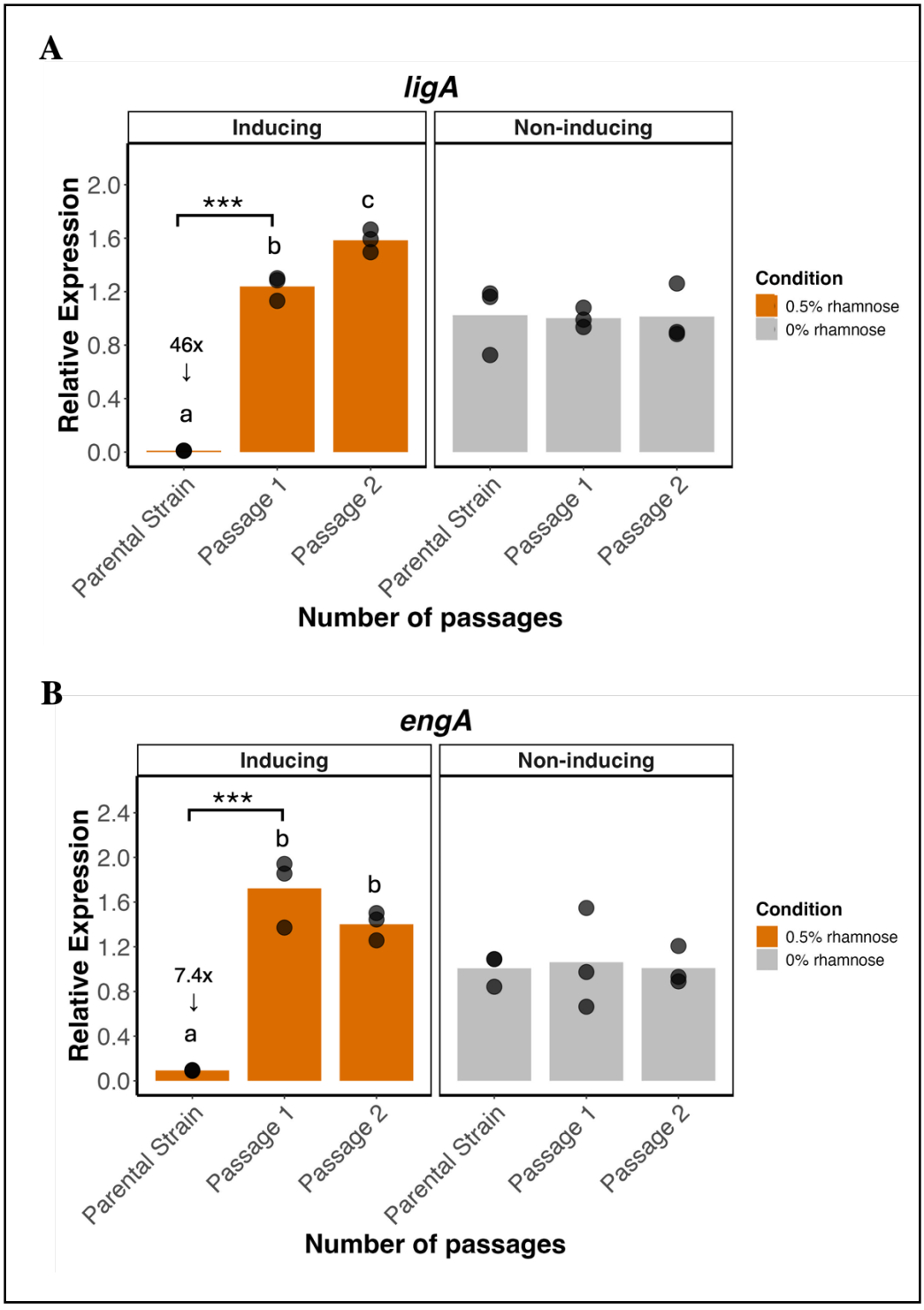

Figure 14. Relative gene expression levels in CRISPRi mutants from Cluster 2.

(A) The CRISPRi *ligA* mutant exhibits gene repression of 46-fold in the parental strain, significantly decreasing in passages one and two under dCas9-inducing conditions. (B) CRISPRi *engA* mutant, demonstrates gene repression of 7.4-fold, significantly decreasing in passages one and two under dCas9-inducing conditions. A one-way ANOVA followed by a Tukey HSD test

was performed to assess for significance between groups for both mutants (***, $p < 0.001$). Bars sharing the same letter indicate no significant difference, while different letters denote significant differences. Black dots represent values from three independent biological replicates. The C_T values, quantification of relative gene expression and fold-changes for all CRISPRi mutants tested are available in the Supplementary Material: Tables S1, S2, and S3.

Table 7. One-way Analysis of Variance (ANOVA) followed by Tukey HSD test to analyze relative gene expression differences between parental strain, passage one and two, under consistent dCas9-inducing conditions of CRISPRi essential gene mutants in Cluster 2.

CRISPRi mutant	*F* statistic [a]	Comparison	*diff*[b]	*df*[c]	*p.adj*[d]
ligA	385.2	1-0	1.228	2	p = 2.00e-06
		2-0	1.574		p = 7.00e-07
		2-1	0.345		p = 2.81e-03
engA	60.57	1-0	1.630	2	p = 0.0001
		2-0	1.308		p = 0.0003
		2-1	-0.321		p = 0.1811

[a]*F* statistic = *f* value from a one-way ANOVA, [b]*diff* = mean difference between passages, [c]*df* = degrees of freedom, [d]*p.adj* = p. value adjusted after Tukey HSD test. Strains are indicated as follows: parental strain (0), passage one (1), passage two (2).

3.4.3 CRISPRi mutants from Cluster 3 display variability in gene repression across passages under dCas9-inducing conditions

Cluster 3 showed the highest diversity in gene expression across passages. For example, gene expression in the parental strain of the CRISPRi *metG* showed a 1.5-fold reduction in gene expression, followed by similar fold changes in passages one and two. However, by passage three, gene expression levels surpassed non-inducing controls (**Figure 15A**). A one-way ANOVA followed by a Tukey HSD test revealed significant differences between the parental strain and passage 3 (Tukey HSD, $diff_{3\text{-}0} = 0.6973$, $p.adj = 0.000001$). On the contrary, gene expression in CRISPRi mutants *trxB* and *parC* exhibited higher levels of gene repression in the parental strain, 52-fold and 32-fold, respectively (**Figure 15B and 15C).** Nonetheless, in passages one and two, gene expression increased significantly in both mutants (*trxB*: Tukey HSD, $diff_{1\text{-}0,\,2\text{-}0} = 2.285, 6.576$, $p.adj = 0.0007, 0.0000003$; *parC*: Tukey HSD, $diff_{1\text{-}0,\,2\text{-}0} = 0.388, 0.853$, $p.adj = 0.0004, 0.000001$).

Nevertheless, gene expression in the CRISPRi *parC* mutant exhibited a 9-fold reduction in passage three, not correlating with the phenotypic results from the short-term evolution assay.

Lastly, gene expression in the CRISPRi *parAB* mutant exhibited an opposite trend, with no apparent repression in the parental strain; however, after one passage under dCas9-inducing conditions, we observed significant gene repression of 1.3-fold (Tukey HSD, $diff_{1\text{-}0} = -1.104$, $p.adj = 0.00004$). Moreover, we observed this gene repression was maintained in passages two and three (**Figure 15D**), a trend not observed in other mutants and not correlating with phenotypic observations from the short-term experimental evolution assay. To assess for significant differences, we compared passages under dCas9-inducing conditions for mutants in Cluster 3 through a one-way ANOVA followed by Tukey HSD tests. This statistical analysis revealed significant differences between parental strains and passage one (**Table 8**). Overall, mutants from this cluster exhibit variability in gene expression among passages, with no observable clear trend.

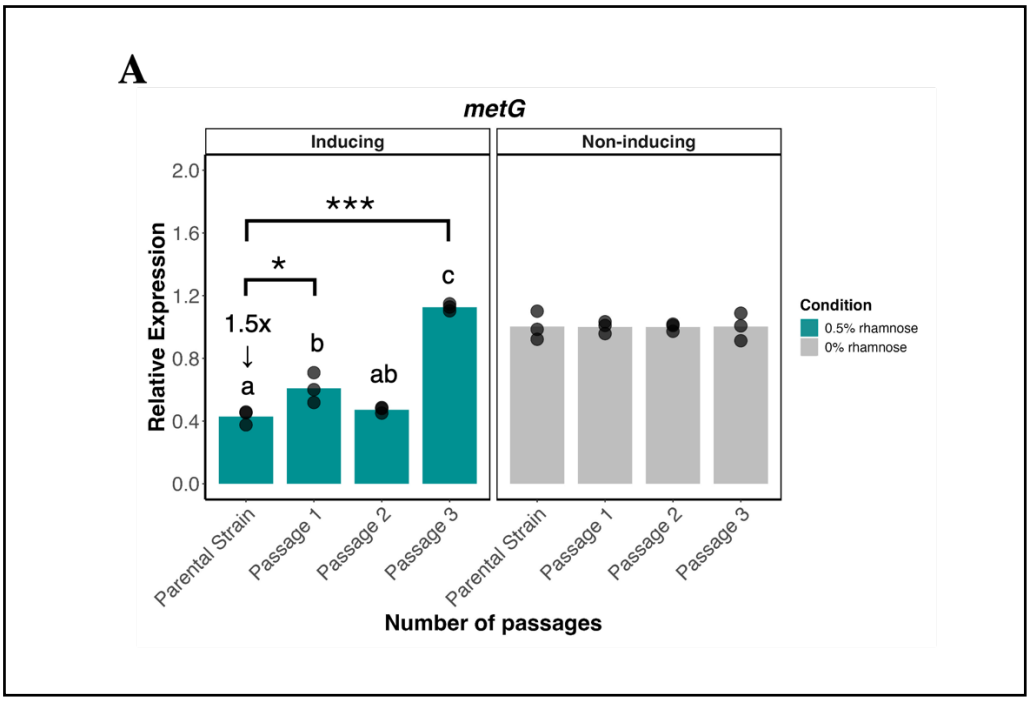

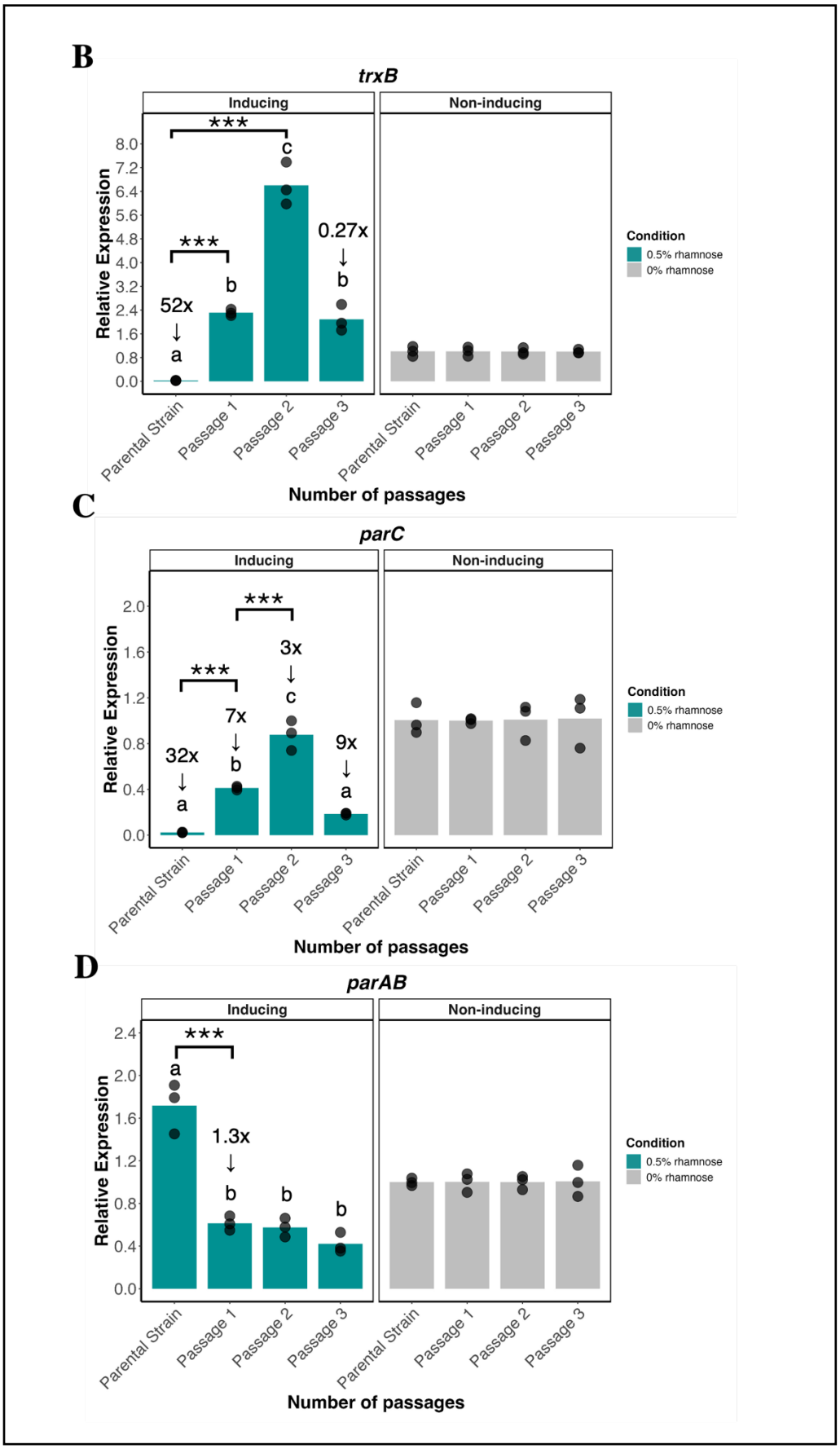
B
trxB
Inducing
Non-inducing
***
***
c
b
b
a
52x
0.27x
Relative Expression
8.0
7.2
6.4
5.6
4.8
4.0
3.2
2.4
1.6
0.8
0.0
Parental Strain
Passage 1
Passage 2
Passage 3
Number of passages
Condition
0.5% rhamnose
0% rhamnose
C
parC
Inducing
Non-inducing
***
***
3x
7x
9x
32x
c
b
a
a
Relative Expression
2.0
1.6
1.2
0.8
0.4
0.0
Parental Strain
Passage 1
Passage 2
Passage 3
Number of passages
Condition
0.5% rhamnose
0% rhamnose
D
parAB
Inducing
Non-inducing
***
a
1.3x
b
b
b
Relative Expression
2.4
2.0
1.6
1.2
0.8
0.4
0.0
Parental Strain
Passage 1
Passage 2
Passage 3
Number of passages
Condition
0.5% rhamnose
0% rhamnose

Figure 15. Relative gene expression levels in CRISPRi mutants from Cluster 3.

(A) CRISPRi *metG* mutant presented mild gene repression throughout all bacterial passages under dCas9-inducing conditions. (B) CRISPRi *trxB* mutant exhibited 52-fold gene repression in the parental strain, outperforming other mutants in this cluster. A sudden drop in gene repression is observed between passages one, two and three under dCas9-inducing conditions, surpassing control levels. (C) A 32-fold gene repression is present in CRISPRi *parC* mutant, significantly decreasing in passages one and two under dCas9-inducing conditions. Gene repression increasing in passage three, not observed in other mutants. (D) CRISPRi *parAB* exhibits an increase in gene repression after one passage under dCas9-inducing conditions and is maintained until passage three, not observed in other mutants. A one-way ANOVA followed by Tukey HSD test was performed to assess for significance between groups for all mutants (***, $p < 0.001$; *, $p < 0.05$). Bars sharing the same letter indicate no significant difference, while different letters denote significant differences. Black dots represent values from three independent biological replicates. The C_T values, quantification of relative gene expression and fold-changes for all CRISPRi mutants tested are available in the Supplementary Material: Tables S1, S2, and S3.

Table 8. One-way Analysis of Variance (ANOVA) followed by Tukey HSD test to analyze relative gene expression differences between parental strain, passage one, two and three, under dCas9-inducing conditions of CRISPRi essential gene mutants in Cluster 3.

CRISPRi mutant	*F* statistic [a]	Comparison	*diff*[b]	*df*[c]	*p.adj*[d]
metG	102.1	1-0	0.180	3	$p = 0.016$
		2-0	0.043		$p = 0.769$
		3-0	0.697		$p = 0.000001$
		2-1	-0.136		$p = 0.062$
		3-1	0.516		$p = 0.00001$
		3-2	0.653		$p = 0.000002$
trxB	126.2	1-0	2.285	3	$p = 0.0007$
		2-0	6.576		$p = 0.0000003$
		3-0	2.063		$p = 0.001$
		2-1	4.291		$p = 0.000008$
		3-1	-0.221		$p = 0.917$
		3-2	-4.513		$p = 0.000005$
parC	95.38	1-0	0.388	3	$p = 0.0004$
		2-0	0.853		$p = 0.000001$
		3-0	0.162		$p = 0.064$

		2-1	0.465		$p = 0.0001$
		3-1	-0.226		$p = 0.012$
		3-2	-0.691		$p = 0.000005$
parAB	55.21	1-0	-1.104	3	$p = 0.00004$
		2-0	-1.142		$p = 0.00003$
		3-0	-1.296		$p = 0.00001$
		2-1	-0.038		$p = 0.985$
		3-1	-0.192		$p = 0.385$
		3-2	-0.153		$p = 0.556$

[a]*F* statistic = *f* value from a one-way ANOVA, [b]*diff* = mean difference between passages, [c]*df* = degrees of freedom, [d]*p.adj* = p. value adjusted after Tukey HSD test. Strains are indicated as follows: parental strain (0), passage one (1), passage two (2), passage three (3).

In summary, RT-qPCR demonstrated that mutants in Cluster 1 experienced severe target gene repression; however, after one passage under dCas9-inducing conditions, target gene expression increased significantly. This trend aligns with the CGP observed in the short-term evolution assay. Gene expression analysis in mutants from Cluster 2 revealed medium to severe gene repression, restoring gene expression levels after one passage under dCas9-inducing conditions. Conversely, this phenotype was not observed during the short-term evolution assay; these mutants showed a different CGP in passage one compared to the parental strain and restored WT growth levels in passage two. Finally, mutants in Cluster 3 were the most diverse, with variable gene repression across passages under dCas9-inducing conditions without any observable trend. These findings led to further investigation of the CGP loss.

3.5 Whole Genome Sequencing (WGS) and sgRNA sequencing reveal CRISPRi stability and uncover single nucleotide polymorphisms (SNPs) related to CGP loss

To determine whether spontaneous mutations contributed to alleviating the CGP, the genomes of the five mutants in Cluster 1 and the NTC mutant were sequenced using Oxford Nanopore Sequencing (ONT). Others have observed spontaneous mutations in the dCas9 gene (Zhao *et al.,* 2016; Liu *et al.,* 2017), causing a frameshift in the reading frame, resulting in premature stop codons. Therefore, this possibility was investigated in our system. Furthermore, the sgRNAs encoded in the plasmid were sequenced for all mutants, as mutations in this sequence can lead to off-target binding of the dCas9 to unintended regions. The sgRNAs encoded in a plasmid were sequenced employing Illumina sequencing for the 16 CRISPRi mutants across all passages and replicates (336 samples). The first goal was to identify mutations in the CRISPRi machinery, such as the dCas9 sequence, rhamnose promoter (PrhaB), rhamnose system transcription regulator genes (*rhaR* and *rhaS*), or the 20 bp nucleotide sgRNA sequence. Mutations in any of these regions would explain the loss of the CGP in the selected CRISPRi mutants.

3.5.1 sgRNA sequencing using Illumina sequencing

The sgRNAs were amplified by PCR with unique combinations of i5 and i7 adaptor sequences. Next, the samples were pooled and sequenced using the Illumina MiSeq platform with a V2 Nano flow cell (1M clusters capacity) for paired-end sequencing. Sequencing was performed at the Donnelly Centre, University of Toronto. The adaptor sequences were obtained from Rahman *et al*., 2024, as these were used during the construction of the CRISPRi library. The synthetic guide RNAs served as barcodes, and the adaptors were used alternatively to generate unique combinations. A total of 336 samples were sequenced, consisting of 7 samples from short-term evolution experiments x 3 biological replicates x 16 mutants. Each sequence was read over 1000x, ensuring high confidence from the sequencing data. The raw data was analyzed by BLAST against the original sgRNA sequence. From the analysis, no mutations were detected in the sgRNAs for any of the mutants, revealing that the encoded sgRNAs are stable across passages under dCas9-inducing and non-inducing conditions in all mutants and replicates.

3.5.2 WGS and a Synteny and Rearrangement Identifier (SyRI) uncover SNPs

To identify SNPs in the genome of CRISPRi mutants from Cluster 1, Oxford Nanopore (ONT) was employed for parental and evolved (passage one) strains. The parental strain selected for sequencing was not grown under dCas9-inducing conditions to avoid stress-driven mutations (MacPhee & Ambrose, 1996; Ram & Hadany, 2012). The evolved mutants were selected from passage one under dCas9-inducing conditions (LB [trimethoprim 100µg/mL] with 0.5% rhamnose overnight). These mutants were those from glycerol stocks generated during the short-term evolution assay. Raw sequencing data was assembled using Flye, a de novo assembler for long reads (Kolmogorov *et al.,* 2019). A total of 12 genomes (6 CRISPRi mutants under both conditions) were assembled with a coverage depth minimum of 150x, in this way, five contigs from all assemblies were generated. Specifically representing three bacterial chromosomes, one megaplasmid, and the vector containing the sgRNA and trimethoprim resistance cassette (pgRNA). Next, to ensure the same starting positions for each contig prior to pairwise alignments, individual contig arrangement was performed in *Geneious Prime* Software (Version 8.1.9). Consequently, SyRI (Synteny and Rearrangement Identifier) (Goel *et al*., 2019), a tool able to identify genomic differences, such as translocations and inversions, as well as SNPs between two genome assemblies, was employed to perform pairwise genome alignment and SNP analysis.

First, we compared the CRISPRi machinery sequences including the dCas9, the rhamnose promoter (PrhaB), and the rhamnose system transcription regulator genes (*rhaR* and *rhaS*), between the parental and evolved mutants. Surprisingly, similar to the sgRNA sequences, no mutations were identified in these regions, which contrasts with previous findings (Zhao *et al.,* 2016; Liu *et al.,* 2017). Subsequently, we analyzed genomic differences and SNPs that could explain the loss of the CGP. Large genomic re-arrangements were not detected between genomes. However, single insertions, deletions and base-substitution changes were detected. Next, we employed Prokka, a prokaryotic genome software, to generate annotations (Seemann T., 2014) to map in which genes (loci) these SNPs were detected. After the annotations were generated, SNPs were individually analyzed using *Geneious Prime* Software. We compared the annotations generated by Prokka against our wild-type and annotated reference genome (GenBank accession

LAUA00000000) previously sequenced by Bloodworth *et al*., 2015, in our laboratory. A flowchart of these steps to analyze SNPs between genomes is shown in **Figure 16.**

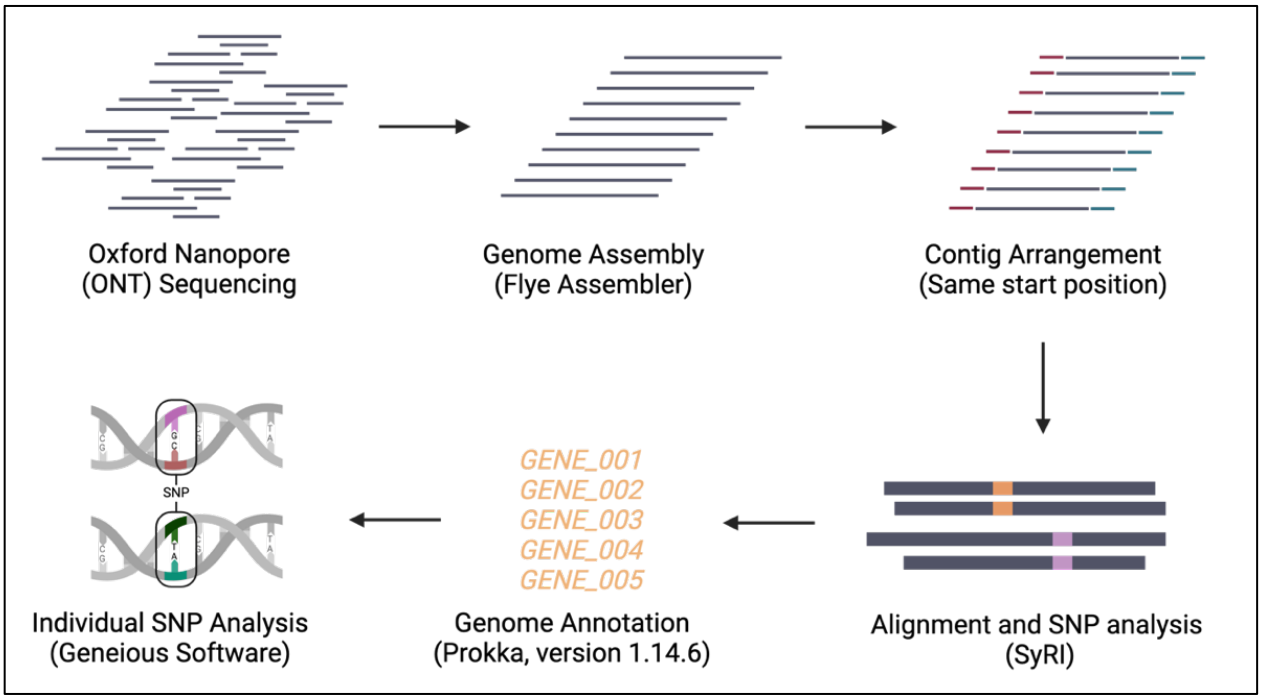

Figure 16. Descriptive workflow of the methodology followed to analyze SNPs in CRISPRi mutants.

Bacterial genomes were sequenced using Oxford Nanopore Technology (ONT), followed by genome assembly using a de novo assembler (Flye). Consecutively, the contigs are arranged at the same starting positions before genome alignment. Afterwards, pairwise comparisons and SNP analyses are performed using SyRI, a tool to detect genomic differences. Genomes are further annotated with Prokka software and visualized in *Geneious Prime* software to identify the affected loci affected by the SNPs detected.

Overall, the SNP analysis indicated a higher frequency of insertions, followed by deletions, with base-substitutional changes being the least frequent (See **Tables S4, S5, S6, S7, S8 and S9**). Chromosome 1 presented a greater mutation frequency among CRISPRi mutants, followed by Chromosome 2 and Chromosome 3. In the megaplasmid, we detected mutations in the CRISPRi *dcw, gatB,* and NTC mutants, predominantly in non-coding sequences. Lastly, a single mutation was identified in the plasmid (pgRNA) of the NTC mutant, which affected the trimethoprim resistance cassette.

3.5.3 SNPs in a LysR transcriptional regulator and a porin might influence the loss of the CGP

Analysis of individual mutants revealed consistent mutations across two loci on Chromosome 2. In the first locus, we observed identical deletion mutations in a LysR-type transcriptional regulator (K562_RS20940, total length: 1143 base pairs), first, at position 920, causing a frameshift in the reading frame, altering the protein sequence (Fan & Chu, 2007); followed by a base-substitutional mutation at position 924, within the same locus, causing the codon to code for a different amino acid, also known as a missense or nonsynonymous mutation (Watford & Warrington, 2023). These identical mutations were present in CRISPRi *atpB* and *dcw* mutants (**Table S4 and S5**). In contrast, only a missense mutation was detected in the CRISPRi *gyrB* mutant, causing the codon to code for a different amino acid (**Table S7**). Notably, identical mutations in the CRISPRi *atpB* and *dcw* mutants occurred at the same positions, affecting the sequences equally (**Figure 17**).

The second locus affected encoded a porin (K562_RS28860, total length: 1140 base pairs), with five CRISPRi mutants presenting mutations in this locus. All strains presented base-substitutional mutations: *gatB* and *gyrB* mutants at position 833, *atpB* and NTC mutants at position 834, and *dnaN* mutant at position 878, coding for a different amino acid; additionally, one strain presented a deletion mutation: *atpB* mutant at position 705 whereas one presented an insertion: NTC mutant at position 704 causing frameshifts in the reading frame (**Tables S4, S6, S7, S8 and S9)**. Interestingly, these mutations occurred at different positions within the coding sequence (CDS), altering the reading frame differently. Porins are outer membrane proteins in gram-negative bacteria that facilitate the entrance of small molecules into the cell, such as vitamins, sugars and even antibiotics (Vergalli *et al.,* 2020). Notably, we identified mutations in this porin across five CRISPRi mutants, albeit at different positions within the CDS. These mutations could impair porin function, potentially disrupting rhamnose uptake and leading to the absence of dCas9 expression, thereby contributing to the observed CGP loss.

First, we investigated the mutations found in the LysR locus as these were identical in two mutants at the same positions. LysR-type transcriptional regulators (LTTRs) have been characterized in *B. cenocepacia* strains K56-2 and H111 as a key regulator involved in quorum

sensing, protease regulation, type II secretion system and colony morphology, with a complex mechanism (Bernier *et al*., 2008; O'Grady *et al*., 2011; Wang *et al*., 2021). Considering that LTTRs can regulate the expression of proteases, we hypothesized that the observed mutations might upregulate a protease, which degrades dCas9, leading to CRISPRi loss of function. This mechanism may explain the absence or reduction of dCas9 abundance correlating with the observed CGP loss.

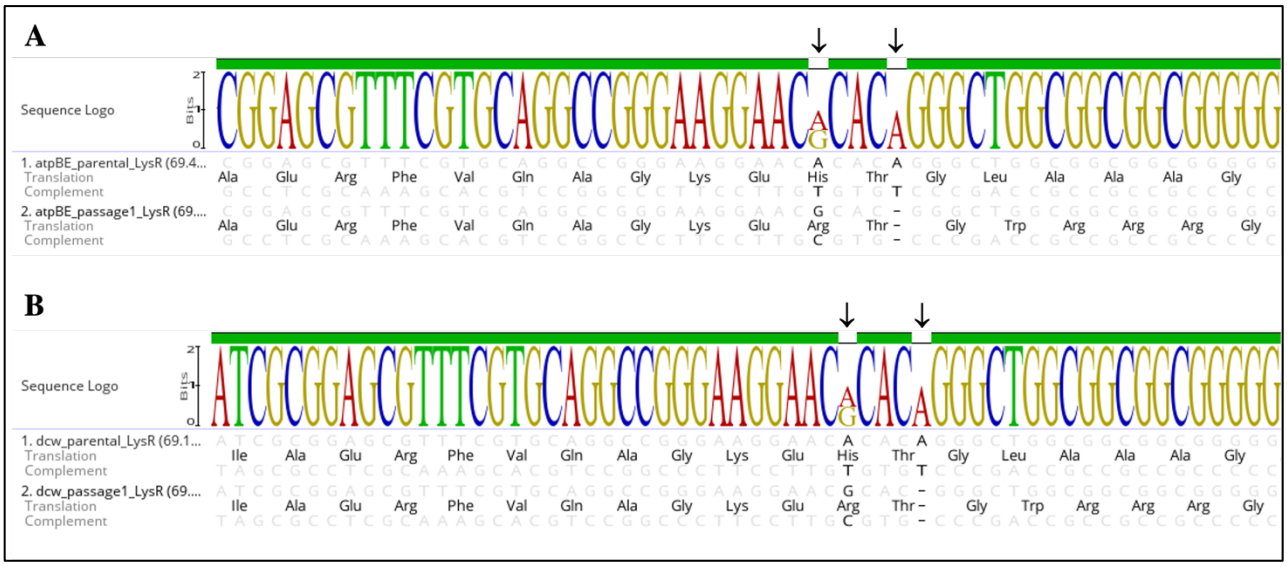

Figure 17. Mutations in a LysR transcriptional regulator alter the amino acid sequence and cause a frameshift in the reading frame.

Comparison of the parental and evolved strains of CRISPRi *atpB* (A) and *dcw* (B) mutants showing identical missense mutations (Position: base pair 920) followed by deletion mutations after four nucleotides (Position: base pair 924). Both mutations result in a frameshift, which may affect the function of the LysR. Visualizations were done in *Geneious Prime* software. The green bar represents the identity between sequences, and the coding amino acid is shown every three nucleotides.

3.5.4 Immunoblot confirms the absence of dCas9 protein abundance in evolved mutants

To investigate whether mutations in LysR affected CRISPRi function, we performed an immunoblot to compare dCas9 protein abundance in evolved strains against several controls. These included the parental strain of a CRISPRi *gyrB* mutant, previously observed to exhibit a severe growth defect, in this way, expected to express dCas9 (**Figure S5**), an evolved NTC mutant lacking a CGP, therefore, expected to express dCas9 and a previously purified dCas9 protein from our laboratory. The CRISPRi mutants tested were those presenting identical mutations (*atpB* and *dcw*), and a missense mutation (*gyrB*).

The immunoblot results revealed the absence of dCas9 in CRISPRi mutants presenting mutations in a LysR transcriptional regulator, supporting the claim that mutations in this regulator may contribute to the loss of the CGP. Positive controls demonstrated the presence of dCas9 under inducing conditions (**Figure 18**). Thus, the absence of dCas9 in evolved mutants indicates this regulator plays a role in CRISPRi function. The LysR-type transcriptional regulator has been characterized as a global regulator, able to repress or activate target genes by binding to the promoter and is widely distributed across bacterial species (Baugh *et al.,* 2023). In *Burkholderia cenocepacia,* it has been characterized as a regulator of diverse mechanisms, principally involved in quorum sensing, protease activity and biofilm formation (O'Grady et al., 2011; Wang et al., 2021). These results indicate that mutations in this regulator might arise as a compensatory response under consistent selective pressure interfering with CRISPRi function.

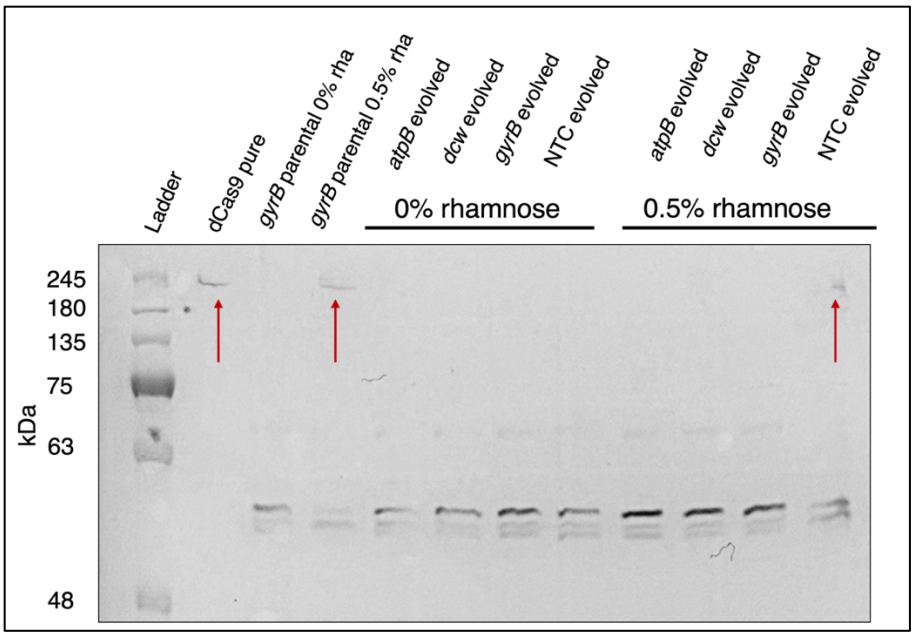

Figure 18. Immunoblot reveals the absence of dCas9 in evolved mutants.

Induction of dCas9 expression for parental control (CRISPRi *gyrB*) and evolved mutants is shown from left to right. The presence of dCas9 (~160 kDa) is detected in positive controls (dCas9 pure and *gyrB* parental strain induced with 0.5% rhamnose). Evolved CRISPRi mutants (*atpB*, *dcw*, and *gyrB*) with mutations in LysR show a lack of dCas9 under dCas9-inducing conditions (0.5% rhamnose). The evolved CRISPRi NTC mutant shows dCas9 expression, although at lower detection levels. Bacterial subcultures from overnights were grown in LB (trimethoprim 100µg/mL) until an OD_{600nm} of 0.7 was reached; after, 0.5% rhamnose was added to induce dCas9 expression for 4 hours. Then, cells were pelleted down and resuspended in TNG buffer (100 mM Tris-HCl, 150 mM NaCl, 10% glycerol, pH 7.4). Cell lysis was done in three sonication cycles of 5 seconds. Soluble proteins were run on an 8% SDS gel. Proteins were transferred by iBlot and blocked in 5% skim milk-TBST. Then, dCas9 was detected using a primary mouse monoclonal antibody (ThermoFisher 10C11A12) and detected by chemiluminescence using a second antibody (goat polyclonal anti-mouse - ThermoFisher G-21060) linked to alkaline phosphatase.

CHAPTER 4: DISCUSSION

4.1 Conserved essential genes as potential targets for gene repression using synthetic biology tools

Essential genes have been under study for decades, however, establishing a set of core genes to understand cellular life is still a challenge. These genes have been established to be evolutionary conserved among species in a variety of environments and have been the target in the antibiotic industry to inhibit bacterial growth (Juhas *et al*., 2012). Methods to study essential genes in bacteria are advancing rapidly, and the application of synthetic biology to comprehend the fundamental processes of life is advancing in parallel. Genetic tools like CRISPRi allow the repression of essential genes and enable us to study their role in growth and survival. This serves to further apply these tools for medical purposes, such as finding new potential drug targets (Fan *et al*., 2020). Additionally, repressing essential genes allows us to control growth or confine microorganisms to a specific environment (Khalil & Collins, 2010; Gallagher *et al*., 2015). Nonetheless, despite these genetic tools being mostly beneficial, the lack of knowledge regarding their long-term genetic stability needs to be addressed. In this study, we investigated the stability of CRISPRi in knocking down essential genes under consistent selective pressure over time.

As our first step, we selected essential functions from different clusters of orthologous gene (COG) categories and repressed their expression in *Burkholderia cenocepacia* K56-2, a versatile species with both pathogenic properties and beneficial traits. We found diverse conditional growth phenotypes (CGPs) among CRISPRi mutants independently of their COG category, meaning that repressing genes related to the same category will not exhibit equal phenotypes. Those categories exhibiting a severe CGP based on an extended apparent lag time were D (cell cycle, cell division and chromosome partitioning), L (replication, recombination and repair), C (energy production and conversion) and J (translation). These data correlate with a previous study investigating which essential genes were more evolutionarily conserved in 23 bacterial genomes (including two *Burkholderia* species) to identify a relationship with the COG functional category (Luo *et al*., 2015). They found categories G, H, I, J, K, and L to be the most conserved categories, followed by C, U, and M. Additionally, another study attempted to create a chromosome-free cell or minimal cell in different bacterial species by expressing different combinations of genes to attempt cell

survival (Fan *et al.,* 2020); they discovered that genes related to energy conversion (C), transcription (I), and translation (J) are preferred to maintain cellular function. Interestingly, COG category D, which involves cell division and peptidoglycan synthesis, was not addressed in any of these studies, despite that essential genes within this category are conserved in gram-negative and gram-positive bacteria (Chen *et al.,* 2001; Kobayashi *et al.,* 2003; Peng & Gao, 2014). This suggests that some essential genes in this category can be species-specific, be found in some bacterial species, and may be absent in others (Garcia *et al*., 2021).

Short- and long-term evolution experiments have been conducted in research laboratories to understand the mechanisms that govern adaptation in microbial communities, focusing on mutations that confer beneficial changes in fitness (Elena & Lenski, 2003; McDonald, 2019). There are studies in *Burkholderia* species performing experimental evolution and studying mutation rates (Pope *et al.,* 2010; Traverse *et al*., 2012; Dillon & Cooper, 2016; Hassan *et al*., 2020); however, these studies focus on those mutations in mechanisms conferring higher pathogenicity or antimicrobial resistance. While it is very important to study the natural selection of mutations in evolved populations, it is also necessary to investigate those mutations that arise when an essential function is compromised. CRISPRi is a genetic tool that allows the study of essential genes by reducing their expression. It has been widely applied to validate antimicrobial targets, studying genes related to virulence in pathogenic species, and inhibiting potential toxins (Hogan *et al.,* 2023; Ghavami & Pandi, 2021; Enright *et al*., 2024). Nonetheless, no studies have investigated CRISPRi stability to consistently repress essential functions.

To address this concern, we performed a short-term experimental evolution assay in CRISPRi essential gene mutants under consistent essential gene repression. We identified that the conditional growth phenotype was compromised after one, two, and three passages for all the mutants tested. Interestingly, the CRISPRi mutants lost the CGP at different time points, with all mutants restoring wild-type growth levels. To date, two other studies using inducible CRISPRi systems to repress essential functions in *Bacillus subtilis* and *Streptococcus pneumoniae* (Zhao *et al.,* 2016; Liu *et al.,* 2017) have observed the loss of conditional growth phenotypes after subculturing the mutants in the presence of the inducers, IPTG and xylose, respectively. Both studies found frameshift mutations in the dCas9 sequence, causing CRISPRi loss of function.

Furthermore, Liu *et al*. (2017), found mutations in the encoded sgRNAs, directing to the possibility of adaptative-induced mutations that relieve selective pressure (Foster, 2007), which will be discussed further. Interestingly, they also observed diversity regarding conditional growth phenotypes when repressing essential functions from different metabolic pathways. However, while they focused on studying the effects of essential gene repression and analyzing the morphology of these mutants to identify new essential functions, they did not investigate CRISPRi stability to consistently repress essential functions. Nonetheless, in this work, we observed that different CRISPRi mutants lose the CGP at different time points, a trend not observed in these studies.

Building on this unique observation, we aimed to cluster the results from our short-term evolution experiment to find a relationship between essential gene function and the timing of CGP loss. Beyond phenotypically characterizing CGP loss in these mutants, we calculated growth parameters from growth curves across passages, in this way, we used this data as an input to identify similarities between essential gene mutants to find a pattern. Using K-medoids, also known as the Partitioning Around Medoids method, an algorithm that randomly selects a data point from the dataset and generates a "medoid" or cluster (Gu *et al*., 2020; Velmurugan & Santhanam, 2010), we identified three clusters. Cluster 1 contained five CRISPRi mutants (*atpB, dcw, dnaN, gatB* and *gyrB*), Cluster 2 contained two CRISPRi mutants *(ligA* and *engA*), and Cluster 3 contained eight CRISPRi mutants (*metG, mrdAB, obgE, trxB, parAB, parC, gmk* and *sodB*) along with the control mutant (NTC).

The cluster distribution somewhat aligned with our phenotypic observations. We expected mutants to cluster based on their CGP loss; however, we identified that the parameters primarily defining the clusters were the time of the apparent lag time and the growth rate rather than the passage at which the CGP was lost, as the pattern identified was related to their growth defect. These results highlight the importance of key growth parameters in understanding the fitness of CRISPRi mutants targeting essential genes. Moreover, this aligns with similar findings that have reported growth rate as the determinant fitness parameter when studying CRISPRi essential gene mutant libraries (Peters *et al*., 2016; Silvis *et al*., 2021; Rahman *et al*., 2024). To further explore

the implications of this cluster distribution and its relationship with essential gene function, we analyzed mRNA expression levels using RT-qPCR to assess whether gene repression corresponded to the observed phenotypic and clustering data.

Conditional growth phenotypes are a key feature observed during essential gene repression mediated by CRISPRi. Several studies using CRISPRi to knock down essential genes have been shown to validate essential gene repression by measuring mRNA expression levels (Peters *et al.,* 2016; Hogan *et al.,* 2023; Wang *et al.,* 2024). Additionally, previous research identifying mutations in the dCas9 sequence has been linked to loss of function (Zhao et al., 2016; Liu et al., 2017), raising the question of whether gene expression is fully restored in the CRISPRi mutants after CGP loss. Based on our results from the short-term evolution experiment, we hypothesized that if the CGP was abolished, gene expression would be restored in all mutants under dCas9-inducing conditions across passages.

To investigate this, we used RT-qPCR to measure mRNA levels in 11 mutants from Clusters 1 and 2, and four representative mutants from Cluster 3, aiming to correlate gene repression with cluster distribution and CGP loss. The mutants selected from Cluster 3 were across different COG categories to address variability across functions. In parental strains, mutants from Cluster 1 exhibited the highest levels of gene repression, up to 78-fold; Cluster 2, composed of two mutants, revealed gene repression of 46-fold and 7.4-fold; and mutants from Cluster 3 exhibited gene repression levels ranging from 52-fold as the highest to 1.3-fold as the lowest. Interestingly, gene repression in the following passages varied across all clusters; for example, mutants from Cluster 1 matched phenotypic data from the short-term experimental evolution assay, exhibiting a significant increase in gene expression after one passage under dCas9-inducing conditions, with gene repression persisting to some degree. Conversely, mutants from Cluster 2 showed increased gene expression after one passage under dCas9-inducing conditions, contradicting the phenotypic data. Lastly, mutants from Cluster 3 displayed high heterogeneity regarding gene repression under dCas9-inducing conditions, with no clear pattern, as some mutants randomly decreased or increased gene expression levels.

When correlating gene expression, mutants from Cluster 1 matched phenotypic data and cluster distribution, suggesting a relationship between severe growth defects, CGP loss and high levels of gene repression. On the contrary, mutants from Cluster 2 differed regarding gene repression levels in the parental strain, although both recovered full gene expression after one passage under dCas9-inducing conditions. In comparison, Cluster 3 exhibited the highest diversity, with the only common pattern being their growth defect in the parental strains, which ranged from medium to mild; nonetheless, when quantifying mRNA expression, we found genes exhibiting significant levels of gene repression (*trxB and parC*). These findings demonstrate that essential gene repression does not correlate with CGP loss, except in mutants in Cluster 1, suggesting that repression of some essential functions affect the conditional growth phenotype more than others.

Interestingly, while analyzing levels of gene repression and functional categories, we observed that mutants in COG category L (replication, recombination, and repair) exhibited the highest levels of gene knockdown compared to mutants from other categories, suggesting that genes ensuring accurate DNA repair are more susceptible to repression, potentially compromising the ability of bacterial cells to maintain growth. In line with our findings, work by Peters *et al.* (2016) in CRISPRi *Bacillus subtilis* mutants, found essential gene networks between functional categories and gene repression. Their findings revealed a higher correlation between essential genes involved in cell wall biosynthesis and DNA replication, COG M and L, respectively, aligning with our results. Given these observations, we next focused on Cluster 1 to perform WGS, as these mutants displayed the strongest correlation between gene repression and CGP loss.

4.2 Spontaneous mutations may affect CRISPRi function

To explore the underlying genetic causes of CGP loss, we sequenced the genomes of mutants in Cluster 1, along with the NTC mutant, before and after consistent selective pressure. We aimed to uncover any spontaneous mutations that might contribute to the loss of CRISPRi function, expecting to find similarities with previous studies, which detected spontaneous mutations in the dCas9 sequence. The first study, performed in *Bacillus subtilis* (Zhao *et al.*, 2016) *investigated* the role of an essential phosphatase involved in the cell envelope synthesis for antibiotic purposes. They observed CRISPRi mutants without sensitivity to xylose, their inducer

for dCas9, and sequenced strains to identify mutations causing this phenotype. WGS revealed frameshift mutations in the dCas9 CDS, indicating loss of function. To address this, they introduced a second copy of the dCas9 gene and a second sgRNA targeting the same gene. These modifications allowed for a mild increase in gene repression. The second study assessed to identify new essential functions in *Streptococcus pneumoniae (*Liu *et al*., 2017) by repressing genes through CRISPRi and characterizing their conditional growth phenotypes. Their observations were similar to ours in terms of growth defects, with a variety of CGPs. Nonetheless, they noted that after subculturing these mutants in the presence of the inducer (IPTG), the mutants alleviated the CGP. They performed WGS, and detected mutations in the sgRNAs and the dCas9 sequence, where the latter indicated loss of function.

From WGS in CRISPRi mutants from Cluster 1 and the NTC control, we did not detect any spontaneous mutations affecting the dCas9 coding sequence (CDS) or any element of the CRISPRi machinery, such as the rhamnose promoter, transcription regulator genes *rhaR* and *rhaS*, or encoded sgRNAs. On the contrary, from our single nucleotide polymorphism (SNP) analysis, we identified mutations consistently in two loci across CRISPRi mutants from Cluster 1.

The first locus affected was a LysR-type transcriptional regulator (K562_RS20940) in three CRISPRi mutants, specifically for two mutants, identical mutations at the same positions were detected. CRISPRi mutants *atpB* and *dcw* presented both mutations at identical positions: a deletion mutation that caused a frameshift in the reading frame and a base-substitution change that coded for a different amino acid. In contrast, CRISPRi *gyrB* mutant presented only a base-substitution change at another position of the CDS. This LysR-type regulator belongs to a family of transcriptional regulators (LTTR) and is one of the most characterized in bacteria due to its conserved DNA-binding domain (N-terminal region) across species, including *Escherichia coli, Salmonella enterica, Pseudomonas aeruginosa*, and *Burkholderia cenocepacia* (Maddocks & Oyston, 2008). On the other hand, the C-terminal has been identified as the effector-binding domain that recognizes coinducers to activate gene transcription (Schell, 1993; Modrzejewska *et al*., 2021). It plays a role as a dual regulator, acting as an activator by recognizing a coinducer and binding to a promoter region to recruit an RNA polymerase and activate transcription. Alternatively, it can function as a repressor when the coinducer is not present, by binding to DNA

and interfering with an RNA polymerase, repressing transcription (Baugh *et al,* 2023). Moreover, it has been identified to regulate genes or operons involved in survival processes, such as quorum sensing (QS), virulence, biofilm formation, oxidative stress response among many others (Maddocks & Oyston, 2008; Giannopoulou *et al.,* 2021).

Evidence in *Burkholderia cenocepacia* has demonstrated this regulator influences biofilm formation, virulence, and protease activity; however, mutations in this gene, such as insertions and base-substitution changes, were proven to alter the activity of these mechanisms by increasing or decreasing its activity. Research by Bernier *et al*. (2008) and O'Grady *et al*. (2011) detected spontaneous changes in colony morphology in *B.cenocepacia* K56-2, where the phenotypes with shiny colonies were related to increased virulence and biofilm formation. They identified mutations in ShvR (BCAS0225), a LysR-type regulator, negatively regulating protease production, biofilm formation, and the type II secretion system, which secretes extracellular proteases and lipases. These studies identified and annotated this regulator by BLAST against *B. cenocepacia* J2315 sequenced by Holden *et al*. (2009), detecting ShvR in chromosome 3. Another study by Wang *et al*. (2021), found a novel LysR-type in *B.cenocepacia* H111; they demonstrated that it regulates gene transcription by binding to the promoter and positively regulates protease and biofilm formation. They created a LysR (BCAL3178) deletion mutant and observed that protease activity and biofilm formation decreased, and after complementation, both levels increased. Similarly, this LysR-type regulator was assessed by homology against *B. cenocepacia* J2315 sequenced by Holden *et al*. (2009), with BCAL3178 detected in chromosome 1.

Based on previous studies and the results from our SNPs analysis, we hypothesize that spontaneous mutations in this LysR regulator, lead to CRISPRi loss of function. Evidence suggests this global regulator can act as an activator or repressor of proteases. Nonetheless, we recognize these studies measure extracellular protease activity. However, we identified the absence of dCas9 by immunoblot in the strains containing mutations in this LysR-type regulator. One possibility might be that mutations in this regulator result in unregulated mechanisms involved in protease activity, such as the type II secretion system. If unregulated, proteases are not being secreted extracellularly and are potentially degrading intracellular dCas9, explaining CRISPRi loss of function. Nonetheless, more studies are needed to confirm this hypothesis. Lastly, to compare our

results with those mentioned previously, we performed a BLAST of our LysR sequence against *B. cenocepacia* J2315 sequenced by Holden *et al.,* 2009, and we found a 99% identity in chromosome 2. Overall, our results revealed the absence of dCas9 in all evolved mutants, except for the NTC control, which showed the presence of dCas9.

The second locus tag affected across CRISPRi mutants was a porin (K562_RS28860). The mutations were found at different positions of the coding sequence, including a silent mutation. Porins are found in the outer membrane of gram-negative bacteria, and their function relies on controlling the entrance of small molecules, like sugars, into the cell (Galdiero *et al.,* 2012; Roy *et al.*, 2021). Modifications in porins have been widely reviewed as a mechanism contributing to antibiotic resistance in gram-negative bacteria (Pagés *et al.,* 2008; Zhou *et al.*, 2023; Kherroubi *et al.*, 2024), primarily due to alterations in cell permeability. Accordingly, we propose that mutations in this porin might compromise rhamnose uptake, failing to activate the rhamnose promoter and consequently preventing dCas9 expression. However, further investigation is needed to confirm a relationship between the mutations and the cell's ability to introduce rhamnose.

4.3 CRISPRi genetic stability and limitations

CRISPRi is a genetic tool that allows the gene repression of targeted genes; however, it has some limitations to consider when consistently repressing essential genes. One study created a mobile CRISPRi tool, which consists of transferring the CRISPRi machinery between species through conjugation, and they measured the genomic integration stability across different bacterial species. They found that the machinery is maintained for approximately 50 generations proving that the CRISPRi machinery is stable across passages (Peters *et al.,* 2019). However, the conditions were not under selective pressure or consistently repressing essential genes. Our work supports that statement, given that we identified all the CRISPRi elements present in parental and evolved strains under non-inducing and dCas9-inducing conditions, respectively. Nonetheless, we demonstrated that the CRISPRi machinery is compromised due to spontaneous mutations.

An interesting study in *Cupriavidus necator* (Wang *et al.,* 2024) repressed the expression of *mutS*, a gene involved in DNA repair, for approximately three days with the approach to identify

how bacteria would adapt under consistent repression. They found higher mutation rates in these mutants and tolerance against hydrogen peroxide, indicating adaptation. However, they did not perform whole genome sequencing to underlie the mutations involved. In a different study done by Gallagher *et al.,* 2015, they genetically modified *E. coli* populations to create essential gene mutants dependent on biotin; in this way, these mutants could not express these essential products without biotin. Consequently, they performed a short-term evolution experiment (110 generations) and found that mutants escaped this conditional growth phenotype; after sequencing their genomes, they found identical mutations in a *mutS* gene.

Although neither study assessed for essential gene repression, they showed that under consistent selective pressure, mutants with compromised functions escape conditional growth phenotypes or acquire adaptation mechanisms. Compared with our study, we identified mutations in a LysR transcriptional regulator, causing frameshifts and changes in amino acids, potentially transcribing a nonfunctional protein (McDonald, 2019), that might compromise its regulatory function. The mutations we identified were in an environment under consistent selective pressure, suggesting these are adaptative mutations (Elena & Lenski, 2003; Foster, 2007), as they confer a selective advantage that allows CRISPRi mutants to escape the conditional growth phenotype.

To finalize this discussion, we want to address the phenomenon of gene essentiality and how CRISPRi excels in demonstrating this spectrum. Our findings revealed that genes involved in DNA replication and repair are the most affected by gene repression, indicating that these mechanisms play a key role, if not the most critical, in bacterial growth. Moreover, this category has been addressed as one of the most conserved genes in comparative analysis across species; however, we acknowledge that this essentiality can depend on the environment (Rancati *et al.,* 2018; Hogan & Cardona, 2022) and be species-specific. Toward our long-term goal, we elucidated CRISPRi as an effective tool for short-term bacterial growth inhibition, by repressing essential genes. Nonetheless, to tackle *Burkholderia*'s pathogenic properties and enhance its biotechnological potential other approaches need to be investigated.

CHAPTER 5: CONCLUSIONS AND FUTURE DIRECTIONS

Synthetic biology tools to study essential genes are becoming more popular due to their performance and applications in the medical and biotechnological industries. However, there are limited studies about their genetic stability over time. In this work, we explored effectiveness and limitations of CRISPRi to achieve consistent gene repression *in Burkholderia cenocepacia* K56-2 mutants. We focused on investigating the genetic stability of CRISPRi and loss of function under consistent selective pressure to repress essential genes during a short-term experimental evolution assay (~72 generations).

We identified distinct conditional growth phenotypes exhibiting diverse growth defects, from severe to medium and mild, primarily affecting genes involved in DNA replication, recombination, and repair. Under selective pressure across bacterial passages, CRISPRi mutants alleviated the conditional growth phenotype with increased gene expression. Through whole genome sequencing, we proved that the CRISPRi machinery is stable across passages, with no mutations found. Instead, we discovered mutations in other genes, specifically a porin and a global regulator, potentially triggering a compensatory mechanism under consistent essential gene repression, which led to CRISPRi loss of function. These findings contribute to a better understanding of *Burkholderia* adaptation under the selective pressure of CRISPRI-based essential gene repression.

Evolution experiments play an important role in uncovering survival mechanisms and revealing genotypic-phenotypic relationships when essential genes are repressed. Our study provides new insights into CRISPRi genetic stability under consistent selective pressure. The mutations found in genes encoding a LysR-type transcriptional regulator and a porin, may cause insufficient levels to dCas9 in evolved mutants and CRISPRi loss of function, which leads to the alleviation of the CGP. Here, we highlight the intricate relationship between essential gene repression, adaptative-induced mutations, and conditional growth phenotypes. Moreover, future work performing WGS on mutants from Clusters 2 and 3 could enable us to identify whether

identical mutations in the same genes arise as a compensatory mechanism alleviating gene knockdown.

As potential future directions for this research, we propose several alternatives. First, to confirm that mutations in the LysR-type regulator leads to unregulated protease activity, we can quantify protease gene expression by RT-qPCR, expecting increased expression levels. Similarly, to confirm that mutations affect porin function and prevent rhamnose uptake, resulting in a lack of dCas9 expression, we can perform RT-qPCR to measure dCas9 expression levels. On the other hand, to improve CRISPRi efficacy to repress essential genes under consistent selective pressure, we could introduce a second chromosomally encoded dCas9, similarly to Zhao *et al*. (2016), aiming for increased gene repression across passages and maintained growth inhibition.

Another alternative is to introduce genes encoding a porin or a LysR-type regulator and induce overexpression to restore their function, thereby preventing CRISPRi loss of function and maintaining the conditional growth phenotype. Finally, we could explore other strategies to contain genetically modified organisms in a confined environment, such as auxotrophy, which has the objective of creating cells dependent on an external supply or using a xenobiological approach, which creates cells dependent on synthetic metabolites, controlling both escape and proliferation (Lee *et al*., 2018). In essence, this research underscores the importance of experimental evolution in understanding the mechanisms involved in adaptation when repressing essential functions, recognizes CRISPRi efficacy to repress essential gene expression, and aims to improve genetic tools for future biotechnology applications.

CHAPTER 6: APPENDIX

6.1 Supplementary tables

Table S 1. Data collected (Ct values) from 11 CRISPRi essential gene mutants under dCas9-inducing conditions across different passages, to calculate relative gene expression using the comparative Ct method.

Sample Name	Target Genes	CT												CT Avg	CT SD	ΔCt(test samples)	ΔΔCT	2-ΔΔCT	Percent Expreession	Fold K/D vs Non-Inducing
		Rep 1				Rep 2				Rep 3										
		T1	T2	T3	Avg	T1	T2	T3	Avg	T1	T2	T3	Avg							
Ind	*atpBE_24*	23.2733021	23.7116566	22.8553371	23.2801	23.2410793	23.5803699	22.9937534	23.2717	23.2551746	23.2980709	23.1463261	23.2332	23.262	0.0250198	5.129	5.80508867	0.0178852	1.788521577	55.91210153
Ind	*dnaN_24*	25.7020226	25.5403194	25.7666321	25.6697	25.7752972	25.3974304	25.6686096	25.6138	26.1884766	Undetermine	25.6132984	25.9009	25.728	0.15221737	6.156056828	6.30199676	0.0126739	1.267389026	78.90237168
Ind	*gyrB_24*	27.52211	27.3912735	27.4203472	27.4446	27.7045097	27.4178066	27.2244949	27.4489	27.786787	27.6580963	27.6630173	27.7026	27.532	0.14774648	7.310047997	6.08390194	0.0147422	1.474222471	67.83236719
Ind	*gatB_24*	25.5228996	25.8422184	25.811758	25.7256	25.8439159	25.5320187	25.9846783	25.7869	25.7770309	25.5149193	25.565218	25.6191	25.711	0.08492141	6.563113954	5.38992543	0.023849	2.384903287	41.93042148
Ind	*dcw_24*	21.9344959	22.2344475	22.339592	22.2870	22.2363491	22.4331799	22.5230522	22.3975	22.1137524	22.1778984	22.4621983	22.1458	22.277	0.12616223	3.460892465	2.16887146	0.2223846	22.2384562	4.496715019
Ind	*atpBE_48*	20.0332413	20.1548347	20.2020073	20.1784	20.5104351	20.4502392	20.514967	20.4919	20.0349731	20.0045662	19.9901466	20.0198	20.230	0.24024834	0.346458011	3.28200319	0.102806	10.28060312	9.727055779
Ind	*dnaN_48*	21.9510098	21.6263275	21.6168766	21.7314	21.7069416	21.6371956	21.7229843	21.6890	21.8039112	21.6256084	21.6837463	21.7044	21.708	0.02144517	1.692381329	1.61524942	0.3264085	32.64085104	3.06364561
Ind	*gyrB_48*	21.4790745	20.8456459	20.7785511	20.8121	20.8029175	19.8588562	20.0627499	20.4328	20.4431896	20.4986591	20.5856285	20.5092	20.585	0.20059897	2.076324463	0.19744958	0.8720909	87.20908991	1.14666946
Ind	*gatB_48*	20.8613758	20.4127865	20.7107086	20.6616	20.699934	20.6602192	20.7967815	20.7190	20.4655533	20.9051552	20.7586765	20.7098	20.697	0.03080683	2.376219432	-0.1428047	1.1040494	110.4049361	0.905756604
Ind	*dcw_48*	20.4016762	19.8147449	19.782896	19.9998	19.7398281	20.3768406	20.2949562	20.1372	19.6891098	20.0506344	20.296442	20.0121	20.050	0.0760496	0.271511502	0.10998917	0.926595	92.659502	1.079220132
Ind	*ligA_24*	29.8194485	29.4851208	29.545969	29.6168	29.5174694	29.3479538	29.5708694	29.4788	29.4573307	29.5663395	29.39501	29.4729	29.523	0.08146926	11.96092733	5.54368952	0.0214379	2.143794582	46.64626024
Ind	*engA_24*	24.7470207	24.5639553	25.0385704	24.7832	25.0984306	24.9844036	25.1129551	25.0653	24.8734512	25.3668575	25.1884499	25.1429	24.997	0.18930187	6.89391009	2.89157444	0.1347564	13.47563875	7.420798512
Ind	*ligA_48*	23.8944111	24.2458115	24.4166451	24.1856	24.2747326	23.8305759	23.7344456	23.9466	24.0426922	24.2010841	24.1653194	24.1364	24.090	0.12621544	5.454528385	-0.4901962	1.4046359	140.4635914	0.711928258
Ind	*engA_48*	19.9914188	20.0315514	19.9568119	19.9933	19.9768829	20.0714912	20.3709545	20.1398	19.9805546	19.9845963	19.9529076	19.9727	20.035	0.09111276	1.694670783	-1.3580091	2.5633121	256.3312064	0.390120272
Ind	*ligA_72*	23.7064323	23.7124882	23.540638	23.6532	23.8038273	23.9294357	22.6696606	23.4676	23.6266422	23.3603497	23.6799278	23.5556	23.559	0.09281342	5.187854343	-1.1120928	2.1615898	216.1589782	0.462622468
Ind	*engA_72*	19.9256973	19.8404484	19.7903976	19.8522	20.1305656	20.0614872	20.094141	20.0954	20.0233517	19.665575	19.8387985	19.8426	19.930	0.14327486	1.982007556	-1.4326098	2.6993457	269.9345734	0.370460141
Ind	*parAB_24*	20.8846493	20.8299255	20.7306862	20.8151	20.7058716	20.6681595	20.7549591	20.7097	20.6990509	20.8854656	20.7159462	20.7668	20.764	0.05277426	1.756873449	-1.0719967	2.102341	210.2340993	0.47566023
Ind	*parAB_48*	21.6578178	21.5465813	22.034193	21.6022	21.0890484	20.4826126	20.3433475	20.7858	21.5198689	21.7191391	21.8565063	21.6195	21.336	0.47640483	2.279200872	0.45233345	0.7308598	73.08597809	1.368251512
Ind	*parAB_72*	21.9258652	22.0244923	21.9381561	21.9628	22.0942211	21.9433765	21.8661366	21.9679	22.3110428	22.2983799	22.2186317	22.2760	22.069	0.17936806	2.596423467	-0.1758997	1.1296687	112.9668688	0.885215294
Ind	*parAB_96*	22.292099	22.8363476	22.8489285	22.6591	23.2234764	22.5545769	22.6537075	22.8106	21.8264866	21.9288349	21.9689388	21.9081	22.459	0.48330557	3.114921146	0.15636423	0.8972835	89.728349	1.11447498
Ind	*parC_24*	29.2447109	29.5456066	29.5124454	29.4343	29.5497551	29.5226173	29.5335941	29.5353	29.1992149	29.1089249	29.081995	29.1300	29.367	0.21095328	10.45716137	5.01861297	0.0308494	3.084941693	32.41552351
Ind	*parC_48*	28.2121792	28.1609821	28.3057346	28.2263	28.2366219	28.2192631	27.9901428	28.1487	27.9756851	28.518549	Undetermine	28.2471	28.207	0.05188023	7.271853235	2.83736515	0.1399162	13.99161934	7.147135551
Ind	*parC_72*	28.1403179	27.3837738	27.6300697	27.7181	27.8594265	27.9590111	27.7663422	27.8616	28.2040806	28.6171436	28.7371979	28.5195	28.033	0.4273338	7.079787572	1.77493477	0.2922075	29.2207524	3.422225364
Ind	*parC_96*	27.6217136	28.1890831	28.1622963	27.9910	28.2724209	28.2570267	28.223671	28.2510	28.3283615	28.6190548	28.3816547	28.4430	28.228	0.22684786	7.017671797	3.22136561	0.1072191	10.72191412	9.326692875
Ind	*trxB_24*	32.3565521	32.9778175	32.7328911	32.6891	32.654789	32.3558502	32.668663	32.5598	32.3593025	31.7690639	32.7988167	32.3091	32.519	0.19321701	12.31522412	5.7191391	0.0189831	1.898311951	52.6783809
Ind	*trxB_48*	27.2098522	27.3438835	27.0376492	27.1971	27.0852432	27.0257378	27.0937996	27.0683	27.195158	27.2457371	27.3402386	27.2604	27.175	0.09790872	7.48593945	-1.2139346	2.3196941	231.9694119	0.43109132
Ind	*trxB_72*	26.7424278	26.541172	26.5355835	26.6064	26.8464031	26.8782463	27.1992817	26.9746	26.6563816	26.9891834	26.5567265	26.7341	26.772	0.18698402	6.005841361	-1.6231793	3.0805316	308.0531589	0.324619297
Ind	*trxB_96*	26.8804932	26.5258465	25.9902039	26.4655	26.7120266	26.1242771	26.6750278	26.5038	25.8676929	26.3035221	27.0663605	26.4125	26.461	0.04582363	6.950537788	-1.8779134	3.6754308	367.5430825	0.272076948
Ind	*metG_24*	24.2542019	24.4595413	24.3082008	24.3406	24.3112354	24.3307171	24.3866634	24.3429	24.1131763	24.0936279	23.8692436	24.0253	24.236	0.18268319	4.615176943	0.60467805	0.6576181	65.76181179	1.520639369
Ind	*metG_48*	23.038208	23.1106586	22.9628716	23.0372	22.395546	Undetermine	22.0648232	22.2302	22.8274403	22.9749432	22.8096104	22.8707	22.713	0.42608926	4.105880525	-0.9103332	1.8794795	187.9479539	0.53206219
Ind	*metG_72*	24.8343945	24.65201	24.6916161	24.7260	24.7014904	24.7873554	24.7838688	24.7576	24.8644733	24.7881451	24.8411007	24.8312	24.772	0.05400199	3.524437375	2.65856086	0.1583775	15.83774828	6.314028877
Ind	*metG_96*	24.0261765	24.3628693	24.1366272	24.1752	24.0411777	24.2662373	24.1592331	24.1555	24.0452728	24.2982559	24.2430687	24.1955	24.175	0.01999239	3.383145438	0.69001664	0.6198467	61.98467004	1.613302127

$\Delta Ct(\text{test samples}) = Ct(\text{target gene in test}) - \Delta Ct(\text{reference genes in test})$

$\Delta Ct(\text{calibrator samples}) = Ct(\text{target gene in calibrator}) - \Delta Ct(\text{reference genes in calibrator})$

$\Delta\Delta Ct = \Delta Ct(\text{test samples}) - \Delta Ct(\text{calibrator samples})$

RQ (Relative Quantification) = $2^{-\Delta\Delta Ct}$

Table S 2. Data collected (Ct values) from 11 CRISPRi essential gene mutants under non-inducing conditions across different passages, to calculate relative gene expression using the comparative Ct method.

Sample Name	Target Genes	CT												CT Avg	CT SD	ΔCt(calibrator samples)
		Rep 1				Rep 2				Rep 3						
		T1	T2	T3	Avg	T1	T2	T3	Avg	T1	T2	T3	Avg			
Non-ind	*atpBE_24*	17.00704	17.1920109	17.1836052	17.127552	17.1907864	16.9747353	17.1334038	17.0996418	18.1280155	18.1670914	18.1325836	18.1425635	17.4565858	0.59423802	-0.676352183
Non-ind	*dnaN_24*	19.8576756	19.2629166	19.4607468	19.527113	19.5231056	19.4426575	19.2092648	19.3916759	19.395628	19.3562908	19.3267174	19.3595454	19.4261114	0.08893298	-0.145939933
Non-ind	*gyrB_24*	20.7587166	22.1235218	21.5813904	21.4878763	21.078928	20.4915085	21.357151	21.2180395	21.9827003	21.2943516	23.9968948	21.638526	21.4481472	0.21303992	1.226146062
Non-ind	*gatB_24*	19.8952389	20.2448826	20.075901	20.0720075	20.4522762	20.5285549	20.5084362	20.4964224	20.1198845	20.4473133	20.6128407	20.3933462	20.320592	0.22136369	1.173188527
Non-ind	*dcw_24*	20.1912041	20.0504169	20.2168064	20.1528091	20.0402431	20.2506847	20.1915703	20.1608327	20.2126236	20.016861	19.8008633	20.0101159	20.1079193	0.08479512	1.29202101
Non-ind	*atpBE_48*	17.1652641	17.248764	17.1243973	17.1794751	16.9604778	16.8934135	16.9040527	16.9193147	16.7520752	16.7525463	16.7311935	16.7452717	16.9480205	0.21852043	-2.93554518
Non-ind	*dnaN_48*	20.3627682	20.0776787	20.1738262	20.2047577	20.2295704	20.569416	19.9060173	20.2350012	20.0420971	19.7328472	19.7431355	19.8393599	20.0930396	0.22021288	0.077131907
Non-ind	*gyrB_48*	20.4587784	20.6944599	19.6672268	20.2734884	20.5104694	20.4031315	20.1181107	20.3439039	20.5330238	20.601696	20.4983311	20.5443503	20.3872475	0.14053666	1.878874885
Non-ind	*gatB_48*	21.0428944	20.803318	21.0718346	20.9726823	20.9018841	20.6912861	20.8256245	20.8062649	20.538475	20.8608952	20.8202209	20.7398637	20.8396036	0.11993636	2.519024107
Non-ind	*dcw_48*	20.030777	20.1504211	19.7344685	19.9718889	19.9753819	19.9974117	19.96558	19.9794579	19.3109055	20.097105	20.1951752	19.8677286	19.9396918	0.06243676	0.161522335
Non-ind	*ligA_24*	24.0398293	23.6276951	23.5287838	23.7321027	23.5578632	23.7679157	23.9678593	23.7645461	24.9105415	24.3297081	24.0821095	24.4407864	23.9791451	0.40012207	6.417237812
Non-ind	*engA_24*	21.9676514	21.9198513	22.0552769	21.9809265	22.0540791	21.9177761	21.9745884	21.9821479	22.14011	22.8408489	22.0797424	22.3535671	22.1055472	0.21479245	4.002335654
Non-ind	*ligA_48*	24.8047619	24.4854374	24.783762	24.6913204	24.526165	24.2675438	24.6542664	24.4826584	24.5973873	24.5664101	24.5317497	24.5651824	24.5797204	0.10508795	5.944724613
Non-ind	*engA_48*	20.7985649	20.9828777	20.8433208	20.8749212	21.4964142	21.4752617	21.6559753	21.5425504	21.7853832	21.7599888	21.7414646	21.7622789	21.3932501	0.4621351	3.05267991
Non-ind	*ligA_72*	24.7189999	24.8239937	24.7767658	24.7732531	24.7597542	24.8051281	24.6811962	24.7486928	24.5371933	24.8116665	24.123539	24.4907996	24.6709152	0.15646732	6.299947103
Non-ind	*engA_72*	20.999464	21.3860111	21.5507889	21.312088	21.1021767	20.9273071	21.4757519	21.1684119	21.9119816	21.359684	21.5507851	21.6074835	21.3626611	0.22386204	3.414617327
Non-ind	*parAB_24*	21.6677017	21.9212036	21.7503071	21.7797375	21.7295094	21.9866619	21.9226894	21.8796202	21.9069557	21.8001461	21.8375092	21.8482037	21.8358538	0.05107378	2.828870138
Non-ind	*parAB_48*	21.1204453	20.5373039	20.8806763	20.8461418	20.7721462	20.7481976	20.8063965	20.7755801	20.91749	21.1976528	20.9712925	21.0288118	20.8835112	0.13068637	1.826867421
Non-ind	*parAB_72*	21.9707851	22.2535477	22.2893658	22.1712329	22.1548119	22.29072	22.1914711	22.2123343	22.394659	22.357748	22.3002911	22.3508994	22.2448222	0.09413613	2.772323185
Non-ind	*parAB_96*	22.0006104	21.9344788	22.3368969	22.090662	22.443388	22.3380165	22.1410847	22.3074964	22.609005	22.2082386	22.7143993	22.5105476	22.302902	0.20998052	2.958556917
Non-ind	*parC_24*	24.1274261	23.9504204	24.3343487	24.1373984	24.4284344	24.357296	24.4234543	24.4030615	24.5858421	24.2490234	24.6751022	24.5033226	24.3479275	0.1890898	5.438548406
Non-ind	*parC_48*	25.1365814	25.6014271	25.334343	25.3574505	25.3552914	25.3361588	25.3443375	25.3452625	25.5629559	25.3038559	25.3550377	25.4072831	25.3699987	0.03285929	4.434488085
Non-ind	*parC_72*	26.4840908	26.0081291	25.9417458	26.1446552	26.0386715	26.1640015	26.0892048	26.0972926	26.4330692	26.4906235	26.6734142	26.532369	26.2581056	0.23869668	5.304852804
Non-ind	*parC_96*	26.4337158	25.0159492	24.7575226	25.4023959	24.6685886	24.8299332	24.7842274	24.7609164	24.7583294	24.8930569	24.921669	24.8576851	25.0069991	0.34582509	3.796306186
Non-ind	*trxB_24*	27.1807175	27.0328217	26.9318275	27.0484556	27.0034809	26.6544895	26.6833591	26.7804432	26.6881428	26.5616035	26.4650517	26.5715993	26.800166	0.23903914	6.596085019
Non-ind	*trxB_48*	28.9783382	28.6344299	28.2822647	28.6316776	28.2565498	28.4201927	27.8879948	28.1882458	28.7962627	28.0825272	28.1641502	28.3476467	28.38919	0.22461598	8.69987403
Non-ind	*trxB_72*	28.4974194	28.0479069	28.0994415	28.2149226	28.528244	28.3697968	28.4421234	28.4467214	28.4413795	28.4938602	28.6338482	28.5230293	28.3948911	0.16045942	7.629020691
Non-ind	*trxB_96*	28.0714951	28.3048477	28.3123989	28.2295806	28.7715549	28.0939751	28.294508	28.3866793	28.5041275	28.4709301	28.2228336	28.3992971	28.338519	0.09455415	8.828451157
Non-ind	*metG_24*	23.82658	23.7426243	23.6779022	23.7490355	23.7149239	23.802557	23.4415684	23.6530164	23.7205524	23.2494907	23.5083065	23.4927832	23.6316117	0.12946015	4.010498895
Non-ind	*metG_48*	23.4560661	23.6039848	23.6663113	23.5754541	23.7551537	23.7487278	23.5515137	23.6851317	23.6240635	23.9410725	23.2603912	23.6085091	23.6230316	0.05626255	5.016213735
Non-ind	*metG_72*	22.2612782	21.9959431	22.0409565	22.0993926	21.9021549	22.22645	22.1320057	22.0868702	21.9447498	22.2586212	22.2552471	22.1528727	22.1130452	0.03505536	0.865876516
Non-ind	*metG_96*	23.3001041	23.3055534	23.4854965	23.363718	23.4586849	23.4202518	23.5464993	23.4751453	23.5575809	23.510025	23.7845726	23.6173929	23.4854187	0.12714907	2.693128798

Table S 3. Data collected (Ct values) from 11 CRISPRi essential gene mutants under dCas9-inducing conditions targeting a sigma factor as an internal control across different passages to calculate relative gene expression using the comparative Ct method.

Sample Name	Target Genes	CT												CT Avg
		Rep 1				Rep 2				Rep 3				
		Ct1	Ct2	Ct3	Avg	Ct1	Ct2	Ct3	Avg	Ct1	Ct2	Ct3	Avg	
sigE +	*atpBE_24*	17.52996826	18.4570675	18.1278629	18.0382996	17.9676056	18.3382072	18.1751766	18.1603298	18.188158	18.2742386	18.1381569	18.2001845	18.132938
sigE +	*dnaN_24*	19.83037949	19.7381229	19.2836037	19.6173687	19.5479183	19.476532	19.6679497	19.5641333	19.4980392	19.5807133	19.5252037	19.5346521	19.5720514
sigE +	*gyrB_24*	20.30334854	20.2381115	20.2722092	20.2712231	20.3175793	20.5607605	20.2565994	20.3783131	19.6029358	20.1695137	20.2769527	20.0164674	20.2220012
sigE +	*gatB_24*	19.05046463	18.9448872	19.3706455	19.1219991	18.9422836	19.5337849	18.9682388	19.1481024	18.9943295	19.2693386	19.2526588	19.172109	19.1474035
sigE +	*dcw_24*	18.74577904	18.8821793	18.6563492	18.7614358	18.8467236	18.7055168	18.8595791	18.8039398	18.8754196	18.9258595	18.8456783	18.8823191	18.8158983
sigE +	*atpBE_48*	20.04813576	20.1225529	20.0843925	20.0850271	19.8770504	19.967865	20.065588	19.9701678	19.558176	19.675106	19.5532246	19.5955022	19.8835657
sigE +	*dnaN_48*	20.24504089	20.0499077	20.0668621	20.1206036	19.9933891	20.0419559	19.9622707	19.9992053	19.9450912	19.8848591	19.9537926	19.9279143	20.0159077
sigE +	*gyrB_48*	18.9599762	18.5956936	18.711607	18.7557589	18.3962421	18.6975212	18.209837	18.4345334	18.0306244	18.5718594	18.4019928	18.3348255	18.5083726
sigE +	*gatB_48*	17.86261749	18.3937759	18.1058006	18.1207314	18.3329678	18.2777691	18.6192894	18.4100087	18.3045712	18.394022	18.5944023	18.4309985	18.3205795
sigE +	*dcw_48*	19.96414375	19.9080296	19.6630383	19.8450705	19.9476967	19.9692345	19.8013535	19.9060949	19.2852879	20.0096092	19.4551315	19.5833429	19.7781694
sigE +	*ligA_24*	17.71389198	17.6193981	17.6657505	17.6663469	17.5064487	17.5908298	17.5209408	17.5394065	17.4253616	17.5869141	17.4276295	17.4799684	17.5619072
sigE +	*engA_24*	17.79661179	18.1255665	17.7853546	17.902511	18.1048203	18.3108406	18.2544422	18.2233677	18.3041782	18.0320225	18.2150669	18.1837559	18.1032115
sigE +	*ligA_48*	18.77375221	18.7168007	18.8706112	18.7870547	18.6150894	18.7675323	18.3107128	18.5644449	18.3625984	18.5442142	18.7536507	18.5534878	18.6349958
sigE +	*engA_48*	18.5314064	18.3226051	18.4113159	18.4217758	18.5628128	18.8083496	18.5314445	18.6342023	17.9917202	17.9265079	17.9789696	17.9657326	18.3405702
sigE +	*ligA_72*	18.52718163	18.4554729	18.4413013	18.474652	18.3211994	18.3753033	18.3613377	18.3526134	18.3663654	18.2894592	18.2010918	18.2856388	18.3709681
sigE +	*engA_72*	18.00193596	17.7901325	17.962204	17.9180908	17.8155708	17.8269043	18.240675	17.96105	17.9500446	17.9667168	17.9782104	17.9649906	17.9480438
sigE +	*parAB_24*	19.10668373	19.1105747	19.1696167	19.1289584	18.0210323	19.0819435	19.0579891	18.7203217	19.2813892	19.0242023	19.2094212	19.1716709	19.0069837
sigE +	*parAB_48*	19.62987137	19.1569176	19.1638336	19.3168742	18.389492	18.4246674	18.241724	18.3519611	19.0384121	19.7177029	19.7471733	19.5010961	19.0566438
sigE +	*parAB_72*	19.77316284	19.3775215	19.5857658	19.5788167	19.145977	19.231308	19.7937622	19.3903491	19.6404495	19.3264465	19.3780975	19.4483312	19.472499
sigE +	*parAB_96*	19.64496803	19.087204	19.5380116	19.4233945	19.7108612	19.0795135	19.6066608	19.4656785	19.1614647	18.8653946	19.4050274	19.1439622	19.3443451
sigE +	*parC_24*	18.885849	18.934248	18.9988346	18.9396439	18.9634724	19.0706673	18.7094193	18.9145196	18.9225006	18.9798355	18.7195854	18.8739738	18.9093791
sigE +	*parC_48*	20.77205467	20.9502144	20.9574261	20.8932317	20.9512749	20.7908688	21.043314	20.9284859	20.8260059	21.0282478	21.1001892	20.9848143	20.9355106
sigE +	*parC_72*	20.56778336	20.7744884	20.68009	20.6741206	20.9775276	20.9601059	21.0037422	20.9804586	21.3330555	21.1107693	21.1717129	21.2051792	20.9532528
sigE +	*parC_96*	20.88072395	20.9737663	21.159586	21.0046921	21.1887894	21.2927361	21.3633823	21.2816359	21.4119396	21.4651127	21.1602001	21.3457508	21.2106929
sigE +	*trxB_24*	19.95870972	20.2529621	20.5064735	20.2393818	20.0154381	20.221735	20.1062698	20.114481	20.2226639	20.2932472	20.2592297	20.2583803	20.204081
sigE +	*trxB_48*	19.60082626	19.8623829	19.6424561	19.7018884	19.422493	19.743433	19.7895317	19.6518192	19.6123276	19.7614346	19.768959	19.7142404	19.689316
sigE +	*trxB_72*	20.55774689	20.667078	21.0775928	20.7674726	20.9090462	20.9925556	20.5897808	20.8304609	20.7027016	20.5040722	20.8922596	20.6996778	20.7658704
sigE +	*trxB_96*	19.15276146	19.4248657	19.1944313	19.2573528	19.3053112	19.2806168	19.8562927	19.4807402	19.7338581	19.9534492	19.689024	19.7921104	19.5100678
sigE +	*metG_24*	20.18387032	20.1084175	19.1889038	19.8270639	19.5755901	19.6916695	20.1656609	19.8109735	19.0733891	19.5166588	19.0858555	19.2253011	19.6211128
sigE +	*metG_48*	18.70789719	18.2833881	19.7757549	18.9223468	18.3137455	18.4690475	18.2800198	18.3542709	18.7665195	18.428091	18.4368973	18.543836	18.6068179
sigE +	*metG_72*	21.08831215	21.2605534	21.327261	21.2253755	21.3126659	21.2264957	21.2891502	21.276104	21.2209339	21.3630352	21.1361103	21.2400265	21.2471686
sigE +	*metG_96*	20.73831749	20.8033886	20.8402081	20.7939714	20.7951012	20.9075165	20.6980553	20.8002243	20.9128742	20.9226551	20.5124931	20.7826742	20.7922899

Table S 4 . Single Nucleotide Polymorphisms (SNPs) Analysis from Pairwise Alignment between parental (0% rhamnose) and passage one (0.5% rhamnose) strains from CRISPRi *atpB* mutant.

#	Nucleotide in parental strain	Nucleotide in evolved strain	Mutation type	Mutation effect	Locus Tag	Gene
Chromosome 1						
1	t	a	Substitution	None	NA	NA
2	.	g	Insertion	None	NA	NA
3	g	a	Substitution	None	NA	NA
4	t	.	Deletion	None	NA	NA
5	a	.	Deletion	None	NA	NA
6	a	.	Deletion	None	NA	NA
7	t	.	Deletion	None	NA	NA
8	.	g	Insertion	None	NA	NA
9	c	.	Deletion	Frameshift in reading frame	K562_RS04280	Polysaccharide deacetylase family protein
10	.	g	Insertion	None	NA	NA
11	.	a	Insertion	None	NA	NA
12	t	g	Substitution	Missense	K562_RS00935	Site-specific integrase
13	.	g	Insertion	None	NA	NA
14	.	t	Insertion	None	NA	NA
Chromosome 2						
1	c	.	Deletion	Frameshift in reading frame	**K562_RS28860**	**Porin**
2	c	g	Substitution	Missense	**K562_RS28860**	**Porin**
3	t	.	Deletion	None	NA	NA
4	.	g	Insertion	None	NA	NA
5	t	.	Deletion	Frameshift in reading frame	**K562_RS20940**	**LysR family transcriptional regulator**
6	t	c	Substitution	Missense	**K562_RS20940**	**LysR family transcriptional regulator**
7	.	t	Insertion	None	NA	NA
Chromosome 3						
1	.	c	Insertion	None	NA	NA
Megaplasmid: No mutations detected						
Plasmid (pgRNA): No mutations detected						

Table S 5. Single Nucleotide Polymorphisms (SNPs) Analysis from Pairwise Alignment between parental (0% rhamnose) and passage one (0.5% rhamnose) strains from CRISPRi *dcw* mutant.

#	Nucleotide in parental strain	Nucleotide in evolved strain	Mutation	Effect	Locus Tag	Gene
Chromosome 1						
1	.	a	Insertion	None	NON CDS	NA
2	.	a	Insertion	None	NON CDS	NA
3	.	a	Insertion	None	NON CDS	NA
4	.	g	Insertion	None	NON CDS	NA
5	.	t	Insertion	None	NON CDS	NA
6	.	c	Insertion	Frameshift in reading frame	K562_RS01030	DUF2957 domain-containing protein
7	t	.	Deletion	None	NON CDS	NA
8	.	a	Insertion	None	NON CDS	NA
9	.	a	Insertion	None	NON CDS	NA
10	.	a	Insertion	None	NON CDS	NA
11	.	g	Insertion	None	NON CDS	NA
12	.	g	Insertion	None	NON CDS	NA
13	c	.	Deletion	Frameshift in reading frame	K562_RS12695	UvrD-helicase domain-containing protein
Chromosome 2						
1	.	c	Insertion	None	NON CDS	NA
2	g	.	Deletion	Frameshift in reading frame	K562_RS28815	mauD (methylamine dehydrogenase accessory protein)
3	.	a	Insertion	None	NON CDS	NA
4	.	c	Insertion	None	NON CDS	NA
5	t	.	Deletion	None	NON CDS	NA
6	.	c	Insertion	Frameshift in reading frame	K562_RS18055	mqo (malate dehydrogenase)
7	.	t	Insertion	Frameshift in reading frame	**K562_RS18170**	**LysR family transcriptional regulator**
8	a	g	Substitution	Missense	**K562_RS20940**	**LysR family transcriptional regulator**
9	a	.	Deletion	Frameshift in reading frame	**K562_RS20940**	**LysR family transcriptional regulator**

Chromosome 3						
1	.	c	Insertion	Frameshift in reading frame	K562_RS33215	Autotransporter-associated beta strand repeat-containing protein
2	a	.	Deletion	None	NA	NA
Megaplasmid						
1	g	.	Deletion	None	NON CDS	NA
2	.	c	Insertion	None	NON CDS	NA
Plasmid (pgRNA): No mutations detected						

Table S 6. SNP Single Nucleotide Polymorphisms (SNPs) Analysis from Pairwise Alignment between Parental and Passage 1 strains from CRISPRi *gatB* mutant.

#	Nucleotide in parental strain	Nucleotide in evolved strain	Mutation	Effect	Locus Tag	Gene
Chromosome 1						
1	.	a	Insertion	None	NON CDS	NA
2	.	g	Insertion	None	NON CDS	NA
3	.	c	Insertion	None	NON CDS	NA
4	.	c	Insertion	Frameshift in reading frame	K562_RS12695	UvrD-helicase domain-containing protein
5	g	.	Deletion	Frameshift in reading frame	K562_RS12890	IS66-like element ISBcen19 family transposase
6	.	c	Insertion	None	NON CDS	NA
7	c	.	Deletion	None	NON CDS	NA
8	.	a	Insertion	None	NON CDS	NA
9	.	g	Insertion		K562_RS13495	
10	c	.	Deletion	None	NON CDS	NA
11	.	t	Insertion	None	NON CDS	NA
12	.	t	Insertion	None	NON CDS	NA
13	c	g	Substitution	Missense	K562_RS06160	ABC transporter permease
14	c	.	Deletion	Frameshift in reading frame	K562_RS30545	IS3-like element ISBcen9 family transposase
Chromosome 2						
1	a	.	Deletion	None	NON CDS	NA

2	a	.	Deletion	None	NON CDS	NA
3	g	.	Deletion	None	NON CDS	NA
4	g	c	Substitution	Silent	**K562_RS28860**	**Porin**
5	g	.	Deletion	None	NON CDS	NA
6	.	a	Insertion	None	NON CDS	NA
7	.	g	Insertion	None	NON CDS	NA
8	t	g	Substitution	Missense	K562_RS26990	Efflux RND transporter periplasmic adaptor subunit
Chromosome 3: No mutations detected						
Megaplasmid						
1	t	.	Deletion	None	NON CDS	NA
2	a	.	Deletion	None	NON CDS	NA
Plasmid (pgRNA): No mutations detected						

Table S 7. Single Nucleotide Polymorphisms (SNPs) Analysis from Pairwise Alignment between parental (0% rhamnose) and passage one (0.5% rhamnose) strains from CRISPRi *gyrB* mutant.

#	Nucleotide in parental strain	Nucleotide in evolved strain	Mutation	Effect	Locus Tag	Gene
Chromosome 1						
1	a	.	Deletion	None	NON CDS	NA
2	.	g	Insertion	None	NON CDS	NA
3	c	.	Deletion	Frameshift in reading frame	K562_RS10405	Sugar ABC transporter ATP-binding protein
4	.	t	Insertion	None	NON CDS	NA
5	.	c	Insertion	None	NON CDS	NA
6	c	t	Substitution	None	NON CDS	NA
7	c	g	Substitution	Missense	K562_RS04725	Hypothetical protein
8	a	.	Deletion	None	NON CDS	NA
9	.	g	Insertion	Frameshift in reading frame	K562_RS01770	tssK (type VI secretion system baseplate subunit TssK)
10	.	g	Insertion	None	NON CDS	NA
11	g	t	Substitution	Silent	K562_RS00935	Site-specific integrase
12	.	a	Insertion	None	NON CDS	NA
13	.	t	Insertion	Frameshift in reading frame	K562_RS00260	ABC transporter substrate-binding protein
14	.	t	Insertion	None	NON CDS	NA

15	.	g	Insertion	Frameshift in reading frame	K562_RS14875	MFS transporter
16	.	t	Insertion	None	NON CDS	NA
17	.	t	Insertion	None	NON CDS	NA
Chromosome 2						
1	g	c	Substitution	Missense	**K562_RS28860**	**Porin**
2	.	t	Insertion	None	NON CDS	NA
3	.	g	Insertion	None	NON CDS	NA
4	g	.	Deletion	None	NON CDS	NA
5	.	a	Insertion	None	NON CDS	NA
6	.	g	Insertion	None	NON CDS	NA
7	t	g	Substitution	Missense	K562_RS26990	efflux RND transporter periplasmic adaptor subunit
8	c	t	Substitution	Missense	**K562_RS20940**	**LysR family transcriptional regulator**
9	.	c	Insertion	Frameshift in reading frame	K562_RS18630	TIGR00730 family Rossman fold protein
10	.	t	Insertion	Frameshift in reading frame	K562_RS18470	3-oxoacyl-ACP synthase
11	g	.	Deletion	None	NON CDS	NA
12	.	c	Insertion	None	NON CDS	NA
13	.	a	Insertion	None	NON CDS	NA
14	a	.	Deletion	None	NON CDS	NA
15	g	.	Deletion	None	NON CDS	NA
Chromosome 3						
1	.	c	Insertion		K562_RS31725	IS3 family transposase
2	.	c	Insertion		K562_RS34220	Group II intron reverse transcriptase
3	a	.	Deletion	None	NON CDS	NA
Megaplasmid: No mutations detected						
Plasmid (pgRNA): No mutations detected						

Table S 8. Single Nucleotide Polymorphisms (SNPs) Analysis from Pairwise Alignment between parental (0% rhamnose) and passage one (0.5% rhamnose) strains from CRISPRi *dnaN* mutant.

#	Nucleotide in parental strain	Nucleotide in evolved strain	Mutation	Effect	Locus Tag	Gene
Chromosome 1						
1	g	.	Deletion	None	NON CDS	NA
2	c	.	Deletion	None	NON CDS	NA
3	.	g	Insertion	None	NON CDS	NA
4	t	.	Deletion	None	NON CDS	NA
5	c	.	Deletion	Frameshift in reading frame	K562_RS07970	ABC transporter ATP-binding protein
6	g	.	Deletion	Frameshift in reading frame	K562_RS07545	PAS domain S-box protein
7	a	.	Deletion	None	NON CDS	NA
8	.	a	Insertion	None	NON CDS	NA
9	g	t	Substitution	Silent	K562_RS00935	Site-specific integrase
Chromosome 2						
1	c	.	Deletion	None	NON CDS	NA
2	.	a	Insertion	None	NON CDS	NA
3	g	.	Deletion	Frameshift in reading frame	**K562_RS28860**	**Porin**
4	c	.	Deletion	Frameshift in reading frame	K562_RS30545	IS3-like element ISBcen9 family transposase
5	g	.	Deletion	None	NON CDS	NA
6	g	.	Deletion	None	NON CDS	NA
7	t	.	Deletion	None	NON CDS	NA
8	.	c	Insertion	Frameshift in reading frame	K562_RS20285	ABC transporter ATP-binding protein
Chromosome 3						
1	t	.	Deletion	Frameshift in reading frame	K562_RS32635	Hypothetical protein
Megaplasmid: No mutations detected						
Plasmid (pgRNA): No mutations detected						

Table S 9. SNP Single Nucleotide Polymorphisms (SNPs) Analysis from Pairwise Alignment between Parental and Passage 1 strains from CRISPRi NTC mutant.

#	Nucleotide in parental strain	Nucleotide in evolved strain	Mutation	Effect	Locus Tag	Gene
Chromosome 1						
1	g	.	Deletion	None	NON CDS	NA
2	.	t	Insertion	None	NON CDS	NA
3	c	.	Deletion	Frameshift in reading frame	K562_RS07970	ABC transporter ATP-binding protein
4	c	.	Deletion	Frameshift in reading frame	K562_RS05590	nadB (L-aspartate oxidase)
5	.	a	Insertion	None	NON CDS	NA
6	.	a	Insertion	None	NON CDS	NA
7	g	t	Substitution	Missense	K562_RS00935	Site-specific integrase
8	.	c	Insertion	Frameshift in reading frame	K562_RS05645	IS3-like element ISBcen9 family transposase
9	c	.	Deletion	None	NON CDS	NA
10	g	a	Substitution	None	NON CDS	NA
11	t	.	Deletion	None	NON CDS	NA
12	a	.	Deletion	None	NON CDS	NA
13	a	.	Deletion	None	NON CDS	NA
14	.	t	Insertion	None	NON CDS	NA
15	.	g	Insertion	None	NON CDS	NA
Chromosome 2						
1	.	c	Insertion	Frameshift in reading frame	**K562_RS28860**	**Porin**
2	c	g	Substitution	Missense	**K562_RS2886**1	**Porin**
3	c	.	Deletion	Frameshift in reading frame	K562_RS18630	TIGR00730 family Rossman fold protein
4	g	.	Deletion	None	NON CDS	NA
Chromosome 3: No mutations detected						
Megaplasmid						
1	g	.	Deletion	Frameshift in reading frame	K562_RS34965	*traH* (conjugal transfer protein)
2	.	c	Insertion	None	NON CDS	NA
Plasmid (pgRNA)						
1	g	.	Deletion	Frameshift in reading frame	NA	*dhfr*, trimethoprim resistance gene

6.2 Supplementary figures

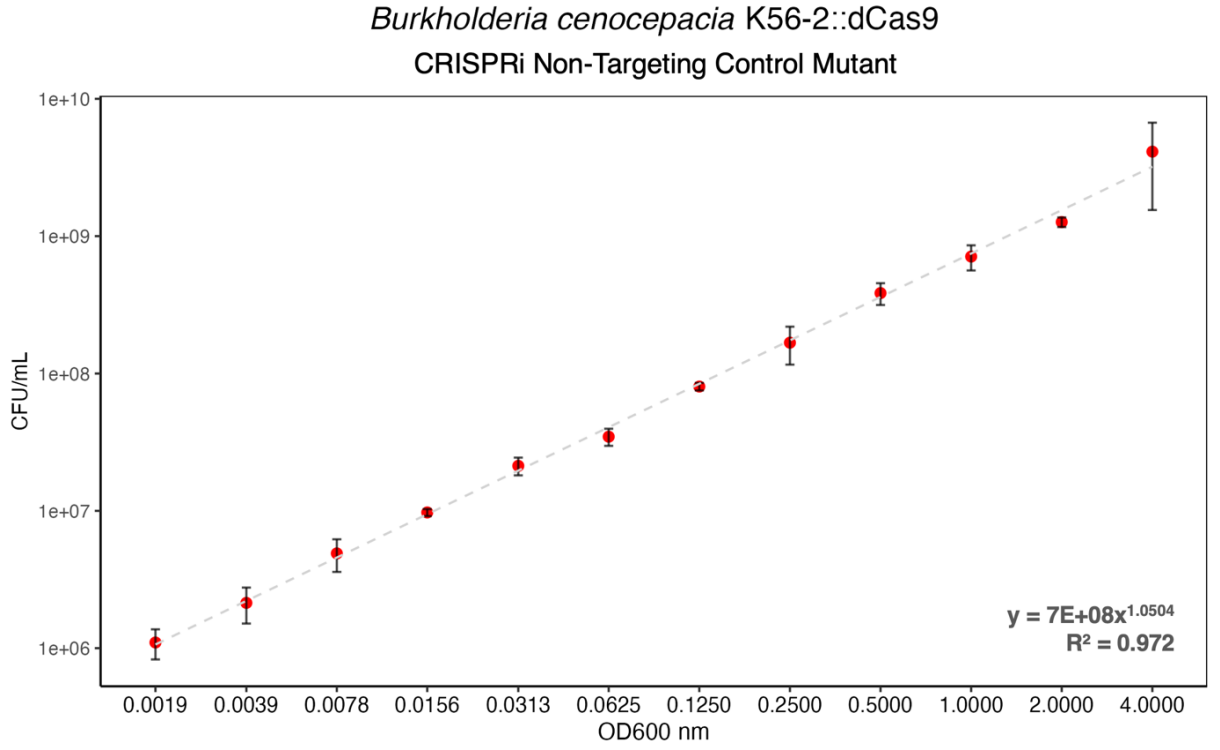

Figure S1. CFU/mL vs Optical Density (OD) in *B. cenocepacia* K56-2::dCas9.

A standard curve was generated using a CRISPRi Non-Targeting Control mutant to assess viable cells by counting colony-forming units (CFU) at different optical densities measured at a wavelength of 600 nm. An initial optical density from an overnight culture (37°C with shaking at 230) was measured (OD_{600nm} 4), followed by 10-fold serial dilutions. A volume of 100 µL was plated onto rich medium agar plates, and colonies between 30 and 300 were counted. Plates were grown at 37°C for two days before colony count. A power equation and R^2 are shown in the right corner. Error bars represent the SD ± mean of three independent biological replicates.

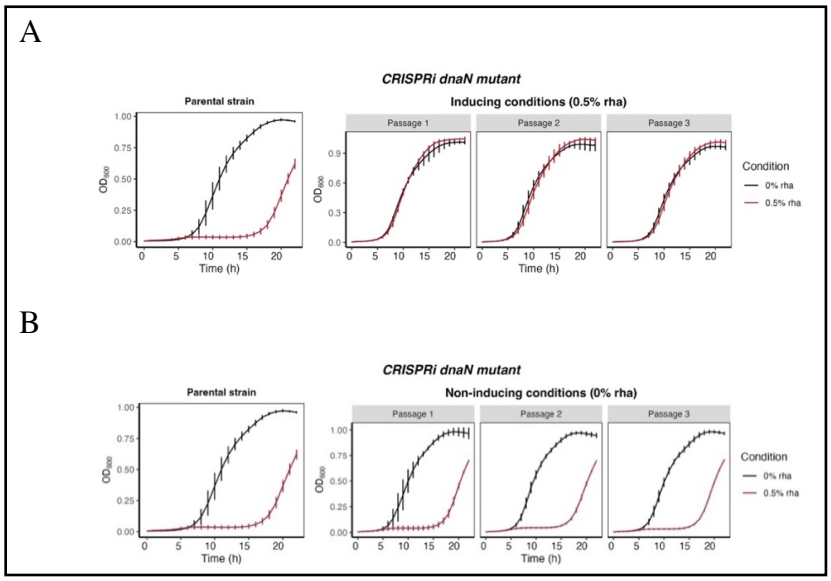

Figure S2. Short-term evolution experiment for CRISPRi *dnaN* mutant under dCas9-inducing and non-inducing conditions.

(A) CGP loss is observed under consistent dCas9-inducing conditions after one bacterial passage. (B) CGP is maintained across bacterial passages under non-inducing conditions. Error bars represent the SD ± mean of three independent biological replicates.

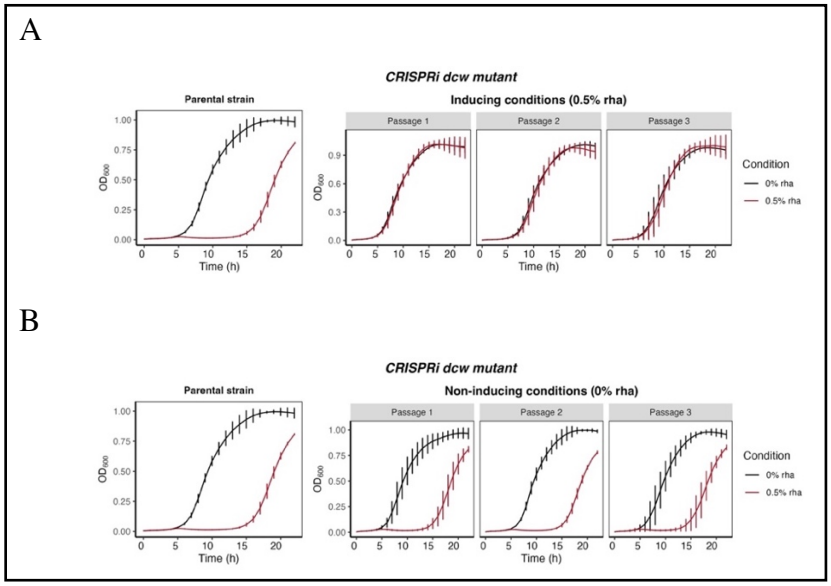

Figure S3. Short-term evolution experiment for CRISPRi *dcw* mutant under dCas9-inducing and non-inducing conditions.

(A) CGP loss is observed under consistent dCas9-inducing conditions after one bacterial passage. (B) CGP is maintained across bacterial passages under non-inducing conditions. Error bars represent the SD ± mean of three independent biological replicates.

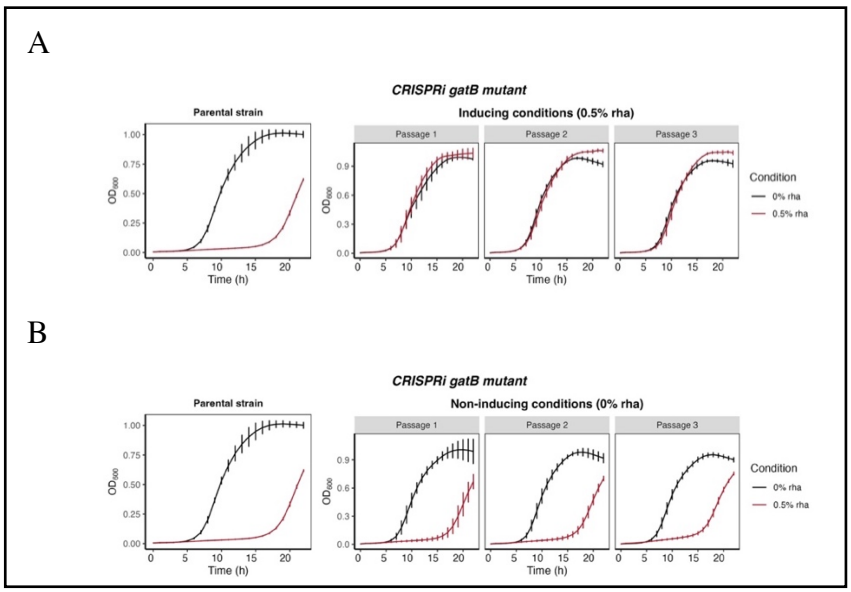

Figure S4. Short-term evolution experiment for CRISPRi *gatB* mutant under dCas9-inducing and non-inducing conditions.

(A) CGP loss is observed under consistent dCas9-inducing conditions after one bacterial passage. (B) CGP is maintained across bacterial passages under non-inducing conditions. Error bars represent the SD ± mean of three independent biological replicates.

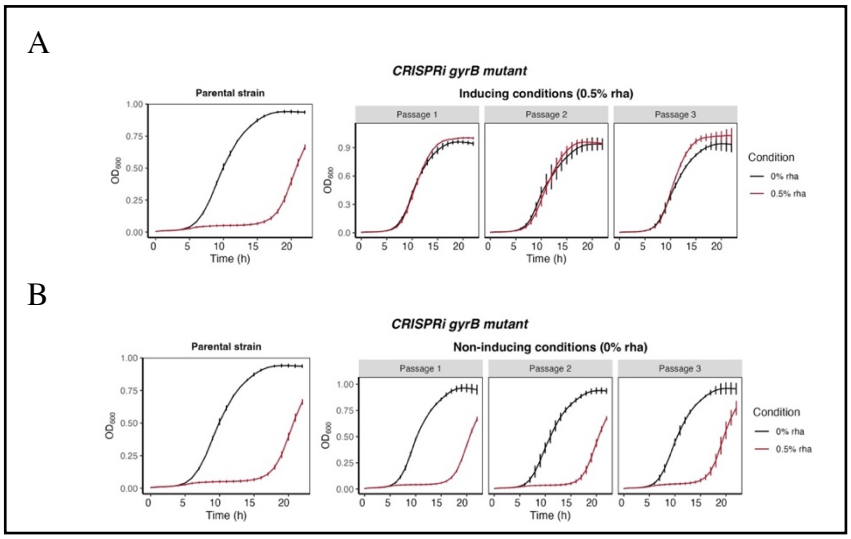

Figure S5. Short-term evolution experiment for CRISPRi gyrB mutant under dCas9-inducing and non-inducing conditions.

(A) CGP loss is observed under consistent dCas9-inducing conditions after one bacterial passage. (B) CGP is maintained across bacterial passages under non-inducing conditions. Error bars represent the SD ± mean of three independent biological replicates.

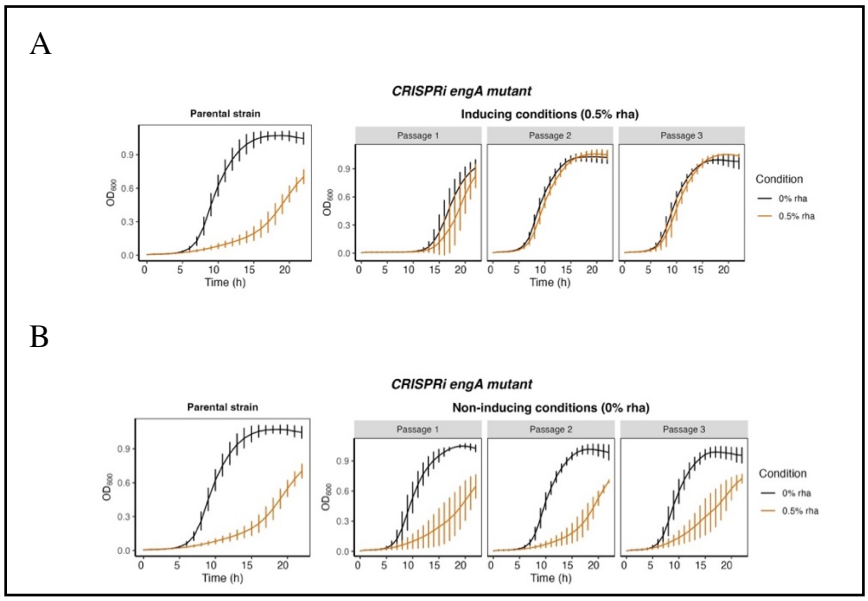

Figure S6. Short-term evolution experiment for CRISPRi *engA* mutant under dCas9-inducing and non-inducing conditions.

(A) CGP loss is observed under consistent dCas9-inducing conditions after two bacterial passages. (B) CGP is maintained across bacterial passages under non-inducing conditions. Error bars represent the SD ± mean of three independent biological replicates.

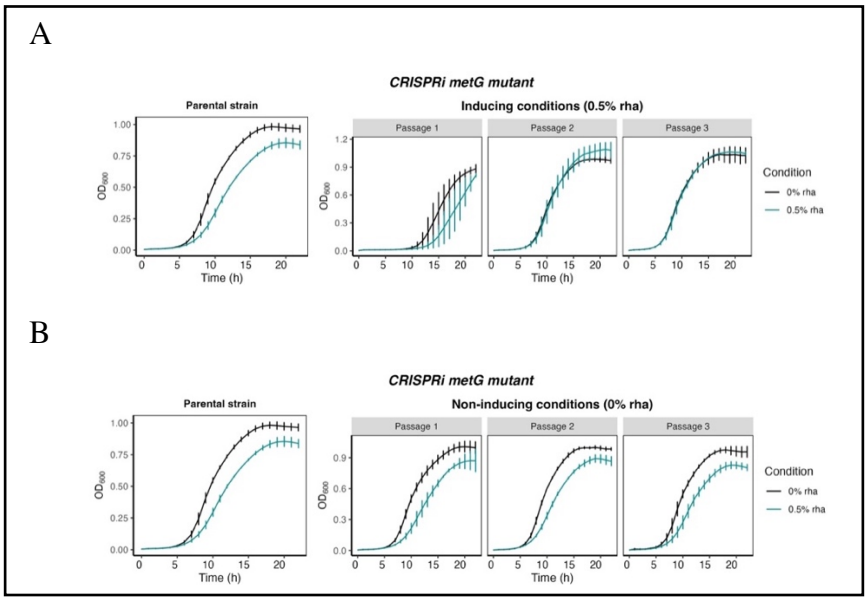

Figure S7. Short-term evolution experiment for CRISPRi *metG* mutant under dCas9-inducing and non-inducing conditions.

(A) CGP loss is observed under consistent dCas9-inducing conditions after two bacterial passages. (B) CGP is maintained across bacterial passages under non-inducing conditions. Error bars represent the SD ± mean of three independent biological replicates.

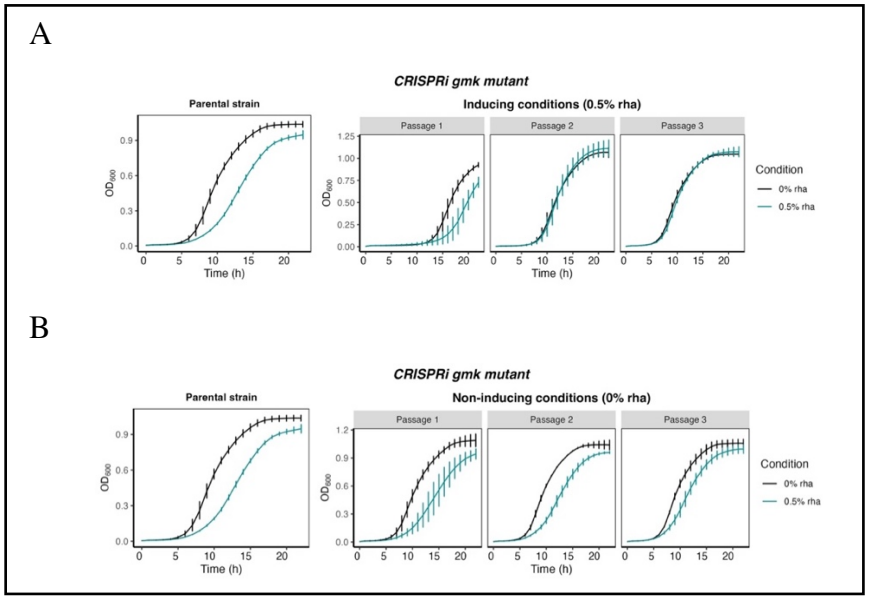

Figure S8. Short-term evolution experiment for CRISPRi *gmk* mutant under dCas9-inducing and non-inducing conditions.

(A) CGP loss is observed under consistent dCas9-inducing conditions after two bacterial passages. (B) CGP is maintained across bacterial passages under non-inducing conditions. Error bars represent the SD ± mean of three independent biological replicates.

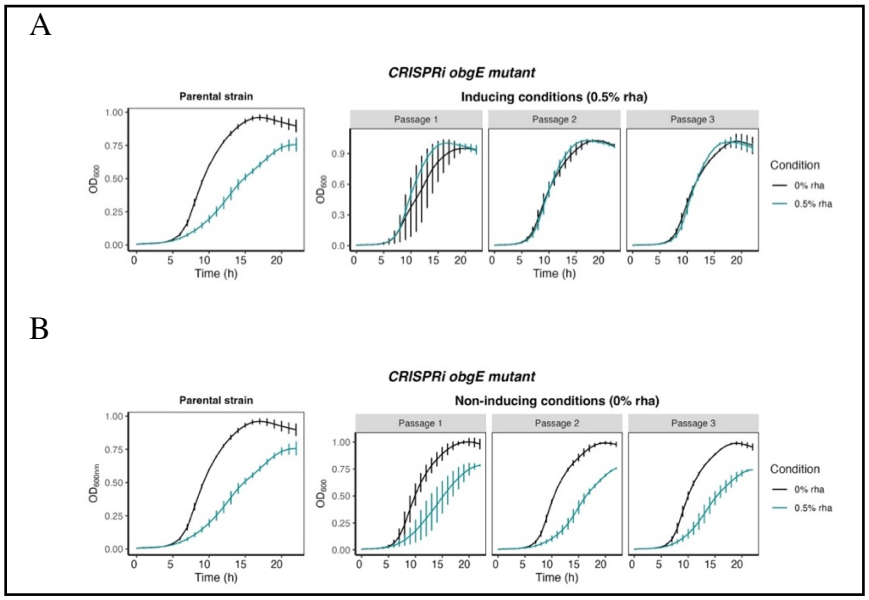

Figure S9. Short-term evolution experiment for CRISPRi *obgE* mutant under dCas9-inducing and non-inducing conditions.

(A) CGP loss is observed under consistent dCas9-inducing conditions after one bacterial passage. (B) CGP is maintained across bacterial passages under non-inducing conditions. Error bars represent the SD ± mean of three independent biological replicates.

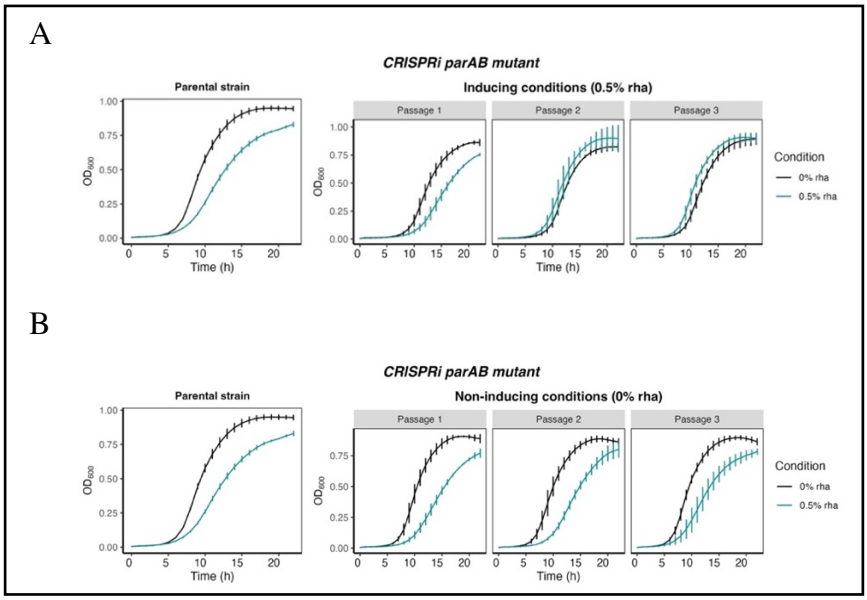

Figure S10. Short-term evolution experiment for CRISPRi *parAB* mutant under dCas9-inducing and non-inducing conditions.

(A) CGP loss is observed under consistent dCas9-inducing conditions after two bacterial passages. (B) CGP is maintained across bacterial passages under non-inducing conditions. Error bars represent the SD ± mean of three independent biological replicates.

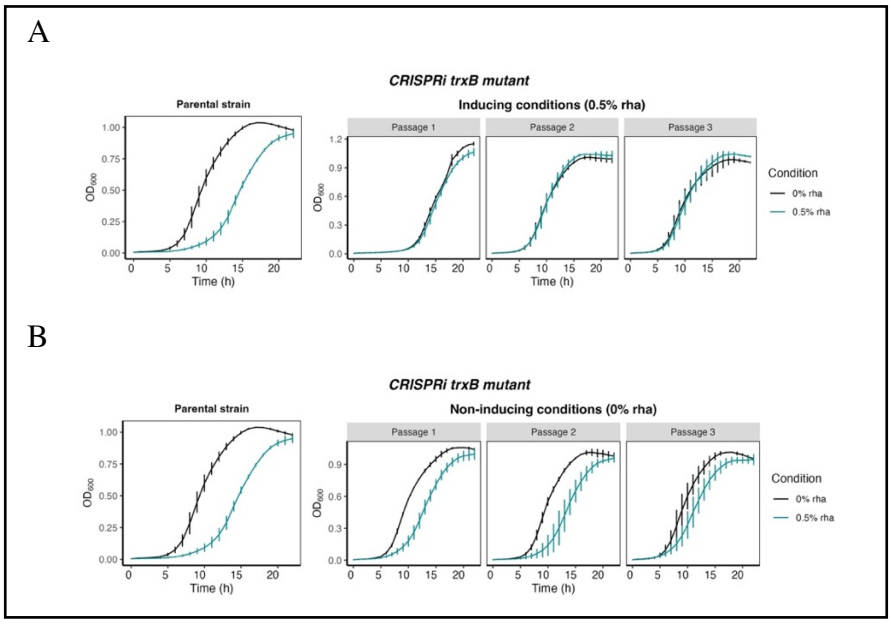

Figure S11. Short-term evolution experiment for CRISPRi *trxB* mutant under dCas9-inducing and non-inducing conditions.

(A) CGP loss is observed under consistent dCas9-inducing conditions after three bacterial passages. (B) CGP is maintained across bacterial passages under non-inducing conditions. Error bars represent the SD ± mean of three independent biological replicates.

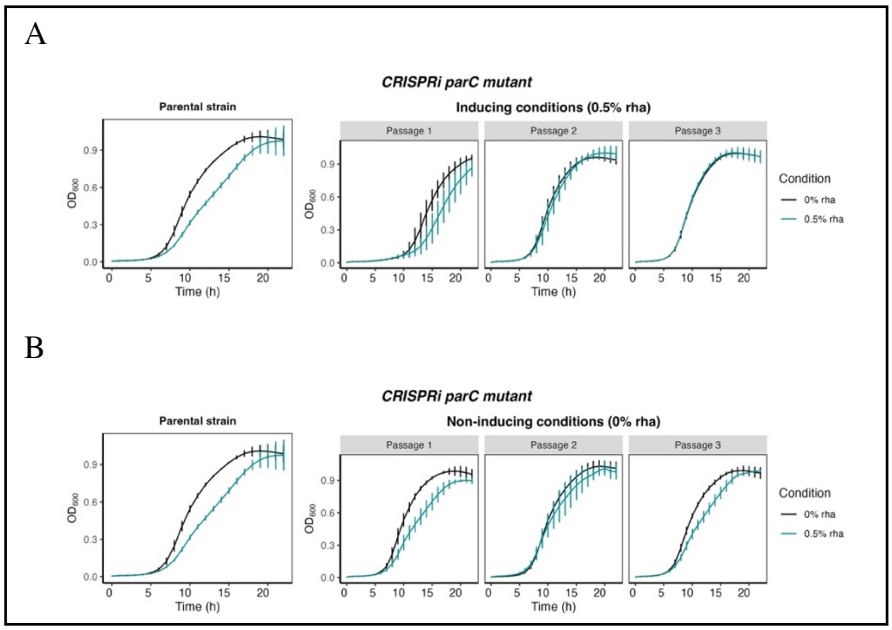

Figure S12. Short-term evolution experiment for CRISPRi *parC* mutant under dCas9-inducing and non-inducing conditions.

(A) CGP loss is observed under consistent dCas9-inducing conditions after two bacterial passages. (B) CGP is maintained across bacterial passages under non-inducing conditions. Error bars represent the SD ± mean of three independent biological replicates.

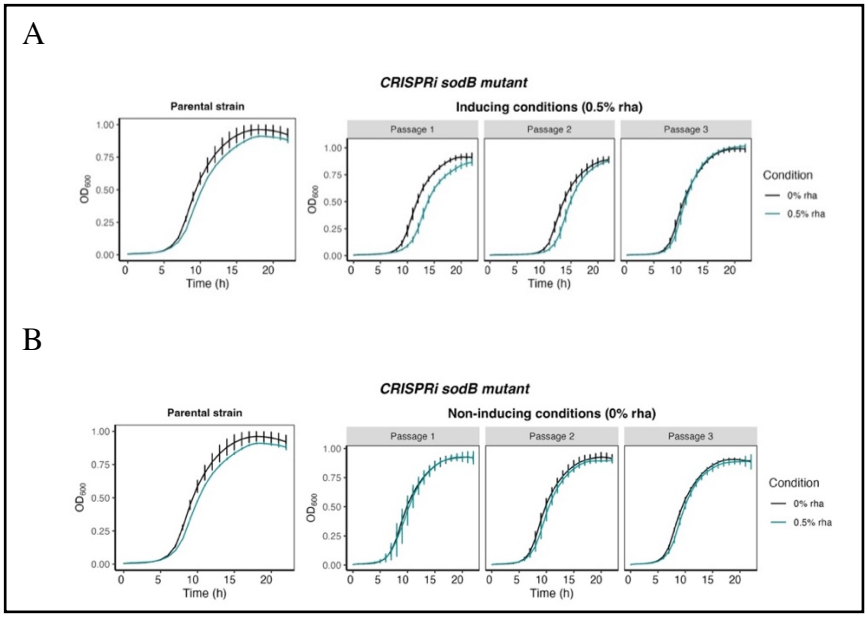

Figure S13. Short-term evolution experiment for CRISPRi *sodB* mutant under dCas9-inducing and non-inducing conditions.

(A) CGP loss is observed under consistent dCas9-inducing conditions after three bacterial passages. (B) CGP is maintained across bacterial passages under non-inducing conditions. Error bars represent the SD ± mean of three independent biological replicates.

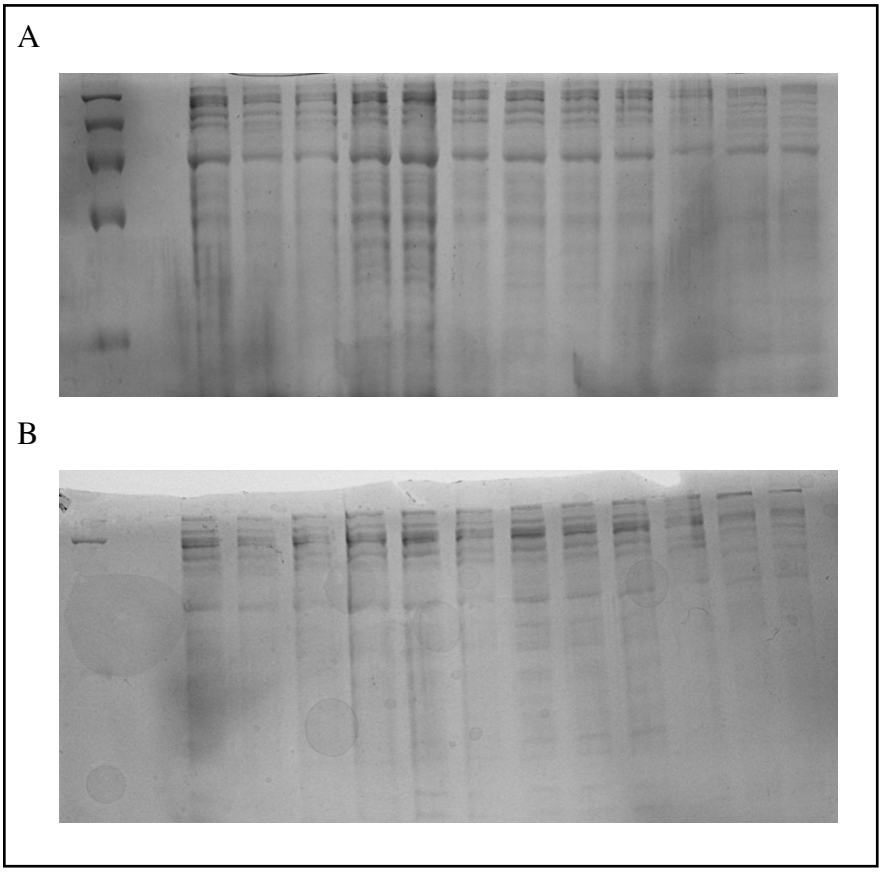

Figure S14. SDS-PAGE loading controls for total protein confirmation.

(A) SDS-PAGE gel stained with Coomassie to demonstrate equal loading before transfer to the polyvinylidene difluoride (PVDF) membrane. (B) SDS-PAGE gel stained with Coomassie after transferring to the PVDF membrane presents the absence of the ladder, demonstrating successful transfer. The first row contains the ladder; the second contains a purified dCas9 control, and the samples are in the same order as in Figure 1.

CHAPTER 7: REFERENCES

1. Acevedo-Rocha, C. G., Fang, G., Schmidt, M., Ussery, D., & Danchin, A. 2013. From essential to persistent genes: a functional approach to constructing synthetic life. *Trends in Genetics*, **29**(5): 273-279. Doi: 10.1016/j.tig.2012.11.001
2. Arnolds K., Dahlin L., Ding L., Wu C., Yu J., Xiong W., Zuniga C., Suzuki Y., Zengler K., Linger J. & Guarnieri M. 2021. Biotechnology for secure biocontainment designs in an emerging bioeconomy. *Current opinion in Biotechnology*, **71**: 25-31. Doi: 10.1016/j.copbio.2021.05.004
3. Azami N.A., Wirjon I.A., Kannusamy S., Teh A. & Abdullah A.A. 2017. Enhanced degradation of polyhydroxyalkanoates (PHAs) by newly isolated *Burkholderia cepacia* DP1 with high depolymerase activity. *Springer Biotech,* **7**:75. Doi: 10.1007/s13205-017-0716-7
4. Baugh A.C., Momany C. & Neidle E.L. 2023. Versatility and Complexity: Common and Uncommon Facets of LysR-Type Transcriptional Regulators. *Annual Review of Microbiology*, **77**: 317-339. Doi:10.116/annurev-micro-050323040543
5. Bengtsson M., Hemberg M., Rorsman P. & Ståhlberg. 2008. Quantification of mRNA in single cells and modelling of RT-qPCR induced noise. *BMC Molecular Biology*, **9**:63. Doi:10.1186/1471-2199-9-63
6. Bernier S.P., Nguyen D. & Sokol P.A. 2008. A LysR-Type Transcriptional Regulator in *Burkholderia cenocepacia* Influences Colony Morphology and Virulence. *Infection and Immunity*, 76: 38-47. Doi: 10.1128/iai.00874-07
7. Bervoets I. & Cahrlier D. 2019. Diversity, versatility and complexity of bacterial gene regulation mechanisms: opportunities and drawbacks for applications in synthetic biology. *FEMS Microbiology Reviews*, **43:** 304–339. Doi: 10.1093/femsre/fuz001
8. Beuter D., Gomes-Filho J.V., Randau L., Díaz-Pascual F., Drescher K. & Link H. 2018. Selective Enrichment of Slow-Growing Bacteria in a Metabolism Wide CRISPRi Library with a TIMER Protein. *ACS Synth. Biol.*, **7**: 2775-2782. Doi: 10.1021/acssynbio.8b00379
9. Bloodworth R.A., Gislason A.S. & Cardona S.T. 2013. *Burkholderia cenocepacia* conditional growth mutant library created by random promoter replacement of essential genes. *Microbiology Open,* **2**(2): 243–258. Doi: 10.1002/mbo3.71

10. Bloodworth, R.A., Selin,C., Lopez De Volder,M.A., Degrossi,J., Drevinek,P., Galanternik,L., Cardona, S.T. 2015. Draft genome sequences of the *Burkholderia contaminans* strains LMG 23361 and FFH2055 and *Burkholderia cenocepacia* K56-2. GenBank, NIH genetic sequence database.
11. Brockhurst M.A., Colegrave N. & Rozen D.E. 2011. Next-generation sequencing as a tool to study microbial evolution. *Molecular Ecology*, **20**: 972-980. Doi: 10.1128/genomeA.00766-15
12. Cai R., Lv R., Shi X., Yang G. & Jin J. 2023. CRISPR/dCas9 Tools: Epigenetic Mechanism and Application in Gene Transcriptional Regulation. *International Journal of Molecular Sciences,* **24**: 14865. Doi: 10.3390/ijms241914865
13. Cardona S.T., Mueller C.L. & Valvano M.A. 2006. Identification of essential operons with a rhamnose-inducible promoter in *Burkholderia cenocepacia*. *Appl Environ Microbiol,* **72**:2547–2555. Doi: 10.1128/AEM.72.4.2547-2555.2006
14. Chen J. & Beckwith J. 2001. FtsQ, FtsL and FtsI require FtsK, but not FtsN, for co-localization with FtsZ during *Escherichia coli* cell division. *Molecular Microbiology*, **42**(2): 395-413. Doi: 10.1046/j.1365-2958.2001.02640.x.
15. Chin J.H., Samian M.R. & Normi Y.M. 2022. Characterization of polyhydroxyalkanoate production capacity, composition and weight synthesized by *Burkholderia cepacia* JC-1 from various carbon sources. *Heliyon Cell Press*, **8**: e09174. Doi: 10.1016/j.heliyon.2022.e09174
16. Coenye T. & Vandamme P. 2003. Diversity and significance of *Burkholderia* species occupying diverse ecological niches. *Environmental Microbiology,* **5**(9):719-29. Doi: 10.1046/j.1462-2920.2003.00471.x.
17. Coenye, T. 2014. The Family *Burkholderiaceae*. In: Rosenberg, E., DeLong, E.F., Lory, S., Stackebrandt, E., Thompson, F. (eds) The Prokaryotes. Springer, Berlin, Heidelberg.
18. Compant S., Nowak J., Coenye T., Clément C. & Barka E.A. 2008. Diversity and occurrence of *Burkholderia* spp. In the natural environment. *FEMS Microbiology Reviews*, **32**:607-626. Doi: 10.1111/j.1574-6976.2008.00113.x.
19. Courtney J.M., Dunbar K.E.A., McDowell A., Moore J.E., Warke T.K., Stevenson M. & Elborn J.S. 2004. Clinical outcome of *Burkholderia cepacia complex* infection in cystic fibrosis adults. *Journal of Cystic Fibrosis*, **3**: 93-98. Doi: 10.1016/j.jcf.2004.01.005.
20. Crow J., Geng H., Sullivan T.J., Soucy S.M. & Schultz D. 2024. Dynamics of drug delivery determines course of evolution of antibiotic responses in bacteria. bioRxiv. doi.org/10.1101/2023.11.29.569327

21. Crozat E., Philippe N., Lenski R., Geiselmann J. & Schneider D. 2004. Long-Term Experimental Evolution in *Escherichia coli*. XII. DNA Topology as a Key Target of Selection. *Genetics,* **169**: 523–532. Doi: 10.1534/genetics.104.035717

22. De Paula C.B.C., De Paula-Elias F.C., Rodrigues M.C., Coelho L.F., De Oliveira N.M.L., De Almeida A.F. & Contiero J. 2021. Polyhydroxyalkanoate Synthesis by *Burkholderia glumae* into a Sustainable Sugarcane Biorefinery Concept. *Front. Bioeng, Biotechnol*., **8**: 631284. Doi: 10.3389/fbioe.2020.631284

23. Deng P., Wang X., Baird S.M., Showmaker K.C., Smith L., Peterson D.G. & Lu S. 2016. Comparative genome-wide analysis reveals that *Burkholderia contaminans* MS14 possesses multiple antimicrobial biosynthesis genes but not major genetic loci required for pathogenesis. *Microbiology Open*, **5**(3): 353–369. Doi: 10.1002/mbo3.333.

24. Depardieu F. & Bikard D. 2020. Gene silencing with CRISPRi in bacteria and optimization of dCas9. *Methods, Elsevier*, **172**, pp. 61-75. Doi: 10.1016/j.ymeth.2019.07.024ff.

25. Depoorter, E., Bull, M.J., Peeters, C., Coenye T., Vandamme P. & Mahenthiralingam E. 2016. *Burkholderia:* an update on taxonomy and biotechnological potential as antibiotic producers. *Appl Microbiol Biotechnol*, **100:**5215–5229. Doi: 10.1007/s00253-016-7520-x

26. Derveaux S., Vandesompele J. & Hellemans J. 2010. How to do successful gene expression analysis using real-time PCR. *Elsevier Methods*, **50:** 227-230. Doi: 10.1016/j.ymeth.2009.11.001

27. Dillon M.M. & Cooper V.S. 2016. The Fitness Effects of Spontaneous Mutations Nearly Unseen by Selection in a Bacterium with Multiple Chromosomes. *Genetics*, **4**:1225-1238. Doi: 10.1534/genetics.116.193060

28. Dillon M.M., Sung W., Lynch M. & Cooper V.S. 2015. The Rate and Molecular Spectrum of Spontaneous Mutations in the GC-Rich Multichromosome Genome of *Burkholderia cenocepacia*. *Genetics*, **200:** 935–946. Doi: 10.1534/genetics.115.176834

29. Dilucca M., Cimini G. & Giansanti A. 2018. Essentiality, conservation, evolutionary pressure and codon bias in bacterial genomes. *Elsevier Gene*, **663**: 178-188. Doi: 10.1016/j.gene.2018.04.017

30. Drevinek P. & Mahenthiralingam E. 2010. *Burkholderia cenocepacia* in cystic fibrosis: epidemiology and molecular mechanisms of virulence. *Clin Microbiol Infect,* **16**:821-830. Doi: 10.1111/j.1469-0691.2010.03237.x.

31. Eberl L. 2006. Quroum sensing in the genus *Burkholderia*. International Journal of Medical Microbiology, *Elsevier*, **296**: 103–110. Doi: 10.1016/j.ijmm.2006.01.035.

32. Eberl, L. & Vandamme. P. 2016. Members of the genus *Burkholderia*: good and bad guys. *F1000Research*, **5:**1007. Doi: 10.12688/f1000research.8221.1.

33. Elena S. F & Lenski R.E. 2003. Evolution experiments with microorganisms: the dynamics and genetic bases of adaptation. *Nature Review Genetics*, **4**(6): 457-469. Doi: 10.1038/nrg1088

34. Elshafie, H. S. & Ippolito, C. 2021. An Overview of Metabolic Activity, Beneficial and Pathogenic Aspects of *Burkholderia* Spp. *Metabolites* **11**(5): 321. Doi: 10.3390/metabo11050321.

35. Enright A.L., Heelan W.J., Ward R.D. & Peters J. 2024. CRISPRi functional genomics in bacteria and its application to medical and industrial research. *Microbiology and Molecular Reviews*, **88**:e00170-22. Doi: 10.1128/mmbr.00170-22

36. Fan C., Davison P., Habgood R., Zeng H., Decker C., Salazar M., Lueangwattanapong K., Townley H., Yang A., Thompson I., Ye H., Cui Z., Schmidt F., Hunter C. & Huang W. 2020. Chromosome-free bacterial cells are safe and programmable platforms for synthetic biology. *Proc. Natl. Acad. Sci.,* PNAS, **117**(2): 6752-6761. Doi: 10.1073/pnas.1918859117

37. Fan H. & Chu J. 2007. A brief review of short tandem repeat mutation. *Genomics Proteomics Bioinformatics*, **5**(1): 7-14. Doi: 10.1016/S1672-0229(07)60009-6.

38. Fleischmann, R. D., Adams, M. D., White, O., Clayton, R. A., Kirkness, E. F., Kerlavage, A. R., Bult, C. J., Tomb, J. F., Dougherty, B. A., Merrick, J. M., McKenney, K., Sutton, G., FitzHugh, W., Fields, C., Gocayne, J. D., Scott, J., Shirley, R., Liu, L., Glodek, A., Kelley, J. M., Weidman, J. F., Phillips, C. A., Spriggs, T., Hedblom, E., Cotton, M. D., Utterback, T. R., Hanna, M. C., Nguyen, D. T., Saudek, D. M., Brandon, R. C., Fine, L. D., Fritchman, J. L., Fuhrmann, J. L., Geoghagen, N. S. M., Gnehm, C. L., McDonald, L. A., Small, K. V., Fraser, C. M., Smith, H. O., & Venter, J. C. 1995. Whole-Genome Random Sequencing and Assembly of *Haemophilus influenzae* Rd. *Science*, **269(**5223): 496-512. Doi: 10.1126/science.7542800.

39. Forster A.C. & Church G.M. 2006. Towards synthesis of a minimal cell. *Molecular Systems Biology*, **2**(45). Doi: 10.1038/msb4100090.

40. Foster P.L. 2007. Stress-induced Mutagenesis in Bacteria. *Crit Rev Biochem Mol Biol*., **42**(5):373-397. Doi: 10.1080/10409230701648494

41. Fuentes D.A.F., Manfredi P., Jenal U. & Zampieri M. 2021. Pareto optimality between growth-rate and lagtime couples metabolic noise to phenotypic heterogeneity in *Escherichia coli*. *Nat. Comm.,* **12**: 3204. Doi: 10.1038/s41467-021-23522-0

42. Galdiero S., Falanga A., Cantisani M., Tarallo R., Della Pepa M.E., D'Oriano V. & Galdiero M. 2012. Microbe-host interactions: structure and role of Gram-negative bacterial porins. *Curr Protein Pept Sci*. **8**:843-854. Doi: 10.2174/138920312804871120
43. Gallagher R., Patel J., Interiano A., Rovner A. & Isaacs F. 2015. Multilayered genetic safeguards limit growth of microorganisms to defined environments. *Nucleic Acids Research,* **43**(3): 1945-1954. Doi: 10.1093/nar/gku1378.
44. Gao W., Zhang W. & Meldrum D.R. 2011. RT-qPCR based quantitative analysis of gene expression in single bacterial cells. *Journal of Microbiological Methods*, **8**: 221-227. Doi: 10.1016/j.mimet.2011.03.008
45. Garcia P.S., Duchemin W., Flandrois J-P., Gribaldo S., Grangeasse C. & Brochier-Armanet C. 2021. A Comprehensive Evolutionary Scenario of Cell Division and Associated Processes in the Firmicutes. *Molecular biology evolution*, **38**(6): 2396-2412. Doi: 10.1093/molbev/msab034
46. García-Romero I. & Valvano M.A. 2020. Complete genome sequence of *Burkholderia cenocepacia* K56-2, an opportunistic pathogen. *Microbiol Resour Announc*, **9**:e01015-20. Doi: 10.1128/MRA.01015-20.
47. Ghavami S. & Pandi A. 2021. Chapter 5 – CRISPR interference and its applications. Progress in Molecular Biology and Translational Science Elsevier, 180: 123-140.
48. Giannopoulou E., Senda M., Koentjoro M.P., Adachi N., Ogawa N. & Senda T. 2021. Crystal structure of the full-length LysR-type transcriptional regulator CbnR in complex with promoter DNA. *The FEBS Journal*, **288**: 4560–4575. Doi: 10.1111/febs.15764
49. Gislason A.S., Turner K., Domaratzki M., & Cardona S.T. 2017. Comparative analysis of the *Burkholderia cenocepacia* K56-2 essential genome reveals cell envelope functions that are uniquely required for survival in species of the genus *Burkholderia*. *Microbial Genomics*, **3**(11): e000140. Doi: 10.1099/mgen.0.000140.
50. Glowicz J., Crist M., Gould C., Moulton-Meissner H., Noble-Wang J., de Man T.J.B., Perry K.A., Miller Z., Yang W.C., Langille S., Ross J., Garcia B., Kim J., Epson E., Black S., Pacilli M., LiPuma J.J. & Fagan R. 2018. A multistate investigation of health care-associated *Burkholderia cepacia* complex infections related to liquid docusate sodium contamination, January-October 2016. 2018. *Am J Infect Control*, **46**(6):649–655. Doi: 10.1016/j.ajic.2017.11.018.

51. Goel M., Sun H., Jiao W. & Schneeberger K. 2019. SyRI: finding genomic rearrangements and local sequence differences from whole-genome assemblies. *Genome Biology,* **20**:277. Doi: 10.1186/s13059-019-1911-0

52. González-Bermúdez, L., Anglada, T., Genescà, A., Martín M. & Terradas M. 2019. Identification of reference genes for RT-qPCR data normalisation in aging studies. *Scientific Reports*, 9:13970. Doi: 10.1038/s41598-019-50035-0

53. Good B.H., McDonald M.J., Barrick J.E., Lenski R.E. & Desai M.M. 2017. The dynamics of molecular evolution over 60,000 generations. *Nature*, **551**: 45-50. Doi: 10.1038/nature24287.

54. Govan J.R.W., Hughes J.E. & Vandamme P. 1996. *Burkholderia cepacia*: medial, taxonomic and ecological issues. *J. Med. Microbiol.*, **45**: 395-407. Doi: 10.1099/00222615-45-6-395.

55. Gu Y., Preisser J.S., Zeng D., Shrestha P., Shah M., Simancas-Pallares M.A., Ginnis J. & Divaris K. (2022). Partitioning around medoids clustering and random forest classification for gis-informed imputation of fluoride concentration data. *Ann Appl Stat*, **16**(1): 551-572. Doi: 10.1214/21-aoas1516

56. Gutiérrez-Santana J.C. & Coria-Jiménez V.R. 2024. *Burkholderia cepacia complex* in cystic fibrosis: critical gaps in diagnosis and therapy. *Ann Med*, **56**(1):2307503. Doi: 10.1080/07853890.2024.2307503

57. Handl J., Knowles J. & Kell D.B. 2005. Computational cluster validation in post-genomic data analysis, *Bioinformatics,* **21**(15):3201–3212. Doi: 10.1093/bioinformatics/bti517

58. Hassan A.A., dos-Santos S.S., Cooper V.S. & Sá-Correia I. 2020. Comparative Evolutionary Patterns of *Burkholderia cenocepacia* and *B. multivorans* During Chronic Co-infection of a Cystic Fibrosis Patient Lung. *Front. Microbiol,* **11**: 574626. Doi: 10.3389/fmicb.2020.574626

59. Higgins S., Sanchez-Contreras M., Gualdi S., Pinto-Carbó M., Carlier A. & Eberl L. 2017. The essential genome of *Burkholderia cenocepacia* H111. *Journal of Bacteriology*, **199**:e00260-17. Doi: 10.1128/JB.00260-17.

60. Ho Y.N., Chiang H.M., Chao C.P., Su C.C., Hsu H.F., Guo C.T., Hsieh J.L. & Huang C. 2015. *In planta* biocontrol of soilborne Fusarium wilt of banana through a plant endophytic bacterium, *Burkholderia cenocepacia* 869T2. *Plant Soil*, **387**: 295–306. Doi: 10.1007/s11104-014-2297-0

61. Hogan A.M. & Cardona S.T. 2022. Gradients in gene essentiality reshape antibacterial research. *FEMS Microbiology Reviews*, **3**: 1-27. Doi: 10.1093/femsre/fuac005

62. Hogan A.M., Rahman A.S.M.Z., Lightly T.J. & Cardona S.T. 2019. A Broad-Host-Range CRISPRi toolkit for silencing gene expression in *Burkholderia*. ACS *Synthetic Biology*, **8**(10): 2372-2384. Doi: 10.1021/acssynbio.9b00232.

63. Hogan A.M., Rahman A.S.M.Z., Motnenko A., Natarajan A., Maydaniuk D., León B., Batun Z., Palacios A., Bosch A. & Cardona S.T. 2023. Profiling cell envelope-antibiotic interactions reveals vulnerabilities to β-lactams in a multidrug-resistant bacterium. *Nature Communications*, **14**:4815. Doi: 10.1038/s41467-023-40494-5

64. Holden M.T.G., Seth-Smith H.M.B., Crossman L.C., Sebaihia M., Bentley S.D., Cerdeño-Tárraga A.M., Thomson N.R., Bason N., Quail M.A., Sharp S., Cherevach I., Churcher C., Goodhead I., Hauser H., Holroyd N., Mungall K., Scott P., Walker D., White B., Rose H., Iversen P., Mil-Homens D., Rocha E.P.C., Fialho A.M., Baldwin A., Dowson C., Barrell B.G., Govan J.R., Vandamme P., Hart C.A., Mahenthiralingam E. & Parkhill J. 2009. The Genome of *Burkholderia cenocepacia* J2315, an Epidemic Pathogen of Cystic Fibrosis Patients. *J Bacteriol,* **191**(1): 261-277. Doi:10.1128/JB.01230-08

65. Holden, M.T.G., Titball, R.W., Peacock, S.J., Cerdeño-Tárraga, A.M., Atkins, T., Crossman, L.C., Pitt, T., Churcher, C., Mungall, K., Bentley, S.D., Sebaihia, M., Thomson, N.R., Bason, N., Beacham, I.R., Brooks, K., Brown, K.A., Brown, N.F., Challis, G.L., Cherevach, I., Chillingworth, T., Cronin, A., Crossett, B., Davis, P., DeShazer, D., Feltwell, T., Fraser, A., Hance, Z., Hauser, H., Holroyd, S., Jagels, K., Keith, K.E., Maddison, M., Moule, S., Price, C., Quail, M.A., Rabbinowitsch, E., Rutherford, K., Sanders, M., Simmonds, M., Songsivilai, S., Stevens, K., Tumapa, S., Vesaratchavest, M., Whitehead, S., Yeats, C., Barrell, B.G., Oyston, P.C.F., & Parkhill, J. 2004. Genomic plasticity of the causative agent of melioidosis, *Burkholderia pseudomallei*. *Proc Natl Acad Sci, PNAS,* **101**(39):14240-14245. Doi: 10.1073/pnas.0403302101.

66. Hunter W.J. & Manter D.K. 2014. Antimicrobial Properties of an Oxidizer Produced by *Burkholderia cenocepacia* P525. *Current Microbiology, Springer*, **68**:610–614. Doi: 10.1007/s00284-013-0515-2.

67. Jones, C., Webster, G., Mullins, A. J., Jenner, M., Bull, M. J., Dashti, Y., Spilker, T., Parkhill, J., Connor, T. R., LiPuma, J. J., Challis, G. L., & Mahenthiralingam, E. 2021. Kill and cure: genomic phylogeny and bioactivity of *Burkholderia gladioli* bacteria capable of pathogenic and beneficial lifestyles. *Microbial Genomics*; 7:000515. Doi: 10.1099/mgen.0.000515

68. Juhas M., Eberl L. & Church G. M. 2012. Essential genes as antimicrobial targets and cornerstones of synthetic biology. *Trends in Biotechnology,* **30**(11): 601-607. Doi: 10.1016/j.tibtech.2012.08.002

69. K. Kobayashi, S. D. Ehrlich, HAS. Albertini, G. Amati, K. K. Andersen, Mr. Arnaud, K. Asai, S. Ashikaga, S. Aymerich, P. Bessieres, F. Boland, S. C. Brignell, S. Bron, K. Bunai, J. Chapuis, L. C. Christiansen, HAS. Danchin, Mr. Washed, E. Dervyn, E. Deuerling, K. Guess, S. K. Guess, O. Three, J. Errington, S. Fillinger, S. J. Foster, Y. Fujita, HAS. Galizzi, A. Gardan, C. Aldermen, T. Fukushima, K. Hey, C. A. Harwood, Mr. Hecker, D. Hosoya, Mr. F. Hullo, H. Kakeshita, D. Karamata, Y. Kasahara, F. Kawamura, K. Koga, P. Koski, A. Kuwana, D. Imamura, Mr. Ishimaru, S. Ishikawa, I. Ishio, D. The Rooster, HAS. Mason, C. Mauel, A. Meima, A. P. Melado, HAS. Moi, S. Moriya, E. Nagakawa, H. Nanamiya, S. Nakai, P. Nygaard, Mr. Ogura, T. Ohanan, Mr. O'Reilly, Mr. O'Rourke, Z. Pragay, H. Mr. Pooley, G. Report, J. P. Rawlins, L. HAS. Rivas, C. Revolt, HAS. Sadaie, Y. Sadaie, Mr. Sarvas, T. Sato, H. H. Saxild, E. Scanlan, W. Schumann, J. F. Mr. L. Seegers, J. Sekiguchi, HAS. Sekowska, S. J. Seror, Mr. Simon, P. Stragier, A. Studer, H. Takamatsu, T. Tanaka, Mr. Takeuchi, H. B. Thomaides, Vagner V., van Dijl J. M., K. Watabe, K. Wipat, H. Yamamoto, M. Yamamoto, Y. Yamamoto, K. Yamane, K. Yata, K. Yoshida, H. Yoshikawa, U. Zuber & N. Ogasawara. 2003. Essential *Bacillus subtilis* genes. *PNAS Biological Sciences,* **100**(8): 4678-4683. Doi:10.1073/pnas.0730515100

70. Kassambara A. 2020. factoextra: Extract and Visualize the Results of Multivariate Data Analyses. R package version 1.0.7. Doi: 10.32614/CRAN.package.factoextra

71. Kaufman L and Rousseeuw PJ (2009). Finding Groups in Data: An Introduction to Cluster Analysis. John Wiley & Sons. USA. 68-71 pp.

72. Kawecki T.J., Lenski R.E., Ebert D., Hollis B., Olivieri I. & Whitlock M.C. 2012. Experimental evolution. *Trends in Ecology & Evolution,* **27**(10): 547-560. Doi: 10.1016/j.tree.2012.06.001 T

73. Khalil A.S. & Collins J.J. 2010. Synthetic biology: applications come of age. *Nature Reviews Genetics*, 11:367-379. Doi:10.1038/nrg2775

74. Kherroubi L., Bacon J. & Rahman K.M. 2024. Navigating fluoroquinolone resistance in Gram-negative bacteria: a comprehensive evaluation. *JAC Antimicrobial resistance*, **6**(4): dlae127. Doi: 10.1093/jacamr/dlae127

75. Kolmogorov M., Yuan J. Lin Y. & Pevzner P.A. 2019. Assembly of long, error-prone reads using repeat graphs. *Nature biotechnology*, **37**:540-546. Doi: 10.1038/s41587-019-0072-8

76. Kubista M., Andrade J.M., Bengtsson M., Forootan A., Jonák J., Lind K., Sindelka R., Sjöback R., Sjögreen B., Strömbom L., Ståhlberg A. & Zoric N. 2006. The real-time polymerase chain reaction. *Molecular Aspects of Medicine,* **27:** 95-125. Doi: 10.1016/j.mam.2005.12.007.

77. Lee J.W., Chan C.T.Y., Slomovic S. & Collins J.J. 2018. Next-generation biocontainment systems for engineered organisms. *Nature Chemical Biology*, **14**: 530-537. Doi: 10.1038/s41589-018-0056-x

78. Leiby N. & Marx C. J. 2014. Metabolic Erosion Primarily Through Mutation Accumulation, and Not Tradeoffs, Drives Limited Evolution of Substrate Specificity in *Escherichia coli*. *PLOS Biology*, **12**(2): e1001789. Doi: 10.1371/journal.pbio.1001789

79. Lengyel A. & Botta-Dukát Z. 2019. Silhouette width using generalized mean-A flexible method for assessing clustering efficiency. *Ecol Evol*, **9**(23):13231–13243. Doi: 10.1002/ece3.5774.

80. Lenski R.E. 2017. Experimental evolution and the dynamics of adaptation and genome evolution in microbial populations. *International Society for Microbial Ecology*, **11**: 2181–2194. Doi: 10.1038/ismej.2017.69

81. Liu G., Yong M.Y.J., Yurieva M., Srinivasan K.G., Liu J., Lim J.S.Y., Poidinger M., Wright G.D., Zolezzi F., Choi H., Pavelka N., Rancati G. 2015. Gene essentiality is a quantitative property linked to cellular evolvability. *Cell*, **163:** 1388–1399. Doi: 10.1016/j.cell.2015.10.069

82. Liu X., Gallay C., Kjos M., Domenech A., Slager J., Kessel S.P., Knoops K., Sorg R.A., Zhang J.R., & Veening J. 2017. High-throughput CRISPRi phenotyping identifies new essential genes in *Streptococcus pneumoniae*. *Molecular Systems Biology*, **13**(5):931. Doi: 10.15252/msb.20167449.

83. Llunar-Senar M., Delgado J., Chen W-H., Lloréns-Rico V., O'Reilly F.K., Wodke J.A.H., Unal E.B., Yus E., Martínez S., Nichols R.J., Ferrar T., Vivancos A., Schmeisky A., Stülke J., van Noort V., Gavin A-C., Bork P. & Serrano L. 2015. Defining a minimal cell: essentiality of small ORFs and ncRNAs in a genome-reduced bacterium. *Molecular Systems Biology,* **11**: 780. Doi: 10.15252/msb.20145558

84. Luo H., Gao F. & Lin Y. 2015. Evolutionary conservation analysis between the essential and nonessential genes in bacterial genomes. *Scientific Reports*, **5**: 13210. Doi: 10.1038/srep13210.

85. Luo H., Lin Y., Liu T., Lai F., Zhang C., Gao F. & Zhang R. 2020. DEG 15, an update of the Database of Essential Genes that includes built-in analysis tools. *Nucleic Acids Research,* **49**: D677–D686. Doi: 10.1093/nar/gkaa917

86. Maddocks S.E. & Oyston P.C.F. 2008. Structure and function of the LysR-type transcriptional regulator (LTTR) family proteins. *Microbiology,* **154:** 3609-3623. Doi: 10.1099/mic.0.2008/022772-0

87. Maechler M, Rousseeuw P, Struyf A, Hubert M, Hornik K (2024). cluster: Cluster Analysis Basics and Extensions. R package version 2.1.8 Doi: 10.32614/CRAN.package.cluster

88. Maechler M., Rousseeuw P., Struyf A., Hubert M., Hornik K. 2023. *cluster: Cluster Analysis Basics and Extensions*. R package version 2.1.6

89. Mandell D., Lajoie M.J., Mee M.T., Takeuchi R., Kuznetsov G., Norville J.E., Gregg C.J., Stoddard B. & Church G.M. 2015. Biocontainment of genetically modified organisms by synthetic protein design. *Nature*, **518**(7537): 55-60. Doi: 10.1038/nature14121

90. Mardis E.R. 2008. Next-Generation DNA sequencing methods. *Annu. Rev. Genomics Hum. Genet***, 9**:387–402. Doi: 10.1146/annurev.genom.9.081307.164359

91. McDonald M.J. 2019. Microbial Experimental Evolution - a proving ground for evolutionary theory and a tool for discovery. *EMBO Reports*, **20**:e46992. Doi: 10.15252/embr.201846992

92. McElroy K.E., Hui J.G., Woo J.K., Luk A.W., Webb J.S., Kjelleberg S., Rice S.A. & Thomas T. 2014. Strain-specific parallel evolution drives short-term diversification during *Pseudomonas aeruginosa* biofilm formation. *PNAS*, **111**(14): E1419-E1427. Doi: 10.1073/pnas.1314340111

93. McPhee D.G. & Ambrose M. 1996. Spontaneous mutations in bacteria: chance or necessity?. *Genetica* **97**: 87-101. Doi: 10.1007/BF00132585.

94. Mingorance J., Tamames J. & Vicente M. 2004. Genomic channeling in bacterial cell division. *Journal of Molecular Recognition*, **17**: 481-487. Doi: 10.1002/jmr.718

95. Mitchell S.L. & Simner P.J. 2019. Next-Generation Sequencing in Clinical Microbiology: Are We There Yet?. *Clin Lab Med,* **39**:405–418. Doi: 10.1016/j.cll.2019.05.003.

96. Modak S., Chattopadhyay T. & Chattopadhyay A.K. 2020. Unsupervised classification of eclipsing binary light curves through K-medoids clustering. *Journal of applied statistics,* **47**(2): 376-392. Doi: 10.1080/02664763.2019.1635574.

97. Molin S., Klemm P., Poulsen L.K., Biehl H., Gerdes K. & Anderson P. 1987. Conditional Suicide system for containment of bacteria and plasmids. *Nature Biotechnology*, **5**: 1315-1318. doi: 10.1038/nbt1287-1315

98. Mustafa A.S. 2024. Whole Genome Sequencing: Applications in Clinical Bacteriology. *Med Princ Pract,* **33**(3): 185–197. Doi: 10.1159/000538002

99. Novak M., Pfeiffer T., Ackermann M. & Bonhoeffer S. 2009. Bacterial growth properties at low optical densities. *Antonie van Leeuweenhoef*, **96**(3):267–274. Doi: 10.1007/s10482-009-9342-7

100. O'Grady E.P., Nguyen D.T., Weisskopf L., Eberl L. & Sokol P.A. 2011. The Burkholderia cenocepacia LysR-Type Transcriptional Regulator ShvR Influences Expression of Quorum-Sensing, Protease, Type II Secretion, and afc Genes. *ASM Journal of Bacteriology,* 193: 163-176. Doi: 10.1128/JB.00852-10

101. Pagès J., James C. & Winterhalter M. 2008. The porin and the permeating antibiotic: a selective diffusion barrier in Gram-negative bacteria. *Nature Reviews Microbiology,* **6:** 893-903. Doi: 10.1038/nrmicro1994.

102. Peng C. & Gao F. 2014. Protein Localization Analysis of Essential Genes in Prokaryotes. *Scientific Reports*, **4**:6001. Doi: 10.1038/srep06001.

103. Peters J.M. Colavin A. Shi H., Czarny T.L., Larson M.H., Wong S., Hawkins J.S., Lu C.H.S., Koo B., Marta M., Shiver A.L., Whitehead E.H., Weissman J.S., Brown E.D., Qi L.S., Huang K.C. & Gross C.A. 2016. A Comprehensive, CRISPR-based Functional Analysis of Essential Genes in Bacteria. *Cell*, 165: 1493-1506. Doi: 10.1016/j.cell.2016.05.003

104. Peters J.M., Koo B.-M., Patino R., Heussler G.E., Hearne C.C., Qu J., Inclan Y.F., Hawkins J.S., Lu C.H.S., Silvis M.R., Harden M.M., Osadnik H., Peters J.E., Engel J.N., Dutton R.J., Grossman A.D., Gross C.A. & Rosenberg O.S. 2019. Enabling genetic analysis of diverse bacteria with mobile CRISPRi. *Nature microbiology*, 4(2): 244-250. Doi: 10.1038/s41564-018-0327-z.

105. Peters J.M., Silvis M.R., Zhao D., Hawkins J.S., Gross C.A. & Qi L.S. 2015. Bacterial CRISPR: Accomplishments and Prospects. *Current Opinion in Microbiology*, **27**:121-126. Doi: 10.1016/j.mib.2015.08.007

106. Pope C.F., Gillespie S. H., Moore J.E. & McHugh T.D. 2010. Approaches to measure the fitness of *Burkholderia cepacia* complex isolates. *Journal of Medical Microbiology,* **56**:679-686. Doi: 10.1099/jmm.0.017830-0

107. Qi L., Larson M.H., Gilbert L.A., Doudna J., Weissman J.S., Arkin A.P. & Lim W.A. 2013. Repurposing CRISPR as an RNA-Guided Platform for Sequence Specific Control of Gene Expression. *Cell,* **152**(5): 1173-1183. Doi: 10.1016/j.cell.2013.02.022

108. Ragupathi N.K.D. & Veeraraghavan B. 2019. Accurate identification and epidemiological characterization of *Burkholderia cepacia complex*: an update. *Ann Clin Microbiol Antimicrob*, **18**:7. Doi: 10.1186/s12941-019-0306-0

109. Rahman A.S.M.Z., Syroegin E.A., Timmerman L., Novomisky-Nechcoff J., Devarajan A., Polikanov Y.S. & Cardona S.T. 2024. Rationally Designed Pooled CRISPRi-seq Uncovers a Novel Inhibitor of Bacterial Peptidyl-tRNA Hydrolase. *Cell Reports,* **43**(11): 114967. Doi: 10.1016/j.celrep.2024.114967

110. Ram Y. & Hadany L. 2012. The evolution of stress-induced hypermutation in asexual populations. *Evolution*, **66**(7): 2315–2328. Doi: 10.1111/j.1558-5646.2012.01576.x

111. Rana A., Patton D., Turner N.T., Dillon M.M., Cooper V.S. & Sung W. 2021. Precise measurement of the fitness effects of spontaneous mutations by droplet digital PCR in *Burkholderia cenocepacia*. *Genetics,* **219**(2): iyab117. Doi: 10.1093/genetics/iyab117

112. Rancati G., Moffat J., Typas A. & Pavelka N. 2018. Emerging and evolving concepts in gene essentiality. *Nature Review Genetics,* **19**:34-39. Doi: 10.1038/nrg.2017.74

113. Rhodes K.A. & Schweizer H.P. 2016. Antibiotic resistance in *Burkholderia* species. Drug Resist Update, **28:**82-90. Doi: 10.1016/j.drup.2016.07.003

114. Rocha D.J.P.G., Castro T.L.P., Aguiar E.R.G.R. & Pacheco L.G.C. 2020. Gene Expression Analysis in Bacteria by RT-qPCR. *Methods in Molecular Biology*, **2065**: 119-137. Doi: 10.1007/978-1-4939-9833-3_10

115. Rocha E.P.C. & Danchin A. 2003. Gene essentiality determines chromosome organisation in bacteria. *Nucleic Acids Research,* **31**(22):6570-6577. Doi: 10.1093/nar/gkg859

116. Rousset F., Cui L., Siouve E., Becavin C., Depardieu F. & Bikard F. 2018. Genome-wide CRISPR-dCas9 screens in *E. coli* identify essential genes and phage host factors. *PLoS, Genetics,* **14(**11): e1007749. Doi: 10.1371/journal.pgen.1007749

117. Roy S., Naha S., Rao A. & Basu S. 2021. CRISPR-Cas system, antibiotic resistance and virulence in bacteria: Through a common lens, Chapter Five. *Progress in Molecular Biology and Translational Science*, **178**: 123-174. Doi: 10.1016/bs.pmbts.2020.12.005

118. Rozen D. & Lenski R.E. 2000. Long-Term Experimental Evolution in *Escherichia coli*. VIII. Dynamics of a Balanced Polymorphism. *The American Naturalist,* **155**: 24-35. Doi: 10.1086/303299

119. Sanger F., Nicklen S. & Coulson R. 1977. DNA sequencing with chain-terminating inhibitors. *Proc. Nati. Acad. Sci.*, **74**(12): 5463-5467. Doi: 10.1073/pnas.74.12.5463

120. Satam H., Joshi K., Mangrolia U., Waghoo S., Zaidi G., Rawool S., Thakare R.P., Banday S., Mishra A.K., Das G. & Malonia S.K. Next-Generation Sequencing Technology: Current Trends and Advancements. *Biology (Basel),* **12**(7):997. Doi: 10.3390/biology12070997

121. Schmittgen T.D. & Livak K.J. 2008. Analyzing real-time PCR data by the comparative C_T method. *Nature Protocols*, **3**(6): 1101-1108. Doi: 10.1038/nprot.2008.73

122. Sfeir M.M. 2018. *Burkholderia cepacia complex* infections: More complex than the bacterium name suggest. *Journal of infection,* **77**:166-170. Doi: 10.1016/j.jinf.2018.07.006

123. Silvis M.R., Rajendram M., Shi H., Osadnik H., Gray A.N., Cesar S., Peters J.M., Hearne C.C., Kumar P., Todor H., Huang K.C., Gross C.A. 2021. Morphological and Transcriptional Responses to CRISPRi Knockdown of Essential Genes in *Escherichia coli*. *Microbial genetics,* **12(5)**:mbio.02561-21. Doi: 10.1128/mbio.02561-21

124. Slatko B.E., Gardner A.F. & Ausubel F.M. 2018. Overview of next generation sequencing technologies. *Curr Protoc Mol Biol*, **122**(1): e59. Doi: 10.1002/cpmb.59

125. Sprouffske, K. & Wagner, A. 2016. Growthcurver: an R package for obtaining interpretable metrics from microbial growth curves. *BMC Bioinformatics*, **17**: 172. Doi: 10.1186/s12859-016-1016-7

126. Stano, P. 2010. Synthetic biology of minimal living cells: primitive cell models and semi-synthetic cells. *Systems and Synthetic Biology*, **4**:149-156. Doi: 10.1007/s11693-010-9054-3

127. Tavares M., Kozak M., Balola A. & Sá-Correia I. 2020. *Burkholderia cepacia complex* Bacteria: a Feared Contamination Risk in Water-Based Pharmaceutical Products. *Clinical Microbiology Reviews,* **33**(3): e00139-19. Doi: 10.1128/CMR.00139-19

128. Tenaillon O., Barrick J., Ribeck N., Deatherage D.E., Blanchard J.L., Dasgupta A., Wu G.C., Wielgoss S., Cruveiller S., Médigue C. Schneider D. & Lenski R.E. 2016. Tempo and mode of genome evolution in a 50,000-generation experiment. *Nature*, 536(7615):165-70. Doi: 10.1038/nature18959

129. Traverse C.C., Mayo-Sith Leslie M., Poltak S.R. & Cooper V.S. 2012. Tangled bank of experimentally evolved *Burkholderia* biofilms reflects selection during chronic infections. *Proc Natl Acad Sci, PNAS*, **110**(3): E250-E259. Doi: 10.1073/pnas.1207025110

130. Trespidi G., Scoffone V.C., Barbieri G., Riccardi G., De Rossi E. & Buroni S. 2020. Molecular Characterization of the *Burkholderia cenocepacia dcw* Operon and FtsZ Interactors as New Targets for Novel Antimicrobial Design. *Antibiotics,* **9**:841. Doi: 10.3390/antibiotics9120841

131. Ussery D.W., Kiil K., Lagesen K., Sicheritz-Pontén T., Bohlin J. & Wassenaar T.M. 2009. The genus *Burkholderia:* analysis of 56 genomic sequences. *Microbial pathogenomics*, **6**:40-157. Doi: 10.1159/000235768

132. Van den Bergh B., Swings T., Fauvart M. & Michiels J. 2018. Experimental Design, Population Dynamics, and Diversity in Microbial Experimental Evolution. *Microbiol Mol Biol Rev ASM,* **82**(3): e00008-18. Doi: 10.1128/MMBR .00008-18.

133. Velmurugan T. & Santhanam T. 2010. Computational Complexity between K-Means and K-Medoids Clustering Algorithms for Normal and Uniform Distributions of Data Points. *Journal of Computer Science* **6**(3): 363-368. Doi: 10.3844/jcssp.2010.363.368

134. Vergalli J., Bodrenko I.V., Masi M., Moynié L., Acosta-Gutiérrez S., Naismith J.H., Davin-Regil A., Ceccarelli M., van den Berg B., Winterhalter M. & Pagès J. 2020. Porins and small-molecule translocation across the outer membrane of Gram-negative bacteria. *Nature Reviews Microbiology*, **18**(3): 164-176. Doi: 10.1038/ s41579-019-0294-2

135. Vial L., Groleau M.C., Dekimpe V. & Déziel E. 2007. *Burkholderia* Diversity and Versatility: An Inventory of the Extracellular Products. *J. Microbiol. Biotechnol*, **17**(9): 1407–1429.

136. Wang K., Li X., Yang C., Song S., Cui C., Zhou X. & Deng Y. 2021. A LysR family transcriptional regulator modulates *Burkholderia cenocepacia* biofilm formation and protease production. *Applied Environmental Microbiology*, **87**:e00202-21. Doi: 10.1128/AEM .00202-21.

137. Wang Y., Zhao Y., Bollas A., Wang Y. & Au K.F. 2021. Nanopore sequencing technology, bioinformatics and applications. *Nature Biotechnology*, **39**(11): 1348–1365. Doi: 10.1038/s41587-021-01108-x

138. Wang Z., Pan H., Ni S., Li Z. & Lian J. 2024. Establishing CRISPRi for Programmable Gene Repression and Genome Evolution in *Cupriavidus necator*. *ACS Synth. Biol.,* **13**(3):851-861. Doi: 10.1021/acssynbio.3c00664

139. Watford S. & Warrington S.J. 2023. Bacterial DNA mutations. Treasure Island (FL): StatPearls Publishing. Available from:https://www-ncbi-nlm-nih-gov.uml.idm.oclc.org/books/NBK459274

140. Wick R., Judd L.M. & Holt K.E. 2019. Performance of neural network basecalling tools for Oxford Nanopore sequencing. *Genome Biol*, **20**(1): 129. Doi: 10.1186/s13059-019-1727-y

141. Wick R., Judd L.M., Gorrie C.L. & Holt K.E. 2017. Unicycler: Resolving bacterial genome assemblies from short and long sequencing reads. *PLoS Comput Biol,* **13**(6): e1005595. Doi: 10.1371/journal.pcbi.1005595

142. Wong Y., Ghany M.A.E., Naeem R., Lee K., Tan Y., Pain A. & Nathan S. 2016. Candidate essential genes in *Burkholderia cenocepacia* J2315 identified by genome-wide TraDIS. *Front. Microbiol.*, **7**:1288. Doi: 10.3389/fmicb.2016.01288

143. Wu X., Kriz A.J. & Sharp P. 2014. Target specificity of the CRISPR-Cas9 system. *Quantitative Biology*, **2**(2):59-70. Doi: 10.1007/s40484-014-0030-x

144. Yabuuchi E., Kosako Y., Oyaizu H., Yano I., Hotta H., Hashimoto Y., Ezaki T. & Arakawa M. 1992. Proposal of *Burkholderia* gen. nov. and transfer of seven species of the genus *Pseudomonas* homology group II to the new genus, with the type species *Burkholderia cepacia* (Palleroni and Holmes 1981) comb. nov. *Microbiol Immunol.,* **36**(12):1251-75. Doi: 10.1111/j.1348-0421.1992.tb02129.x

145. Zhao H., Sun Y., Peters J.M., Gross C.A., Garner E.C. & Helmann J.D. 2016. Depletion of Undecaprenyl Pyrophosphate Phosphatases Disrupts Cell Envelope Biogenesis in *Bacillus subtilis*. *Journal of Bacteriology*, **198**(21): 2925-2935. Doi: 10.1128/JB.00507-16

146. Zhou, G., Wang, Q., Wang, Y., Wen, X., Peng, H., Peng, R., Shi, Q., Xie, X., & Li, L. 2023. Outer Membrane Porins Contribute to Antimicrobial Resistance in Gram-Negative Bacteria. *Microorganisms*, **11**(7): 1690. Doi: 10.3390/microorganisms11071690

147. Zocca, V.F.B., Corrêa, G.G., Lins, M. R. da C.R., de Jesus, V.N., Tavares, L. F., Amorim, L. A. da S., Kundlatsch G.E. & Pedrolli, D. B. 2021. The CRISPR toolbox for the gram-positive model bacterium *Bacillus subtilis*. *Critical Reviews in Biotechnology,* **42**(6): 813–826. Doi: 10.1080/07388551.2021.1983516

148. Zorraquino V., Kim M., Rai N. & Tagkopoulos I. 2016. The Genetic and Transcriptional Basis of Short and Long Term Adaptation across Multiple Stresses in *Escherichia coli*. *Mol. Biol. Evol.*, **34**(3):707–717. Doi:10.1093/molbev/msw269